RPSEA

Final Report

Document Number 09123.14.Final

Robert Zubrin, Mark Berggren, James Siebarth, Colin Apke, Boris Nizamov, Thomas Henshaw
Pioneer Astronautics
http://www.pioneerastro.com/

Reid Grigg, Chongwei Xiao, Ephraim Schofield
Petroleum Recovery Research Center
New Mexico Institute of Mining and Technology
http://baervan.nmt.edu/

Green Oil™: CO_2 – Enhanced Oil Recovery For America's Small Oil Producers

Contract Number 09123-14

August 9, 2013

Robert Zubrin, Principal Investigator
President, Pioneer Astronautics
11111 W. 8th Avenue, Lakewood, CO 80215
303-980-0890

This report was prepared by *Pioneer Astronautics* as an account of work sponsored by the Research Partnership to Secure Energy for America, RPSEA. Neither RPSEA members of RPSEA, the National Energy Technology Laboratory, the U.S. Department of Energy, nor any person acting on behalf of any of the entities:

a. MAKES ANY WARRANTY OR REPRESENTATION, EXPRESS OR IMPLIED WITH RESPECT TO ACCURACY, COMPLETENESS, OR USEFULNESS OF THE INFORMATION CONTAINED IN THIS DOCUMENT, OR THAT THE USE OF ANY INFORMATION, APPARATUS, METHOD, OR PROCESS DISCLOSED IN THIS DOCUMENT MAY NOT INFRINGE PRIVATELY OWNED RIGHTS, OR

b. ASSUMES ANY LIABILITY WITH RESPECT TO THE USE OF, OR FOR ANY AND ALL DAMAGES RESULTING FROM THE USE OF, ANY INFORMATION, APPARATUS, METHOD, OR PROCESS DISCLOSED IN THIS DOCUMENT.

THIS IS A FINAL REPORT. THE DATA, CALCULATIONS, INFORMATION, CONCLUSIONS, AND/OR RECOMMENDATIONS REPORTED HEREIN ARE THE PROPERTY OF THE U.S. DEPARTMENT OF ENERGY.

REFERENCE TO TRADE NAMES OR SPECIFIC COMMERCIAL PRODUCTS, COMMODITIES, OR SERVICES IN THIS REPORT DOES NOT REPRESENT OR CONSTIITUTE AND ENDORSEMENT, RECOMMENDATION, OR FAVORING BY RPSEA OR ITS CONTRACTORS OF THE SPECIFIC COMMERCIAL PRODUCT, COMMODITY, OR SERVICE.

THIS PAGE INTENTIONALLY LEFT BLANK

Signature Page

Name: Robert Zubrin

Signature: _____

Company Title: President

Robert M Zubrin,
Principal Investigator
President, Pioneer Astronautics
Date: 8/9/13

Abstract

The Green Oil™ technology is an innovative, a truck-portable renewable energy system that generates and separates CO_2 and H_2 for CO_2-Enhanced Oil Recovery for small oil producers. The CO_2 and H_2 are generated by the steam-oxygen reforming of biomass, which is followed by product gas clean-up, conditioning, and gas separation to create a high purity CO_2 stream for on-site well flooding, and H_2 for carbon free electrical power generation. This technical report discusses the operational testing and analysis results of an automated Green Oil™ steam-oxygen reformer system. The Green Oil™ technology was demonstrated in both batch and continuous modes using charcoal and pine wood biomass fuels over a wide range of temperature, pressure and flow conditions. The milestone of 6,000 SLPM (305,000 SCFD) product gas generation at 10 bar was achieved. A Water Gas Shift reactor was used to enrich the product gas yield of CO_2 and H_2 from the reformer. This approach resulted in the high production yield of H_2 (>45 vol. %), CO_2 (>40 vol. %), and a high CO conversion efficiency of >80%. To achieve long duration operation, a pneumatic conveyance coupled to a pressurized lock-hopper system was designed and constructed. Using this device, continuous operational times of over several hours were demonstrated with the GO™ system. Reactant and product gas composition, flow, temperature, and pressure data from these tests were used to calculate material and energy balances of the reformer system. High carbon conversion efficiencies of more than 95% were achieved. An external olivine catalyst tar destruction reactor was operated and is estimated to reduce tar by 60% based on available kinetic data. A product gas heat recovery system generated steam flow that is more than 50% of the total steam needed for reforming. Results from these data can be used to scale-up the system to 20,000 SLPM (1,000,000 SCFD) of combined driver gas for oil recovery on the scale of 100 barrels per day.

A comprehensive study including reservoir characterization, geomodel construction and reservoir simulation was performed for the Grouse Field Spergen Reservoir, Cheyenne County, Colorado. A reservoir simulation model was constructed and the model prediction of cumulative oil production correlated closely to within 92% of the well history data. Using the model, CO_2 injection rates and oil recovery were modeled for 20 and 40 year schedules, and with constant and recycled CO2 injection. CO_2 breaks through after four years (2016 in this case), and at the end of 2052, recycled CO_2 is almost three times of reformer produced CO_2, or a total injection rate of almost 4MMscf/d. An economic calculator has been designed to calculate several important economic values, including initial or capital investment, net present value, and payout. The main inputs for the calculator include an oil price forecast, current production trend, oil production forecast with CO_2 injection, operational expense, horsepower requirements for compression, and pipeline estimates.

Table of Contents

List of Tables **8**

List of Figures **9**

1. Executive Summary **12**

2. Introduction **14**

2.1. Background 14

2.2. Report Organization 18

3. Report Details **19**

3.1 Experimental Methods and Materials 19

3.1.1 Reformer System Design 19

3.1.1.1 Process Definition and Analysis 20

3.1.1.2. Component Analysis and Design 22

3.1.2. Fabrication and Integration 42

3.1.3 Methodology 46

3.2 Results and Discussion **50**

3.2.1 System Checkout 50

3.2.1.1 System Startup, Operation and Shutdown 51

3.2.2 Phase IIIA System Testing 56

3.2.2.1 Batch Operation with Charcoal: 4000 SLPM Demonstration 56

3.2.2.2 Batch Operation with Pine Pellets: 4000 SLPM, 10 Bar Demonstration 60

3.2.2.3 Water Gas Shift Reactor: Enrichment of CO_2 and H_2 Yield 63

3.2.2.4 Effects of Operating Parameters on Product Gas Composition 67

3.2.2.5 Tar Destruction Reactor 72

3.2.2.6 Preferred Operating Conditions 74

3.2.2.7 Extended Duration Testing 75

3.2.2.8 Phase IIIA Test Summary 86

3.2.3 Phase IIIB System Testing 87

3.2.3.1. Continuous Feed Design and Construction 88

3.2.3.2 Initial Testing 92

3.2.3.3. Operational Testing 93

3.2.3.4. Phase IIIB Test Summary 99

3.2.4. Field Data Collection and Analysis 99

3.2.4.1 Reservoir Simulation and Modeling 99

3.2.4.2 Geomodel Construction and Reservoir Simulations 111

3.2.4.3 Economics of CO2-EOR 125

3.3 Impact to Producers **129**

3.4 Technology Transfer Efforts **130**

3.5 Summary and Conclusions **130**

4. Summary and Recommendations for Future Work **130**

5. References **131**

6. List of Acronyms and Abbreviations 134
Appendix 136
A.1 Process Model..... 136
A.2. Piping and Instrumentation Diagram 137
A.3. Proximate and Ultimate Analysis of Wood Pellet Fuel..... 141
A.4. Test Case Summary 142
A.5. Linear Slider Feed Cup Diagram 144

List of Tables

Table 3.1. Simplified Process Stream Table	19
Table 3.2. Nominal Reactant Flow Rates	21
Table 3.3. Scaling Factor for Steam, Propane and Water for Steam Generator-1 Operation	23
Table 3.4. Oxygen Flow Controller Sizing and Specifications	24
Table 3.5. Hydrogen Flow Controller Specifications	24
Table 3.6 Propane Flow Controller Specifications	24
Table 3.7. Design Summary for Steam Orifice Flow Meter	26
Table 3.8. Biomass Steam Reformer Dimensions	28
Table 3.9. Cyclone Separator Geometry	31
Table 3.10. Design Summary for Backpressure Control Valve	36
Table 3.11. Flow Measurement Instrumentation	38
Table 3.12. Gas Chromatograph Analysis Method	38
Table 3.13. System Material Specifications	40
Table 3.14. Process and Performance Variables	44
Table 3.15. Biomass Fuel Properties	48
Table 3.16. Product Gas Composition	51
Table 3.17. Product Gas Composition with Charcoal (Test 055-12, dry gas basis)	57
Table 3.18. Test 055-12 Data Summary	57
Table 3.19. Test 102-19 Data Summary	60
Table 3.20. Comparison of GO Operating Conditions and Gas Composition with Literature Data	69
Table 3.21. Preferred Operating Conditions (4000 SLPM, 10 bar Operation)	71
Table 3.22. Nominal Biomass Feed Rate to Reformer	75
Table 3.23. Feed Control Program Sequence	77
Table 3.24. Material Balance	83
Table 3.25. Reformer Energy Balance	84
Table 3.26. Phase IIIB Design Criteria.	86
Table 3.27. Baseline Test Results for the Phase IIIB Reformer	92
Table 3.28. Capillary Pressure	106
Table 3.29. Simulation Results for Pintail's Grouse Field Sperger	118
Table 3.30. Simulation Results Comparison for Pintail's Grouse Field Spergen Reservoir Over Sixty Years (12/01/2063) After Two Years of CO_2 Injection	119
Table 3.31. Simulation results comparison for Pintail reservoir in 40 years (12/01/2063)	123
Table 4.1 Advantages of Coal Reforming CO_2-EOR for the Small Producer	131
Table A.1.1. Comparison of Experimental and Process Model Results for the Reformer	137
Table A.3.1. Pine Wood Pellet Report of Analysis	141
Table A.4.1. Test Case Log	142

List of Figures

Figure 2.1. *A comparison of current CO_2 pipelines in the United States*	13
Figure 2.2. *Simplified process diagram of the Green Oil™ EOR-CO_2 system for small oil producers.*	14
Figure 2.3. *Diagram of downdraft gasifier and reaction zones.*	15
Figure 2.4. *Green Oil™ Pilot Test Rig and Support Systems*	16
Figure 3.1. *Simplified Process Flow Diagram for the GO™ System*	20
Figure 3.1. *Simplified Process Flow Diagram for the GO™ System*	23
Figure 3.1. *Simplified Process Flow Diagram for the GO™ System*	28
Figure 3.4. *Biomass steam reformer layout*	29
Figure 3.5. *Photograph of the rotating grate*	31
Figure 3.6. *Cyclone design parameters*	32
Figure 3.7. *Schematic for the Tar Destruction Reactor*	33
Figure 3.8. *Boiler -2 Dimensions*	34
Figure 3.9. *Cut away model view of the water condenser*	36
Figure 3.10. *Screen shot of the Reformer tab user interface*	38
Figure 3.11. *Gas Sampling Line Schematic and GC Instrumentation*	40
Figure 3.12. *The integrated gasifier system*	42
Figure 3.13. *Feed Gas Flow and Back Pressure Control Modules*	43
Figure 3.14. *Integrated Computer and Data Acquisition Control System*	43
Figure 3.15. *Data Acquisition I/O chassis (Left) and Solid State Relay Module (Right)*	44
Figure 3.16. *Final integration and assembly of the Phase IIIA system test bed*	44
Figure 3.17. *Biomass fuel types*	48
Figure 3.18. *Reformer fuel load before and after testing*	51
Figure 3.19. *The reformer bed and gas exit temperature profile*	51
Figure 3.20. *The product gas flow rate*	52
Figure 3.21. *Reformer System Pressure*	53
Figure 3.22. *Radial temperature in the reformer bed*	54
Figure 3.23. *Post-run photographs of thermal damage to pipe and grate.*	55
Figure 3.24. *Reformer performance data with charcoal.*	57
Figure 3.25. *Reformer performance data with charcoal.*	58
Figure 3.26. *Reformer operation with wood pellets.*	60
Figure 3.27. *Reformer operation with wood pellets*	61
Figure 3.28. *Comparison of Product Gas Composition, dry gas basis.*	63
Figure 3.29. *Water vapor concentration and H_2O/CO ratio at the WGS reactor inlet as a function of the Steam/O_2 ratio.*	64
Figure 3.30. *CO_2, H_2, and CO gas outlet concentration as a function of the H_2O/CO ratio at the Water Gas Shift reactor inlet.*	64
Figure 3.31. *Example temperature excursion in the Water Gas Shift Reactor.*	65
Figure 3.32. *Reformer exit temperature as a function of the Equivalence Ratio and Gasification Ratio.*	67

Figure 3.33. *Effect of the Equivalence Ratio (ER) on the product gas (dry gas basis) composition*	67
Figure 3.34. *Effect of the Gasification Ratio (GR) on the product gas (dry gas basis) composition*	67
Figure 3.35. *Effect of the Steam to Oxygen ratio (S/O) on the product gas (dry gas basis) composition*	68
Figure 3.36. *H_2/CO and CO/CO_2 ratio for various S/O and GR values.*	68
Figure 3.37. *Effect of the product was flow rate and gas yield on the GR and ER*	69
Figure 3.38. *A plot of temperature vs. oxygen flow rate for product gas heating*	72
Figure 3.39. *Exit temperature profile for the Tar Destruction Reactor*	73
Figure 3.40. *Continuous biomass feeder assembly for the 4000 SLPM Product Gas demonstration*	76
Figure 3.41. *Constructed continuous biomass feed system for the 4000 SLPM product gas demonstration.*	78
Figure 3.42. *Constructed Phase IIIA 4000 SLPM GO^{TM} reformer system with biomass feed system.*	78
Figure 3.43. *Biomass Feed Assembly Blockage.*	79
Figure 3.44. Reformer Time History.	80
Figure 3.45. *Reformer Time History.*	82
Figure 3.46. *Product Gas Composition (dry basis).*	82
Figure 3.47. *Water Gas Shift Reactor temperatures.*	83
Figure 3.48. *Comparison of the Total Steam Flow Rate (Steam Generator-1 and Steam Generator-2 flow rate) and Steam Generator-2 flow rate*	84
Figure 3.49. *Sliding cup feed valve design*	87
Figure 3.50. *Model drawing of the 450 kg/h feed system showing the integrated configuration of the feed hopper, slider cup valve, and the lock-hopper*	89
Figure 3.51. *Process schematic for 450 kg/h feed system*	90
Figure 3.52. *Design of the new Steam Generator-1 unit*	91
Figure 3.53. *New biomass feed system (450kg/h) in the Pioneer Astronautics' laboratory*	91
Figure 3.54. *Various stages of integration of the new biomass feed system and steam generator into the GO^{TM} reformer system*	92
Figure 3.55. *Completed construction of the Phase IIIB reformer system at the Pioneer Astronautics facility*	92
Figure 3.56. *Fuel plugging in reactor and thermal damage to grate*	94
Figure 3.57. *Thermally damaged grate caused by fuel channel or bridge in reformer*	95
Figure 3.58. *Design of the reformer bed stirrer apparatus*	96
Figure 3.59. *Summary of operating conditions, product gas composition and flow rate for Phase IIIB testing*	98
Figure 3.60. *Map of the Grouse Field, Cheyenne County, Colorado*	100
Figure 3.61. *The formation top map of the Mississipian-St. Louis formation.*	101
Figure 3.62. *The formation top map of the Spergen formation*	102
Figure 3.63. *The formation top map of the Osage formation*	103

Figure 3.64. *Digitized well logs for well 05-017-06446*	104
Figure 3.65. *Comprehensive log for well 05-017-06446*	105
Figure 3.66. *Stratigraphic section of rock units in outcrop and the adjacent Denver Basin*	108
Figure 3.66. *Stratigraphic section of rock units in outcrop and the adjacent Denver Basin*	109
Figure 3.68. *Formation top-depth for Ward's Morrow Reservoir in the Pawnee Pioneer Field*	110
Figure 3.69. *Digitized well logs for well 05-123-19213*	111
Figure 3.70. *Formation top-depth for Grouse Field Spergen Reservoir*	112
Figure 3.71. *3D view of formation porosity for Grouse Field Spergen Reservoir*	113
Figure 3.72. *3D view of formation permeability for Grouse Field Spergen Reservoir*	114
Figure 3.73. *Water-oil relative permeability*	115
Figure 3.74. *Gas-liquid relative permeability*	115
Figure 3.75. *Average reservoir pressure with or without aquifer support***.**	116
Figure 3.76. *The cumulative gas production and gas production rate of seven wells***.**	117
Figure 3.77. *The cumulative oil production and oil production rate of seven wells*	118
Figure 3.78. *Average reservoir pressure and aquifer water influx*	119
Figure 3.79. *Cumulative oil production of Pintail's wells in the Grouse Field with and without two years of CO_2 injection*	121
Figure 3.80. *Oil rate, recycled and injection solvent rate plot*	122
Figure 3.81. *The cumulative oil production of Pintail wells with CO_2 injection in 40 years***.**	123
Figure 3.82. *Oil rate and average pressure comparison between constant new CO_2 of 1 MMSCF/day and constant injection rate of 1 MMSCF/day***.**	124
Figure 3.83. *Economic calculator sheet for CO_2 flooding*	126
Figure 3.84. *Production Trend and CO_2 Forecast*	127
Figure 3.85. *Net Present Value Sensitivities*	128
Figure A.1.1. *Process Model Flow Sheet*	137
Figure A.2.1 *Piping and Instrumentation Diagram*	140
Figure A.2.2 *Piping and Instrumentation Diagram*	141
Figure A.5.1. Slider Cup	144
Figure A.5.2. Slider Cup Housing	144

1. Executive Summary

The objectives of this research effort were 1) to develop a novel biomass reforming apparatus for the co-generation of carbon dioxide (CO_2) and hydrogen (H_2), and 2) to prepare the device for a large scale enhanced oil recovery (EOR) field test for small oil producers. The Green Oil^{TM} technology (abbreviated GO^{TM}) was designed to produce approximately one million cubic feet per day of CO_2 for enhanced oil recovery for the small oil producer. The scale of equipment and investment are significantly lower than traditional CO_2 recovery projects. Since H_2 is also produced, the technology generates clean electrical power to offset small producer capital and operating costs. As part of the program, an analysis and evaluation of small-producer oil fields is performed to identify candidates for demonstrating of the GO^{TM} technology. The satisfactory completion of this effort will enable the assessment of the GO^{TM} technology as an economically viable CO_2-EOR option for small oil producers. Attainment of the research objectives would allow small oil producers to have access to EOR for domestic oil recovery in a timely, scalable, locally field deployable, and cost effective manner.

This report describes the product gas generation, monitoring and operation of a pilot scale biomass gasification system for CO_2-EOR. Results from the pilot operation and analysis was used to design and build a portable 5X field unit that will deliver up 28,000 Nm^3/day, 1,000,000 SCFD of combined driver gas. In addition, the report includes analyses to identify small producer oil field candidates for demonstrating the GO^{TM} technology, and the techno-economic potential of the technology for commercial implementation.

The origin of this project began with NASA Phase I and II SBIR programs that successfully demonstrated a 100 SLPM (5,000 SCFD) CO_2 miniaturized steam reforming apparatus that was built and used to launch balloons to 100,000 ft., and was later flown to refill a balloon at 70,000 ft. Next, a gasification unit based on solid feed from charcoal was designed, built, and demonstrated by Pioneer Astronautics with an output of 1000 SLPM (50,000 SCFD) and a driver gas composition of 35% CO_2 and 55% hydrogen. This represents a scale up of an order of magnitude over the initial device.

The program technical approach included building a steam-oxygen fired biomass reformer on the scale of 4000 SLPM (200,000 SCFD) in Phase IIIA. The initial Phase IIIA unit represents a factor of four scale-up over the 50,000 cf/day Phase II reformer system already built and tested by Pioneer, and demonstrated the switch from charcoal to biomass as a reformer feed stock. The Phase IIIA unit was tested to validate scale up and engineering design. Operation under a range of conditions geared toward enhanced oil recovery was conducted. Based on the initial Phase IIIA results, a Phase IIIB reforming system was built to support a product gas flow rate as high as 20,000 SLPM (350,000 SCFD of CO_2 per day. This unit serves as the basis for a Phase IV production module for oil field testing, with 4 modules being used to achieve the required gas production rate of 1 million cubic feet of CO_2 per day.

In this effort, Pioneer Astronautics' designed, constructed and demonstrated a 4000 SLPM biomass-fired reformer system, and a feed system to support a full scale 20,000 SLPM (1,000,000 SCFD) unit. Performance testing and optimization was conducted to generate high

yields of CO_2 and H_2 for CO_2-EOR and power generation. The key elements developed in this program include the steam-oxygen biomass reformer, continuous solid fuel feed system, product gas cleanup, catalytic enrichment of the CO_2 and H_2 gas yield, heat recovery and auxiliary steam generation, tar destruction, and data acquisition and process equipment control. The performance of the GO™ system was benchmarked by measuring a variety of process parameters over a wide range of conditions with respect to gas quality and operational behavior. To that end, over 40 experiments were performed to evaluate the GO™ test rig. Product gas yields of more than 40 vol.% CO_2 and 45 vol.% H_2 were demonstrated. The highest product gas flow rate generated was 6000 SLPM. All of the key GO™ system fuel handling and reformer operational elements for a full scale system were successfully demonstrated. Future work will focus on system modifications to enable more effective bed stirring to break-up the fuel bridge, and grate operation to remove char and ash buildup. The Green Oil™ project achievements are summarized:

Green Oil™ Achievements
• Designed, fabricated, and tested a biomass-fired, truck portable CO_2-EOR system with - High pressure downdraft steam-oxygen reformer - Continuous biomass feeding - Product gas cleanup and energy recovery - Catalytic enrichment of the CO_2 and H_2 concentration in the product gas - Computer data acquisition and control
• Performance tested and demonstrated the utility of the GO™ system for CO_2-EOR with - 6000 SLPM (305,000 SCFD) product gas operation - 10 bar (150 PSI) operation - > 35 vol.% CO_2 and > 40 vol.% H_2 product gas yield - Energy recovery and steam generation - 13 tonne/day continuous biomass feeding

As part of the Green Oil program effort, oil wells in the four states of Colorado, Ohio, New Mexico and Kansas were evaluated by Petroleum Recovery Research Center (PRRC) for applicability of the proposed technology. In Colorado, the PRRC researchers completed a comprehensive study including reservoir characterization, geomodel build-up and reservoir simulation. Three fields were selected in the Colorado Denver Basin as potential candidates: the Grouse field, the Bison field, and the Pawnee Pioneer field. The Grouse field, operated by Pintail Petroleum LTD, was selected for additional studies for its potential for a Carbon Capture, Utilization, and Storage (CCUS) project. A model of Grouse field was constructed to estimate the oil production (referred to as uplift in this report) after beginning CO_2 injection. The simulation for 20 and 40 years of CO_2 injection was evaluated for risk assessment and uncertainty analysis without CO_2 recycling, using two different bottom-hole pressure (BHP) constraints. The simulation for 40 years of CO_2 injection with produced CO_2 re-injected was used in economic modeling analysis. Data from these models suggest the most profitable

operation is with low BHP, which is equivalent to 2.44 MSCF CO_2 for each incremental barrel of oil produced over the base case.

A basic economic model was developed to evaluate the value of this technology for small oil producers and other end-users. The calculator will also assist in determining the most important cost estimates. The calculator has been designed to calculate several important economic values, including initial or capital investment, net present value, and payout. The main inputs for the calculator include an oil price forecast, current production trend, oil production forecast with CO_2 injection, operational expense, horsepower requirements for compression, and pipeline estimates. A payout time of 92 months was determined. From field experience, first oil breakthrough is usually six to twelve months after the start of CO_2 injection. It is believed that the reservoir model is too homogeneous and thus breakthrough is slower than normal. From and economic standpoint, the earlier breakthrough provides earlier cash flow and thus an earlier payout. The later breakthrough indicates a better sweep and thus a higher ultimate recovery, but poorer economics, due to a later date of return. It is recommended to run future sensitivities to the recovery timing and rate.

2. Introduction

2.1. Background

Currently, trillions of dollars of domestic oil remain underground in apparently tapped-out wells, while Americans pay endless amounts of money to buy oil from foreign nations. America's oil reserve has nearly 400 billion barrels of undeveloped technically recoverable oil resource (Advanced Resources International, 2006). In the U.S. Appalachian region alone, over 10 billion barrels of currently economically unrecoverable petroleum exists. Numerous techniques of Enhanced Oil Recovery (EOR) have been developed over the years, the most promising being CO_2 flooding. It is estimated that over 100 billion barrels of oil would become economically recoverable if an economical source of CO_2 is identified (Advanced Resources International, 2006).

Enhanced Oil Recovery (EOR) using CO_2 injection into the ground is a well-known technique that allows a typical well to increase its overall yield by as much as 40%. However, as currently practiced, EOR requires pipelines to deliver CO_2 from natural reservoirs to oilfields. This technique is only practical for oilfields within limited distance from such reservoirs, as the capital cost of building pipelines over long distances is prohibitive. In general, such pipelines only serve major oilfield customers as the return from EOR from isolated small fields is insufficient to justify the capital cost of pipeline construction, and small producers typically do not have the cash to pay for such construction.

Figure 2.1 compares the location of current CO_2 pipelines and the largest stripper well producing states. It can be readily seen that to provide the small producer with CO_2 an extensive network of pipeline construction is needed to reach remote stripper well sites. This method is not practical for small producers due to the high capital cost of constructing pipelines over long distances to isolated well sites, and long timelines involved in pipeline construction. Naturally,

such pipelines generally serve only major oilfield customers, as the return from CO_2-EOR from isolated small fields is insufficient to justify the capital cost of pipeline construction.

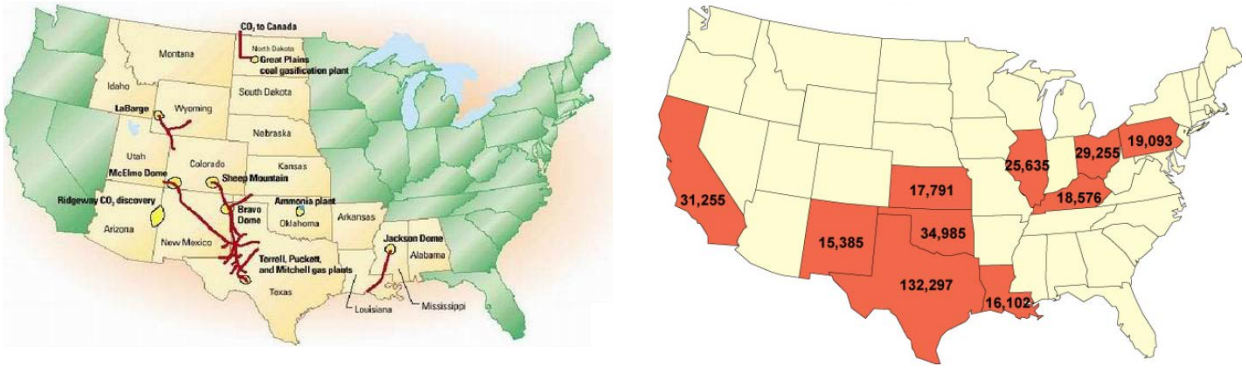

Figure 2.1. *A comparison of current CO_2 pipelines in the United States (European Energy Forum) and top stripper well producer states (Interstate Oil and Gas Compact Consortium)*

To meet this unmet need, Pioneer Astronautics is developing a modular, truck-portable renewable energy system for CO_2-EOR called Green Oil^{TM}. The Green Oil^{TM} technology, or GO^{TM}, works through the steam-oxygen reforming of biomass into CO_2 and hydrogen. This is followed by product gas cleanup, conditioning, CO_2-H_2 enrichment and gas separation to co-generate a high pressure, high purity CO_2 stream for on-site well flooding, and H_2 for carbon-free electrical power for local or grid use. It is designed to generate over 1million cubic feet of CO_2 per day for the recovery of about 100 barrels of oil per day. The hydrogen produced is capable of generating several megawatts of carbon-free electricity. Since the construction of a major central power plant typically takes over 8 years, the prospect of undertaking EOR utilizing their exhaust is generally uninteresting even to medium and large producers who make plans to expand production in response to shifts in oil prices. In contrast, the transportable Pioneer Astronautic system can go directly to the small producer fields where it is needed, and do so in a timely manner. As an additional advantage, the system sequesters more biomass-derived carbon than is released by the burning of the oil it yields, and thus can be said to not only produce carbon-free electricity, but carbon-free oil.

The GO^{TM} system is made up of four primary system components: biomass reformer, gas cleanup and conditioning, gas separator, and gas turbine electrical generation system (Figure 2.2.). The biomass reformer is based on the design legacy of the Imbert downdraft gasifier to minimize the production of tar by-products, flexible fuel turn-down, and low sensitivity to slag formation. However, it unique design is tailored to produce clean, high pressure (> 10 bar), high concentrations of CO_2 for on-site well flooding and H_2 for electrical power for the small producer. It uses oxygen (not air) and steam for higher product yields and reactor temperature control. The use of oxygen beneficially results in heating a smaller gas volume, operation of smaller process equipment, and reduced NO_x generation. The Pioneer Astronautics device uses a Water Gas Shift reactor to further enrich the CO_2 and H_2 yield by catalytically converting residual CO and water to high concentration CO_2 (>35%) and H_2 (>45%) in the gas stream.

Since the Pioneer Astronautics device generates high CO_2 concentration at high pressure, separation and compression energy and cost issues typically encountered with low pressure, low concentration CO_2 from fossil fuel combustion power plants is greatly reduced. To separate the CO_2 from H_2, the Pioneer system uses a methanol-based temperature swing approach. In separate testing, the separator has been demonstrated to operate with over 90% CO_2 separation efficiency at the GO^{TM} operating conditions.

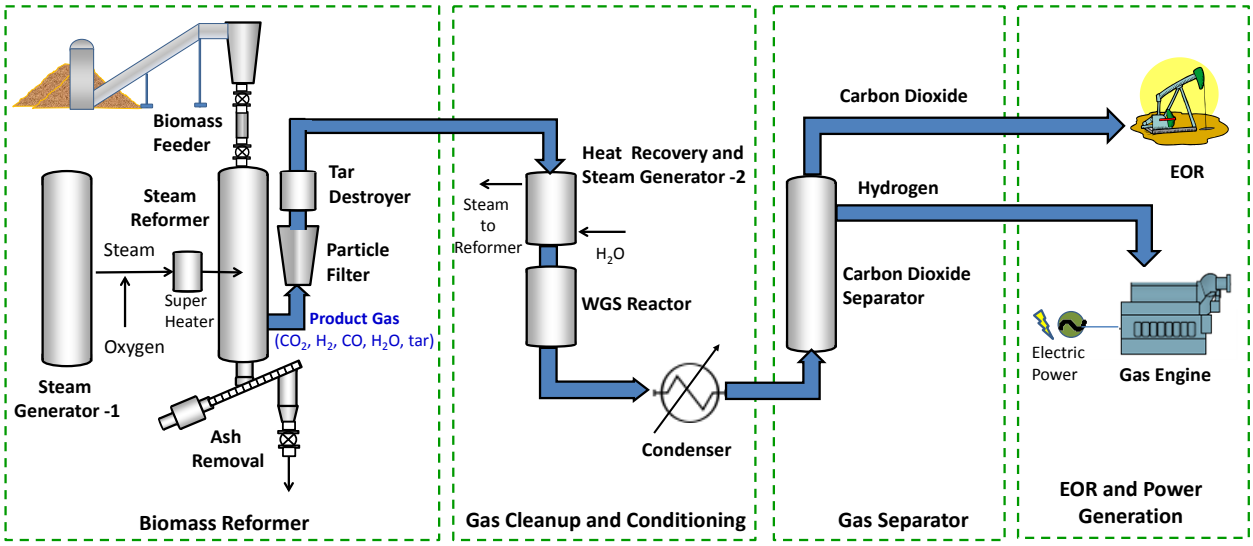

Figure 2.2. *Simplified process diagram of the Green Oil^{TM} EOR-CO_2 system for small oil producers.*

The gasifier is the heart of the GO^{TM} process. Gasification is the partial or incomplete oxidation of carbonaceous material into a useful product or material such as syngas and commercial fuels and chemicals. In the GO^{TM} system, a steam-oxygen gasification agent is used to generate CO_2 for EOR and H_2 for electricity generation. Steam gasification generates a significantly different product distribution than air gasification. Typically, the H_2 content can be quite high with greater than 50 vol. % as compared to a typical value of 15 vol. % with air. The addition of oxygen with steam also enhances tar reduction and provides the heat necessary to make the gasification reaction autothermal. However, steam reforming is endothermic and thus requires a heat source to generate product gas. To supply the necessary heat for steam reforming and reduction, oxygen is added simultaneously to the steam flow to induce exothermic oxidation reactions of the biomass. Optimization of the CO_2 and H_2 gas yields is thus accomplished by adjusting the steam, oxygen and biomass feed ratios.

The gasification is performed in a downdraft configuration in which both the gasification medium and biomass flow down together in the same direction (Figure 2.3). Here the biomass is fed from the top, and the steam-oxygen mixture enters the reactor from the side with the product gas exiting from the bottom. As the gas and biomass flows down in gasifier several characteristic reactions zones set up inside the bed. These include the drying, pyrolysis, oxidation (combustion) and reduction zones as illustrated in Figure x.

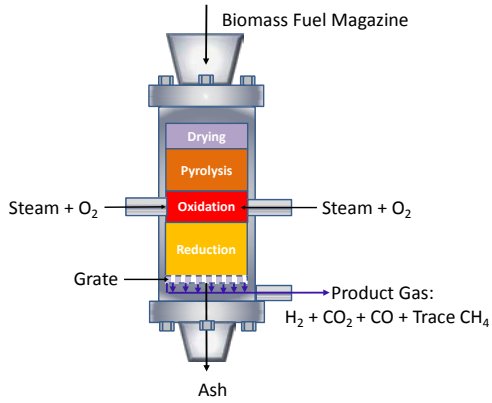

- **Drying**
  - Wet Biomass → Dry Biomass + H_2O (endothermic)
- **Pyrolysis**
  - Biomass → Char + Volatile Gases (H_2, CH_4, H_2O, C_nH_m,, CO_2, CO), Tar
- **Oxidation**
  - $C + 1/2O_2 \rightarrow CO$ — ΔH = -111 kJ/mol
  - Volatiles , Tar + $O_2 \rightarrow CO + H_2O$ — (exothermic)
- **Reduction**
  - $C + CO_2 \leftrightarrow 2CO$ — ΔH = +172 kJ/mol (Boudouard)
  - $C + H_2O \leftrightarrow CO + H_2$ — ΔH = +131 kJ/mol (water-gas)
  - $C + 2H_2 \leftrightarrow CH_4$ — ΔH =-75 kJ/mol (hydrogenation)
- **Shift and Reforming**
  - $CO + H_2O \leftrightarrow CO_2 + H_2$ — ΔH =-41 kJ/mol (water gas shift)
  - $CO + 3H_2 \leftrightarrow CH_4 + H_2O$ — ΔH =-206 kJ/mol (steam-methane reforming)

Figure 2.3. Left: Diagram of downdraft gasifier and reaction zones. Right: Some of the key chemical reactions occurring in the various gasifier zones.

The gasifier zones are reasonably well separated from each other. The zone location and characteristics are a function of the type of reactions occurring and the temperature regimes at that point. For example, in the GO system the pyrolysis, oxidation and reduction zone temperatures are observed at approximately 600°C, 1000°C, and 700°C, respectively. The zone depth is a function of the chemical composition of the gasification agent and biomass, the biomass moisture content and particle size, the mass flow rate of the gasifying agent and biomass, and the temperature. Within each zone numerous reactions occur with the overall result of generating a product gas composed of CO_2, H_2, CO_2, H_2O, and CH_4. Some of the more important reactions are listed in Figure 2.3. Since the drying, pyrolysis and reduction reactions are endothermic; the energy to perform these reaction steps is derived from the exothermic reactions in the oxidation zone. The key performance feature of the downdraft gasifier is that the pyrolysis products, especially the tars, are passed through the high temperature oxidation zone where additional tar decomposition occurs. This benefit allows the product gas to be generated with low tar content so as to minimize the operational impact on downstream machinery.

To test this concept, Pioneer Astronautics designed and fabricated an automated, continuously fed, biomass-based pilot reformer unit. Its construction is presented in Figure 2.4. The system is designed to contain all the unit operations of a full scale, portable CO_2-EOR field unit. The device is modular and can be disassembled and mounted on a portable trailer for field testing.

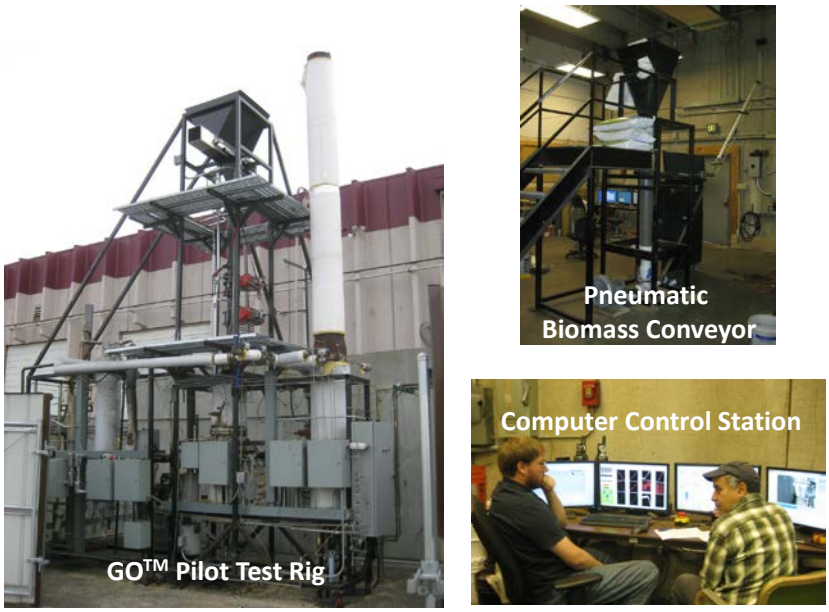

Figure 2.4. Green Oil™ Pilot Test Rig and Support Systems

2.2. Report Organization

This report covers the two year period of performance from February 1, 2011 through January 31, 2013, by Pioneer Astronautics and recounts the main results and conclusions drawn from the GO™ test campaign. Our effort was focused on 1) the design, fabrication, and performance testing a continuously fed biomass reformer, 2) the operability of key unit operations such as the reformer, fuel delivery, CO-shift conversion, tar destruction, ash removal, and heat recovery units, 3) the determination of a preferred operating condition in support of a continuously fed biomass reformer system for a modular, truck-portable on-site CO_2-EOR platform, and 4) the evaluation of small-producer oil fields to identify candidates for demonstration of the Green Oil technology.

Section 3 documents the details of our work performed during this effort. The report is organized into Experimental Methods and Materials presented in Section 3.1, followed by the Results and Discussion in Section 3.2. Section 3.1 describes our first year accomplishments that covered the design, fabrication, and integration of the GO™ reformer system. This included a process definition, the design analysis of key system components, the fabrication and integration of component parts, and the operational parameters and methodology used to test and evaluate the device. Section 3.2 describes our second year achievements starting with the System Startup and Checkout tests in Section 3.2.1, followed by Phase IIIA and IIIB performance testing in Sections 3.2.2 and 3.2.3, respectively. In a parallel effort, the analysis for identifying potential wells and oil fields that might be good test sites for demonstrating the device is presented in Section 3.2.4. This section includes a comprehensive study of site screening, reservoir characterization, geomodel build-up, reservoir simulation, and cost estimates. The combined test and analysis results are placed in context of how the machinery impacts the small oil producer in Section 3.3, and the steps taken to gain technology visibility in Section 3.4.

Finally, Section 4 summarizes the key project accomplishments and future technology development.

3. Report Details

The following sections detail the accomplishments made during the February 2011 – January 2013 reporting period on the GO^{TM} reformer system including operating performance, and field data collection and analysis. The program includes the following technical objectives:

1. Demonstrate 4,000 SLPM (200,000 SCFD) at 10 bar of combined product gas
2. Generate a product gas stream of high CO_2 and H_2 yield from biomass feed stock
3. Determine the operating performance of the system, and select a preferred operating condition for longer duration runs
4. Demonstrate long duration runs of the reformer system
5. Demonstrate scale up of combined product gas flow rate
6. Develop a field deployment model for final candidate fields using key results from field modeling, hardware design and device testing, and projected costs and revenues

To accomplish these objectives, key parametric evaluations of the GO^{TM} device over a wide range of test conditions were performed including system temperature and pressure, material flow rates, product gas composition, and material and energy balances to establish biomass conversion and product gas yield. In addition, modifications and refinements of the GO^{TM} system are performed so as to meet performance goals. System checkout tests were initially performed to verify the system operation. These were followed by performance testing and scale up in batch and continuous operation. The reformer was operated using wood pellet feedstock with oxygen and steam and yielded 6,000 SLPM of product gas at 10 bar, with high yields of CO_2 (>35 vol.%) and H_2 (>40 vol.%). The reformer and associated hardware were carefully inspected during testing to identify areas for improvement or revision for inclusion in subsequent system scale up in Phase IIIB. The GO^{TM} test results are used to validate the scale up of the engineering design in Phase IIIB. In parallel with this test and demonstration program, a field model and economic calculator was constructed to estimate the oil production and economic value of the GO^{TM} process after beginning full scale CO_2 injection. The details of the GO^{TM} system experimental and modeling approach, and the test and modeling results are provided below.

3.1. Experimental Methods and Materials

3.1.1. Reformer System Design

A system design of the Phase IIIA demonstrator was performed which resulted in the establishment of device operating conditions, system equipment size, device material, structural and mechanical components, and automated computer control of the hardware unit operations. The details of the design analysis are presented below. System hardware designs were performed for key operational components including the steam generators, gas delivery, super heater, gasifier, cyclone separator, tar destroyer, water gas shift reactor, and condensers. The design approach and analysis of various hardware units are presented below.

3.1.1.1. Process Definition and Analysis

The Phase IIIA GO gasifier design began with a process definition followed by analyses that specified the system sizing, operating conditions and performance for each component. The GO^{TM} process is based on the high pressure, autothermal reformation of biomass to CO_2, H_2, CO, and CH_4 with steam-oxygen mixtures. The process is performed in a throatless downdraft gasifier to minimize the production of tar by-products, flexible fuel turn-down, and low sensitivity to slag formation. A schematic of process flow diagram and stream summary for the GO^{TM} reformer system is presented in Figure 3.1 and Table 3.1, respectively. The stream data in Table 3.1 was generated using a process model discussed in Appendix A.1. A detailed piping and instrumentation diagram for the GO^{TM} process is given in Section A.2 in the Appendix.

The system contains three main subsystems including (1) the biomass steam reformer, (2) the gas separator, and (3) the gas turbine electrical generator. However, we note the focus of this project effort is the design and test development of the biomass reformer. The process starts by generating high pressure steam with Steam Generator-1, which consists of a tube boiler fired by propane gas. The steam exits the boiler at 180°C and 10 bar (Stream Point 1, SP-1). Oxygen gas flow (SP-13) is mixed with the steam flow (SP-2) and injected into the Super Heater unit. As the steam-oxygen mixture flows into the Super Heater, a small amount of hydrogen gas (SP-14) is added into the Super Heater. An electric cartridge heater inside the Super Heater is activated to ignite the O_2-H_2 mixture to raise the gas temperature to ~ 900K for initiating biomass combustion. The hydrogen addition to the steam-oxygen flow is only on long enough to ignite the biomass. The superheated steam-oxygen mixture (SP-3) is then injected through a circular arrangement seven nozzles into the Biomass Steam Reformer bed where pyrolysis, partial oxidation, and steam reformation occur.

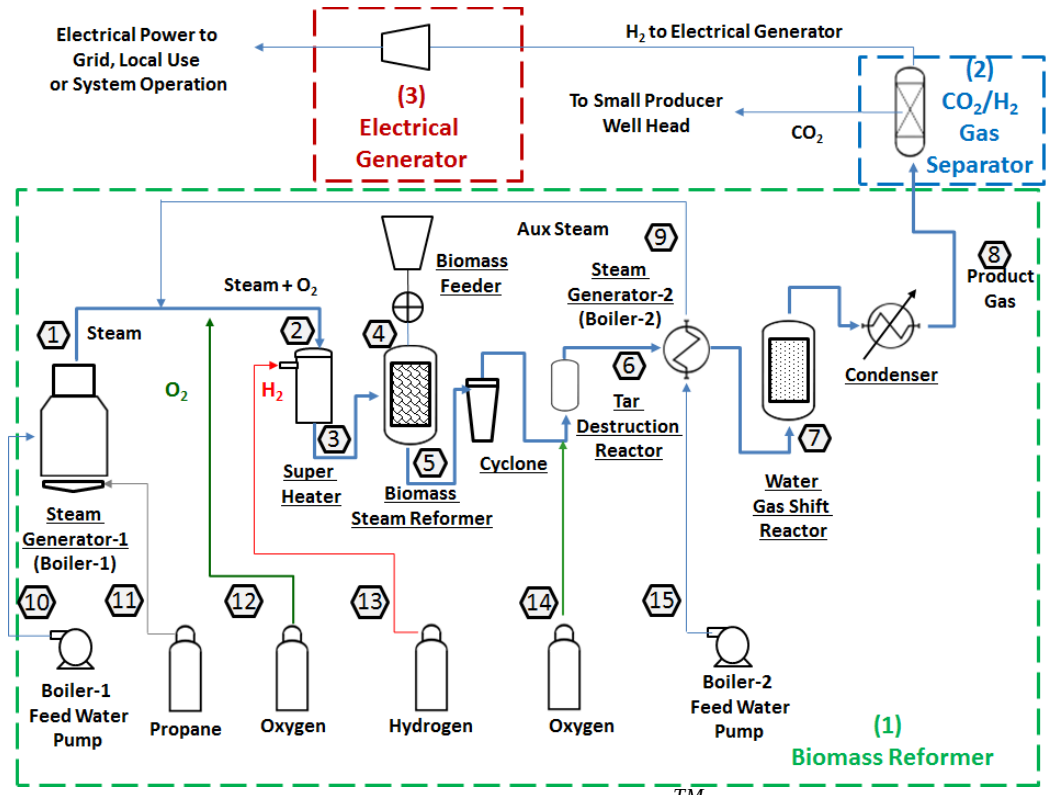

Figure 3.1. *Simplified Process Flow Diagram for the GO™ System*

Table 3.1. Simplified Process Stream Table

	Stream Point				
	1	2	3	4	
Description	SteamGen 1 Out	Combined Stm + O2	Super Heater Out	Biomass In	
Overall pressure	1.0000E+06	1.0000E+06	1.0000E+06	1.0000E+06	Pa
Overall temperature	4.5300E+02	4.5300E+02	6.2500E+02	2.9800E+02	K
Overall flow	1.2000E+00	1.5000E+00	1.5000E+00	2.5550E-01	mol / s
	Stream Point				
	5	6	7	8	
Description	Reformer Out	SteamGen2 In	WGSR In	Condenser In	
Overall pressure	1.0000E+06	1.0000E+06	1.0000E+06	1.0000E+06	Pa
Overall temperature	1.0290E+03	1.1230E+03	1.0000E+06	5.2300E+02	K
Overall flow	3.0500E+00	3.0500E+00	3.0500E+00	2.9700E+00	mol / s
	Stream Point				
	9	10	11	12	
Description	Product Gas Out	SteamGen2 Out	FeedWater-1 In	Propane In	
Overall pressure	1.0000E+06	1.0000E+06	1.0000E+06	1.0000E+05	Pa
Overall temperature	3.0000E+02	4.7500E+02	2.9800E+02	2.9800E+02	J / mol
Overall flow	2.3800E+00	1.1000E+00	1.2000E+00	3.0000E-02	mol / s
	Stream Point				
	13	14	15	16	
Description	Oxygen In-1	Hydrogen In	Oxygen In-2	FeedWater-2 In	
Overall pressure	1.0000E+06	1.0000E+06	1.0000E+06	1.0000E+06	Pa
Overall temperature	2.9800E+02	2.9800E+02	2.9800E+02	2.9800E+02	K
Overall flow	3.0000E-01	3.7000E-02	5.0000E-02	1.1000E+00	mol / s

Biomass is gravity fed (SP-4) into the Reformer by way of a pressurized Biomass Feeder system using a high pressure, lock-hopper assembly. To load the hopper a pneumatic conveyor (dilute phase) shuttles biomass from a dry storage bin to the hopper. The biomass feed rate is determined by balancing the carbon generated in the product gas with the carbon added in the biomass. The product gas exits the bottom of the gasifier (SP-5) and flows to a Cyclone for removing entrained particles in the gas flow. To further reduce tars in the gas flow, a Tar Destruction Reactor consisting of an olivine packed bed is used to catalytically destroy the tar. Here, a small flow of oxygen (SP-15) is injected into the product gas stream to react with the hydrogen. This causes the gas temperature to rise allowing the olivine to catalytically decompose the tar. After the Tar Destruction Reactor the hot product gas (SP-6) is flowed to a heat recovery unit, Steam Generator-2. A second feed water pump delivers water to the steam generator and thermally exchanges with the hot gas to generate steam. This steam (SP-10) is then flowed back to the reformer unit to reduce the steam load of Steam Generator-1. The auxiliary steam is added upstream of the oxygen injection point and combined with the primary steam – oxygen flow. The product gas, H_2, CO_2, CO and CH_4, is then passed to the Water Gas Shift reactor (SP-7) where catalytic conversion of the product gas to even higher yields of CO_2 and H_2 is performed. The product gas from the Water Gas Shift reactor unit (SP-8) is sent to a Condenser where it is cooled down and water removed before being sent to the H_2/CO_2 separator. We note in this project phase the product gas is vented or flared to ambient air in place of the gas separation unit. The gas composition from the Reformer and Water Gas Shift reactor is monitored with Gas Chromatography (GC) for characterizing the gasification process. All units and pipe lines are insulated to minimize heat loss. The design of the system components are discussed in the following sections.

3.1.1.2. Component Analysis and Design

Reactant Feed Rate

The reaction stoichiometry in the steam-oxygen reforming reaction of biomass was used as a basis to determine reactant flow rates for oxygen, steam and biomass, and the suitable equipment size for delivering the fuel to the reformer. The reactant feed rates were based on an average biomass formula of $CH_{1.4}O_{0.6}$ (Reed, T. and Gaur, S, 2001), and the approximate overall reaction for steam – oxygen reforming:

$$3\,C_4H_6O_2 + 12\,H_2O + 2\,O_2 \rightarrow 15\,H_2 + 7\,CO_2 + 4\,CO + CH_4 + 4H_2O \qquad (3.1)$$

For example, using a product gas flow rate of 4000 SLPM and equation 3.1 stoichiometry, the oxygen flow rate is thus 4000(2/31) = 258 SLPM, or 0.37 kg/min. Similarly, the steam and biomass feed rates are 1548 SLPM (1.24kg/min) and 1.49 kg/min, respectively. These data are summarized in Table 3.2.

Table 3.2. Nominal Reactant Flow Rate Design (4000 SLPM Product Gas Flow Rate)

Parameter	Value	Units
O_2 Flow Rate	258 0.37 23.4	SLPM kg/min kg/hr
Steam Flow Rate	1548 1.24 74.4	SLPM kg/min kg/hr
Biomass Flow Rate	1.49 90.0	kg/min kg/hr

Super Heater Chemistry

Hydrogen is added to the steam – oxygen flow and combusted using an electric cartridge heater. The following reaction describes this process using an electrical ignition source:

$$O_2 + 2H_2 + \text{heat} \rightarrow 2H_2O,\ \Delta H_c = -286\ \text{kJ/mol} \tag{3.2}$$

The energy produced from this reaction is used to raise the temperature of the steam-oxygen flow and ignite the biomass in the reformer. In this process it is assumed that oxygen is in excess of hydrogen and hydrogen is completely combusted. The hydrogen flow is on only long enough to raise the temperature of the steam – oxygen flow to near 900K, and until biomass ignition has occurred.

The reaction was conducted in a 15 cm diameter x 60 cm long steel reactor vessel. The steam-oxygen mixture and hydrogen are injected tangentially into reactor so as to induce a swirl in the flow for rapid mixing. To ignite the hydrogen, an electric cartridge heater, 300W, was inserted from the top of the reactor down into the chamber where the steam-oxygen and hydrogen were mixed.

The required hydrogen flow rate to achieve this temperature is calculated by an enthalpy balance approach. Assuming pre-mixed flow and adiabatic conditions, the overall enthalpy balance between gas reactants and products is given by

$$\Delta H = \sum_i n_i \Delta H_i = 0 \tag{3.3}$$

where ΔH_i for species *i* is given by

$$H°_T - H°_{298.15} = A*T + B*T^2/2 + C*T^3/3 + D*T^4/4 + E/T + F - H \tag{3.4}$$

and H_i is the enthalpy (kJ/mol) of species i at temperature T, $\Delta H^o_{298.15}$ is the reference state enthalpy, and n_i is the species mole amount.

The mole amounts of the reactant and product species are taken from the gas flow rate inputs. The coefficients for equation 3.4 are taken from published thermochemical tables (NIST-JANAF Thermochemical Tables, 1998). In this calculation, the reactant starting conditions are:

- T_1 = 453K (180°C), corresponding to 10 bar steam pressure
- H_2O flow rate = 1500 SLPM
- O_2 flow rate = 300 SLPM
- H_2 flow rate = variable to achieve desired temperature increase

T_2 is solved so that the enthalpy balance between reactants and products is zero for a given reactant condition of T_1, H_2O, O_2 and H_2 flow rate. The resulting thermal conditions for a variety of hydrogen flow rates and H_2/O_2 mole ratios are shown in Figure 3.2. For example, a hydrogen flow rate of 80 SLPM is sufficient to generate a steam-oxygen flow temperature of 500°C (773K), which is sufficient to ignite the biomass.

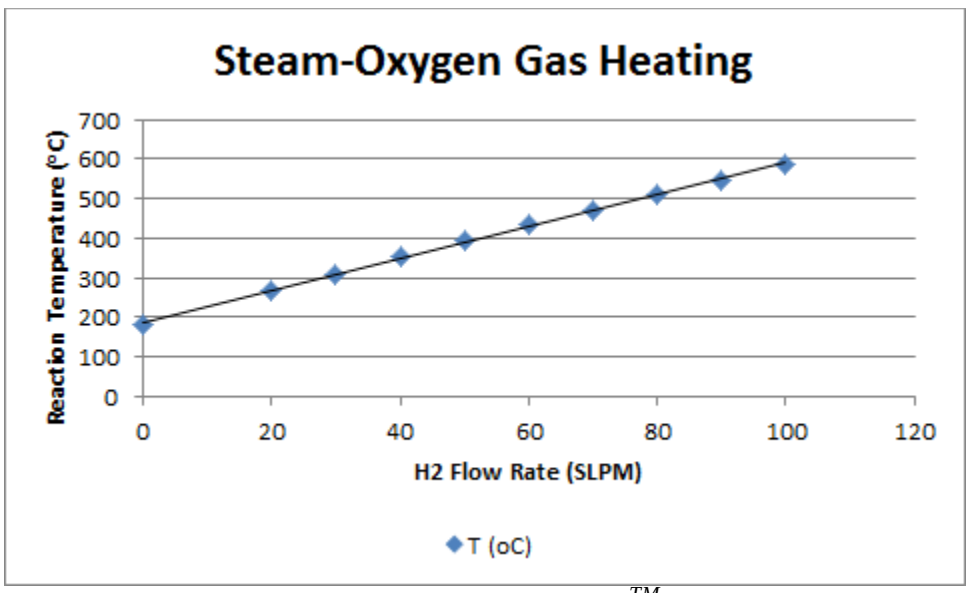

Figure 3.1. *Simplified Process Flow Diagram for the GO™ System*
Steam-Oxygen gas heating as a function of H_2 flow rate. Steam flow rate: 1000 SLPM; Oxygen flow rate: 400 SLPM; Steam – Oxygen Inlet Temperature: T_1 = 180°C.

Steam Generator

A 500,000 BTU/h propane fired boiler was used to generate steam for use in the reformer. To maintain uninterrupted steam flow to the reformer, an automated water delivery system to the boiler was constructed consisting of a high pressure water pump and a water level sensor. The water level sensor consists of four thermocouples spaced every 30 cm along the depth of the boiler that measures the water temperature. Each thermocouple is compared against the calculated boiling point of water at the current pressure inside the boiler, and if any given thermocouple is observed to be at least 10°C above this temperature, the program assumes that it

is out of the water and exposed to steam. The program is directed to watch a particular thermocouple, and if that thermocouple is out of the water, the program opens the water inlet valve to the boiler to bring the water level back up. In the current system, the second thermocouple from the top is the control thermocouple that the program monitors. In addition to this method, the program also watches the temperature of the top most thermocouple, and if it ever exceeds a preset limit, in this case, 270°C, the program assumes that the water level is about to drop below the control thermocouple, as a larger portion of steam is being super-heated. If the top thermocouple exceeds this temperature, the program opens up the water valve to refill the boiler to the point where both the control thermocouple is under water (i.e. less than 10°C above the current boiling point) and the top most thermocouple is below the upper temperature limit.

Using the heat of combustion of propane, heat of vaporization of water, and the sensible heating of water, flow rate correlations between propane, feed water and steam are calculated for Steam Generator-1. The results are tabulated in Table 3.3, and are conveniently used for balancing the water and propane flow during boiler steam generation. Note that these ratios assume a boiler efficiency η of 70%.

Table 3.3. Scaling Factor for Steam, Propane and Water for Steam Generator-1 Operation

Parameter	Value	Units
Steam to Propane Ratio, S/P	36.0	SLPM Steam / SLPM Propane
Steam to Feed Water Ratio, S/FW	78.8	SLPM Steam/GPH Water
Feed Water to Propane Ratio, FW/QP	0.46	GPH Water / SLPM Propane

For example, if 1000 SLPM of steam are desired the propane flow rate is set to 1000/36 = 27.8 SLPM, and the feed water is 1000/79 = 12.7 GPH. In practice the feed rates are typically set to 80% of a nominal feed rate. This action allows the system to be thermally ballasted and prevent overshooting of steam flow rates.

Reactant and Product Gas Measurement

Equipment size for delivering the oxygen, hydrogen and propane gas to the gasifier system was based on the process analysis results discussed above. Oxygen, hydrogen and propane were delivered to the gasifier unit using electronic mass flow controller instrumentation. Mass Flow Controllers (MFCs) were selected to deliver these gases for their stability with respect to changes in inlet temperature and pressure, and backpressure fluctuations. Within the MFCs are built-in PID (proportional/integral/derivative) electronics to keep continuous proportional control through comparing the measured sensor signal to the commanded flow rate. To maintain designed flow rate of the O_2 and H_2 to the gasifier, an external PID loop is executed which based off the gasifier temperature and pressure sensor signals. The development and integration of the external PID to the mass flow controllers is the subject of the software design below. The sizing for the O_2, H_2, and propane mass flow controllers is summarized in Tables 3.4-3.6. The flow controllers are oversized to allow for system scaling.

Table 3.4. Oxygen Flow Controller Sizing and Specifications

Parameter	Value	Units
O_2 Molecular weight	32	kg/kmole
R	0.082	m^3 atm/kmole K
T_{std}	293	K
P_{std}	1	atm
Operating Temperature	293	^oK
Operating Pressure	10 (9.869)	bar (atm)
Target O_2 Standard Volume Flow Rate, Q_{std}	250	SLPM
MFC Size Range	0 - 1000	SLPM
Accuracy	$\pm$ 1	%
Repeatability	$\pm$ 0.2	%
Time Constant	300	ms
Gas Pressure	500	Psi max

Table 3.5. Hydrogen Flow Controller Specifications

Parameter	Value	Units
H_2 Molecular weight	2	kg/kmole
R	0.082	m^3 atm/kmole K
T_{std}	293	K
P_{std}	1	atm
Operating Temperature	293	^oK
Operating Pressure	10 (9.869)	bar (atm)
Target H_2 Standard Volume Flow Rate, Q_{std}	80	SLPM
MFC Size Range	0-500	SLPM
Accuracy	$\pm$ 1	%
Repeatability	$\pm$ 0.2	%
Time Constant	300	ms
Gas Pressure	500	Psi max

Table 3.6 Propane Flow Controller Specifications

Parameter	Value	Units
C_3H_8 Molecular weight	44	kg/kmole
R	0.082	m^3 atm/kmole K
T_{std}	293	K
P_{std}	1	atm
Operating Temperature	293	^oK
Operating Pressure	1(.9869)	bar (atm)
Target H_2 Standard Volume Flow Rate, Q_{std}	42	SLPM

MFC Size Range	0-500	SLPM
Accuracy	$\pm$ 1	%
Repeatability	$\pm$ 0.2	%
Time Constant	300	ms
Gas Pressure	500	Psi max

Orifice plate flow meters based on differential pressure were used to measure the volumetric flow of steam, nitrogen gas purge, and the product gas exiting the device. The orifice design equation for measuring the volumetric flow is shown in equation 3.5:

$$Q = C_d A_2 \sqrt{\frac{2(P_1 - P_2)}{\rho(1-\beta^4)}} \tag{3.5}$$

where Q is the volumetric flow (m^3/s), C_d is the discharge coefficient, A_2 is the orifice area (m^2), β is the ratio of the pipe diameter D to the orifice diameter d, P_1 and P_2 are the upstream and downstream pressure (Pa, kg/ms^2), respectively, and ρ is the gas density.

The approach taken is based on the ISO 5167-1:2003 standard given by the International Organization of Standards for locating upstream and downstream pressure taps and determining the flow discharge coefficient based on β (ISO, 2003). To position the orifice plate, weld neck flanges are used. In such cases the pressure tap distance from the orifice plate is one inch upstream (L_1) and downstream (L_2) from the orifice and is independent of the orifice diameter. This allows C_d to be calculated for a variety of orifice diameters in a single orifice meter. The ISO 5167 standard gives an equation allowing calculation of the orifice discharge coefficient:

$$C_d = 0.5959 + 0.0312\ \beta^{2.1} - 0.1840\ \beta^8 + 0.0029\ \beta^{2.5}(10^6/Re)^{0.75} + 0.0900(L_1/D)[\beta^4/(1 - \beta^4)] - 0.0337(L_2/D)\beta^3 \tag{3.6}$$

for known values of β (d/D), Reynolds number, Re, and L_1 and L_2. To determine C_d, an iteration is performed to get an initial C_d value since the upstream velocity for Re is unknown until C_d is determined. The steam density, ρ = P(MW)/RT, at 300°C and 10 bar is 3.9 kg/m^3. A steam viscosity of 0.02 cP is taken from steam tables. For other gases, the viscosity is estimated from Sutherland's formula (Crane company, 1988):

$$\mu = \mu_o*(a/b)*(T/T_o)^{3/2} \tag{3.7}$$

where $a = 0.555T_o + C$, $b = 0.555T + C$, μ is the viscosity in centipoise at input temperature T, μ_o = reference viscosity in centipoise at reference temperature T_o, T is the input temperature in degrees Rankine, T_o = reference temperature in degrees Rankine, C = Sutherland's constant.

An example calculation for the Boiler-1 steam orifice is given in Table 3.7. Figure 3.3 illustrates the design dimensions, and a photograph of fabricated steam delivery and tail gas orifice plates.

Table 3.7. Design Summary for Steam Orifice Flow Meter

Inputs	Value	Units
Steam MW	18	kg/kmole
Pipe Diameter, D_1	25.4	mm
	0.0254	m
	1	in
Orifice Diameter, D_2	4.85	mm
	0.00485	m
	0.19	in
Measured $\Delta P = P_1 - P_2$ (kPa)	172.5	kN/m^2
	25.0	psi
Fluid Density, ρ	3.908	kg/m^3
Fluid Viscosity, μ	2.000E-05 (0.02)	$N\text{-}s/m^2$ (cP)
Upstream Tap Loc., L_1	25.4	mm
Downstream Tap Loc., L_2	25.4	mm
Assumed Reynolds No., Re	200,000	
Calculations	**Value**	**Units**
Orifice Area, A_2	1.847E+01	mm^2
	1.847E-05	m^2
	2.864E-02	in^2
Diam. Ratio, β	0.191	
Orifice Coeff., C**	0.597	
Measured $\Delta P = P_1 - P_2$ (Pa)	172500	N/m^2
	25.0	psi
Pipe Flow Rate, Q	3.333E-03	m^3/s
	45	kg/hr
	200	LPM
	1006	SLPM
Pipe Velocity, V	180.42	m/s
Velocity is	subsonic	
Calculated Reynolds Number, Re	866,110	

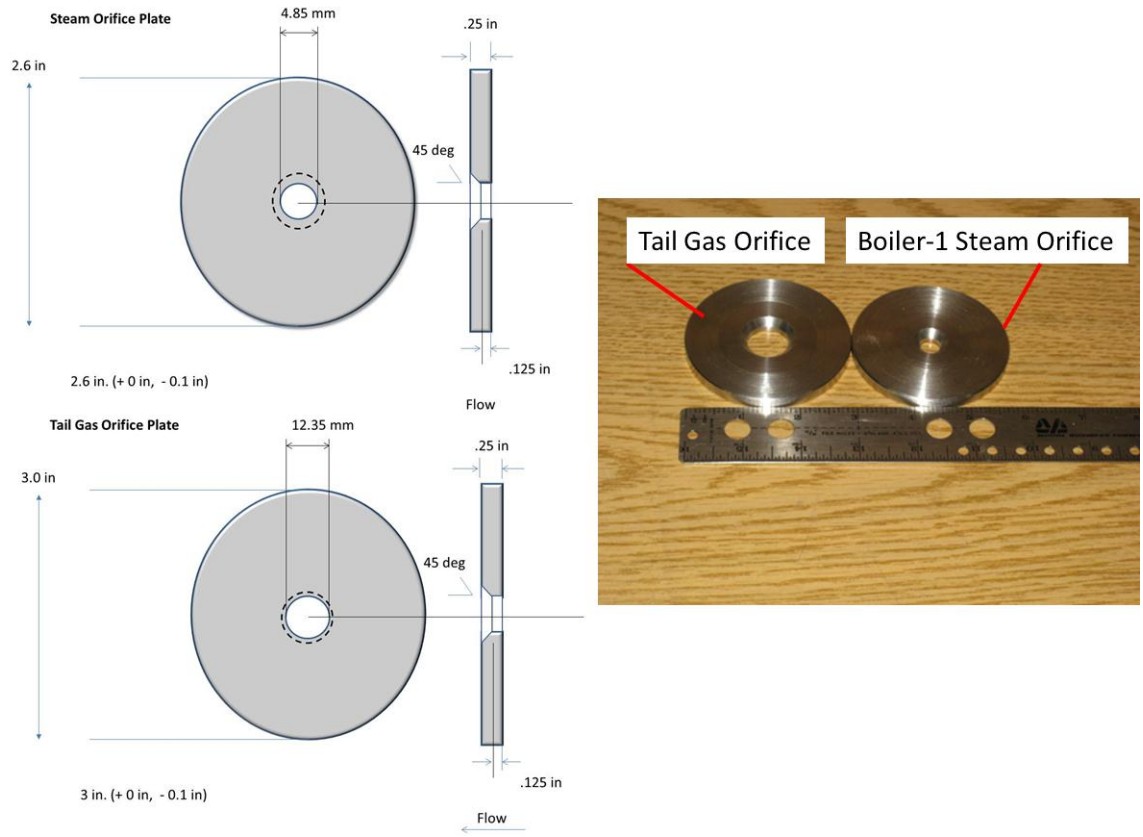

Figure 3.3. *Orifice design and photograph of the Boiler-1 steam orifice and tail gas orifice.*

Downdraft Gasifier Design

The steam-oxygen gasifier is the primary process of the GO^{TM} demonstrator and its design and construction is presented in Figure 3.4. A throatless downdraft design was chosen for maximum unrestricted fuel movement and to minimize the effects of fuel bridging and channeling. The base reformer used in this test consisted of a 25 cm (diameter) x 72 cm (depth) Schedule 40 steel cylindrical vessel (35L). The steam and oxygen gas mixture is injected into a plenum at the bottom of the gasifier and flows upward through a jacket forming a sheath-like flow around the gasifier cylinder. The gas jacket is comprised of an inner and outer steel wall which is separated by about 32 mm (1.3 in). The double-walled jacket helps to keep the pressure drop between across the gasifier to a minimum, and thereby minimizes the possibility of the reformer wall breaching at high pressures and temperatures. The jacket connects to a bank of lower and upper nozzles (tuyeres) for injecting the steam-oxygen mixture into the biomass. The upper and lower nozzle banks are positioned 55 and 32 cm above the grate, respectively. Each nozzle bank consists of seven equally spaced circular nozzles that surround the periphery of the combustion zone. The nozzles are 12.7 mm (1/2 inch) in diameter and staggered so that they are not directly in-line with an opposite nozzle. The nozzles extend slightly inward 38 mm (1.5 in) from the inner gasifier wall into the biomass media and point downward at 45 degrees, which

creates a longer gas penetration path into the media. For a steam flow rate of 1000 SLPM and an oxygen flow rate of 250 SLPM, the gas velocity at the nozzle exit is about 23 m/s. Thermocouples (Type-K, Chromel/Alumel) are placed concentrically inside three of the seven nozzles and extend 2.5 cm from the nozzle exit plane into the biomass bed for radial temperature measurement of the reformer bed. To increase the reformer run time in batch operation, an upper fuel magazine of 30 cm (12 inch) diameter x 92 cm (36 inch) depth was attached to the base reformer. In total, the magazine increases the fuel charge capacity to approximately 110L. This enables the reformer to run for well over an hour and thereby establish sufficient time for parametric evaluations of the reformer. The overall reformer dimensions are summarized in Table 3.8.

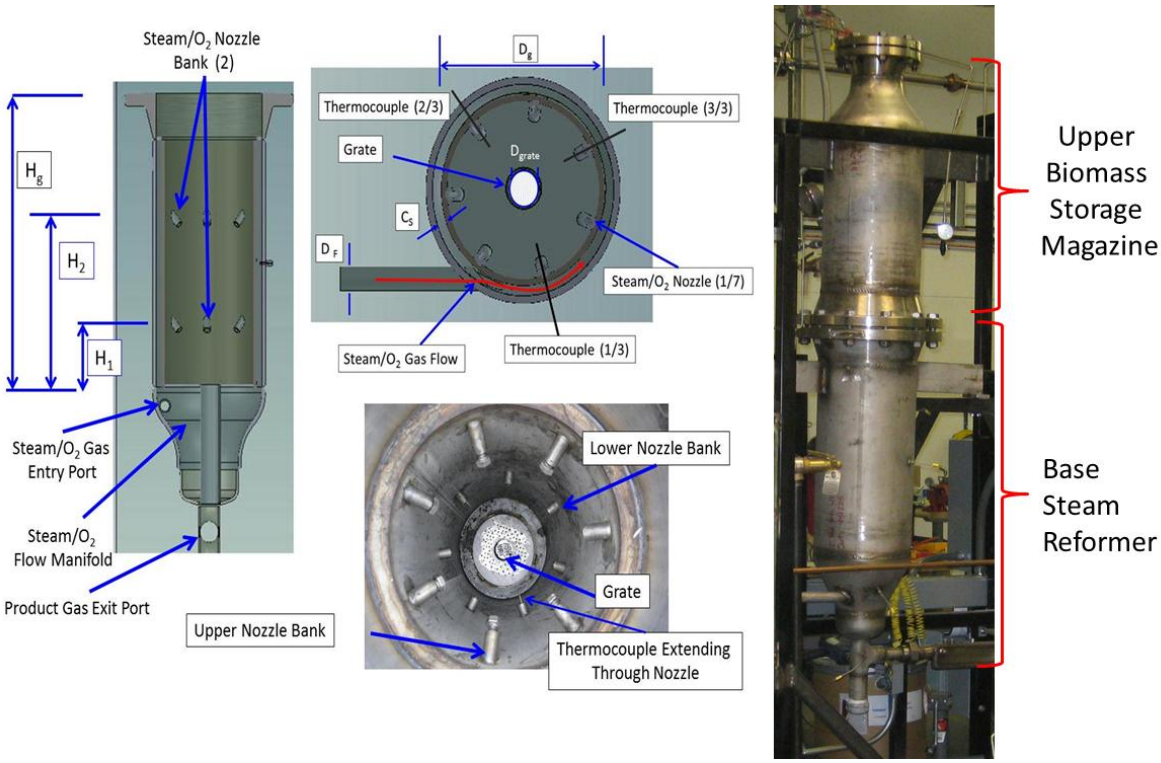

Figure 3.4. *Biomass steam reformer layout. Left: Base reformer geometry. Right: Assembled base steam reformer with additional biomass storage magazine.*

Table 3.8. Biomass Steam Reformer Dimensions

Parameter	Value	Unit
Base Reformer Height, H_g	72	cm
Height From Nozzle (1) to Grate, H_1	32	cm
Height From Nozzle (2) to Grate,H_2	55	cm
Base Reformer Diameter, D_g	25	cm
Base Reformer Volume, V_g	36	L
Upper Magazine Height, H_m	92	cm

Upper Magazine Diameter, D_m	30	cm
Volume of Upper Magazine, V_m	64	L
Single Nozzle Diameter, D_n	6.4	mm
Diameter of Feed Gas Input, D_F	25.4	mm
Inner/Outer Wall Channel Separation, C_S	3.2	cm
Inner Grate Diameter, $D_{in\text{-}grate}$	4	cm
Outer Grate Diameter, $D_{out\text{-}grate}$	18.0	cm
Hole Diameter for Grate, D_s	3.2	mm

The reformer biomass is supported by a concentric, stainless-steel fixed grate system consisting of an 18 cm (7 inch) diameter outer grate, and a 4 cm (1.5 inch) diameter inner grate. Each grate is perforated with 3 mm holes to allow gas and ash to pass through. The inner 4 cm grate is connected to a 3.8 cm (1.5 inch) x 53 cm (21 inch) removable pipe that fixes into place with the outer grate. At the end of a test run the pipe is removed from the reformer bottom for extraction of residual char and ash form the reformer bottom. The removable pipe contains three, 3 cm (width) x 5 cm (height) slots to allow product gas to flow downstream and ash to drop to the reformer bottom. The product gas exits the reformer through a 1 inch side port.

The fixed grate was later modified to a rotating grate for active removal of the char and ash particles, and to keep the pressure drop in the gasifier from building up. The rotating grate consists of three major parts: drive mechanism, shaft and seal, and the grate, and typically operated at 1-2 rpm. The drive mechanism consisted of a ½ horse power, 1720 rpm electric motor with 300X speed reduction, and a variable frequency drive to control the motor speed. The 300X speed reduction was achieved in two stages using a 50X reduction using a gear box, followed by a 6X reduction using two sprockets and a chain. A steel shaft of ½ inch O.D. connected the grate to a sprocket which passed through a shaft seal at the bottom of the gasifier ash bin. The shaft seal was made using two bronze sleeve bearings to reduce the side load on the shaft and a Teflon V-ring bearing. The shaft seal was located approximately 24 inches from the grate. Because the shaft seal was sufficiently far from the grate, the seal temperature never exceed 150°C and the need for cooling or higher temperature packing materials was eliminated. The shaft seal operated reliably during the course of the test campaign. The grate was fashioned from a 7 inch, ¼ inch thick steel plate. It was perforated with numerous ¼ inch holes which gave an open grate area of about 40%. A photograph of the rotating grate assembly is shown in Figure 3.5.

Figure 3.5. *Photograph of the rotating grate*

Cyclone Design

To remove entrained particulates from the producer gas downstream of the gasifier, a cyclone was designed based on the approach given by Koch and Licht, 1977, Casel and Martinez-Benet, 1983, and the calculator posted by Esco Engineering, 1998. The design parameters are defined in Figure 3.6 and summarized in Table 3.9. The design assumptions are based on the flow rate data presented in Table 3.1, a nominal flow velocity of 5 m/s, and a producer gas density of 2.4 kg/m^3. The flow rate in units of m^3/hr from Process Point 4 (between the reformer and the cyclone) is:

$$Q\left(\frac{m^3}{h}\right) = \dot{n}\,\frac{RT}{P} = 11\,\frac{kmole}{h}\left(\frac{0.082\,m^3}{kmole\,K}\right)\left(\frac{1020K}{10\,atm}\right) = 91\,\frac{m^3}{hr} \tag{3.8}$$

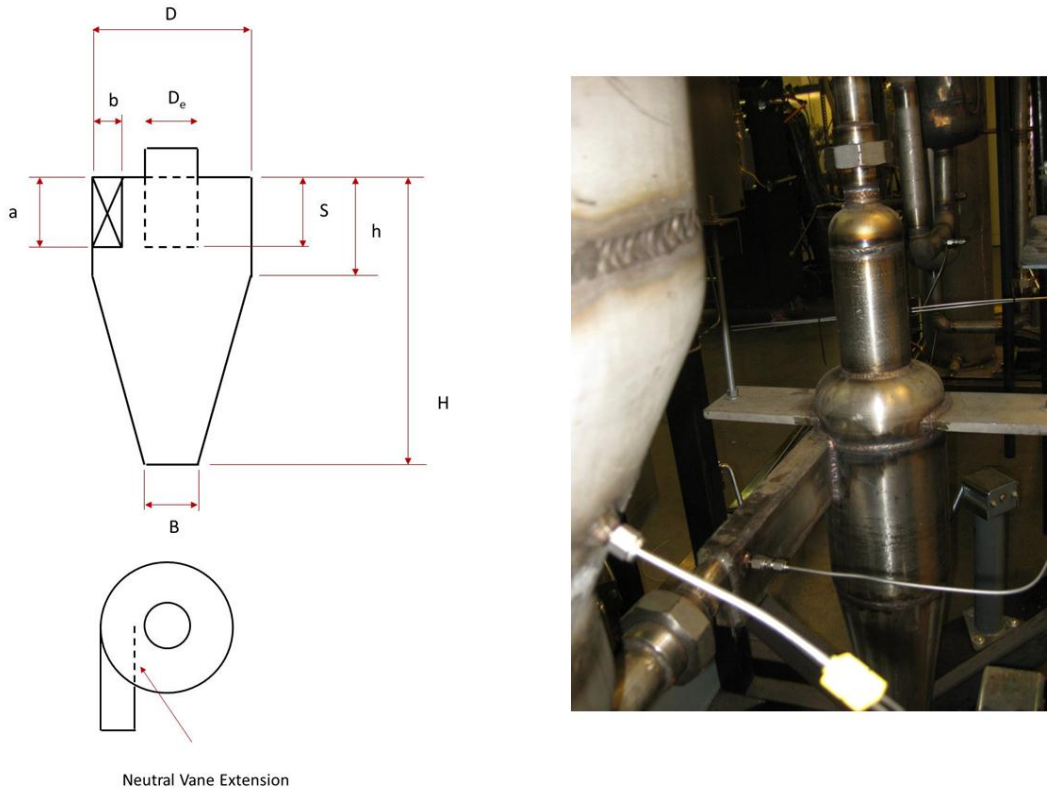

Figure 3.6. *Cyclone design parameters. Left: Cyclone dimensional parameters. Right: Fabricated cyclone*

Table 3.9. Cyclone Separator Geometry

Assumptions	Value	Unit
Flow Rate, Q	91	m^3/h
Inlet velocity, v_i	5.0	m/s
Gas density, ρ_g	2.44	kg/m^3
Calculated Values	**Value**	**Unit**
Inlet Area, A_i	0.30 (469)	m^2 (in^2)
Diameter, D	0.20 (7.9)	m (in)
Inlet height, a	0.10 (4.0)	m (in)
Inlet width, b	0.05 (2.0)	m (in)
Outlet length, S	0.13 (4.9)	m (in)
Outlet diameter, D_e	0.10 (4.0)	m (in)
Cylinder height, h	0.40 (15.8)	m (in)
Overall height, H	0.80 (31.6)	m (in)
Dust outlet diameter, B	0.05 (2.0)	m (in)
Number of velocity heads, H_v	4.49	
Press drop, no Neutral Vane	0.14	kPa (in. water)
Press drop, with Neutral Vane	0.06	kPa (in. water)

Tar Destruction Reactor

A Tar Destruction Reactor was constructed and tested during this period by modifying an existing packed bed reactor. The reaction zone consisted of a 15 cm (diameter) x 30 cm (depth) Schedule 40 steel pipe filled with 9.5 kg of olivine (Prince Minerals) as illustrated in Figure 3.9. The reactor was positioned downstream of the Cyclone. The olivine was kept in place by bracketing the olivine bed with two 3/16 inch perforated steel grates. Between the grates and the catalyst was placed a thin blanket of quartz wool to keep catalyst fines from being entrained in the flow. The lower plate was supported with four, ½ inch steel legs that rested on the bottom of the reactor vessel. Gas entered and exited the reactor through a one inch pipe. The top portion of the reactor was flanged which allowed access to the reactor bed for loading and maintenance. Olivine was selected as the catalyst based on its combined activity and mechanical strength. The olivine particles have roughly an equivalent diameter of 5 mm, which gives a bed porosity or void fraction, ε, of about 0.4. The pressure drop across the reactor with this particle size under operating flow conditions was less than 0.25 atm. (< 4 PSI). The reactor residence is about 0.2 seconds at 4000 SLPM.

To heat the reactor bed to operating temperatures, an oxygen delivery system was designed that injected the small amounts of oxygen just upstream of the olivine reactor bed to react with the hydrogen in the product gas stream. The injector consists of a ¼ inch O.D. stainless steel tube capped on one end and drilled with six, evenly spaced .02 inch diameter holes in tube side wall (Figure 3.7). The injector is placed about 2 cm below the lower grate holding the olivine. The oxygen exits the injector radially and is entrained with the product gas which impinges on a mixing plate that induces a swirl in the flow to ensure rapid mixing and heating of the product gas (Figure 3.7). Thermocouples (TC) were placed into the reactor bed and beneath the lower support plate to monitor the temperature of the catalyst bed and the input gas stream.

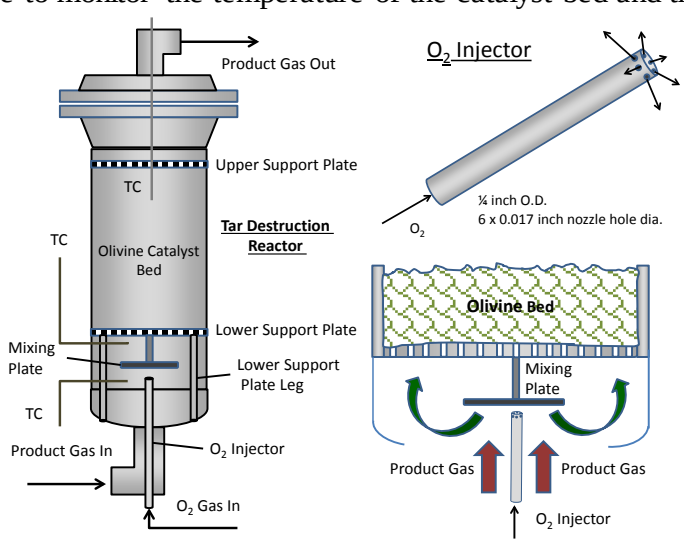

Figure 3.7. *Schematic for the Tar Destruction Reactor. Left: Reactor configuration. Right: Injector and mixing plate concept of operation*

Steam Generator-2

The heat from the hot product gas exiting the Tar Destructor reactor was used in Steam Generator-2 for generating steam. The size of the shell and tube exchanger was based on the heat transfer equation:

$$Q = UA\Delta T_{LM}, \quad (3.9)$$

$$Q = (m_1)(C_{p1})(T_{1in} - T_{1out}) \quad (3.10)$$

$$Q = (m_2)(C_{p2})(T_{2in} - T_{2out}) \quad (3.11)$$

where Q is rate of heat transfer, U is the mean overall heat transfer coefficient, A the heat transfer surface area, ΔT_{LM} the logarithmic mean temperature difference (LMTD) the size the unit,), m is the mass flow rate, C_p is specific heat capacity, fluid 1 is the producer gas (hot fluid), and fluid 2 is water (cold fluid). The LMTD is defined as:

$$\Delta T_{LM} = = [(T_{1in} - T_{2out}) - (T_{1out} - T_{2in})]/\ln[(T_{1in} - T_{2out})/(T_{1out} - T_{2in})] \quad (3.12)$$

The Boiler-2 dimensions are presented in Figure 3.8.

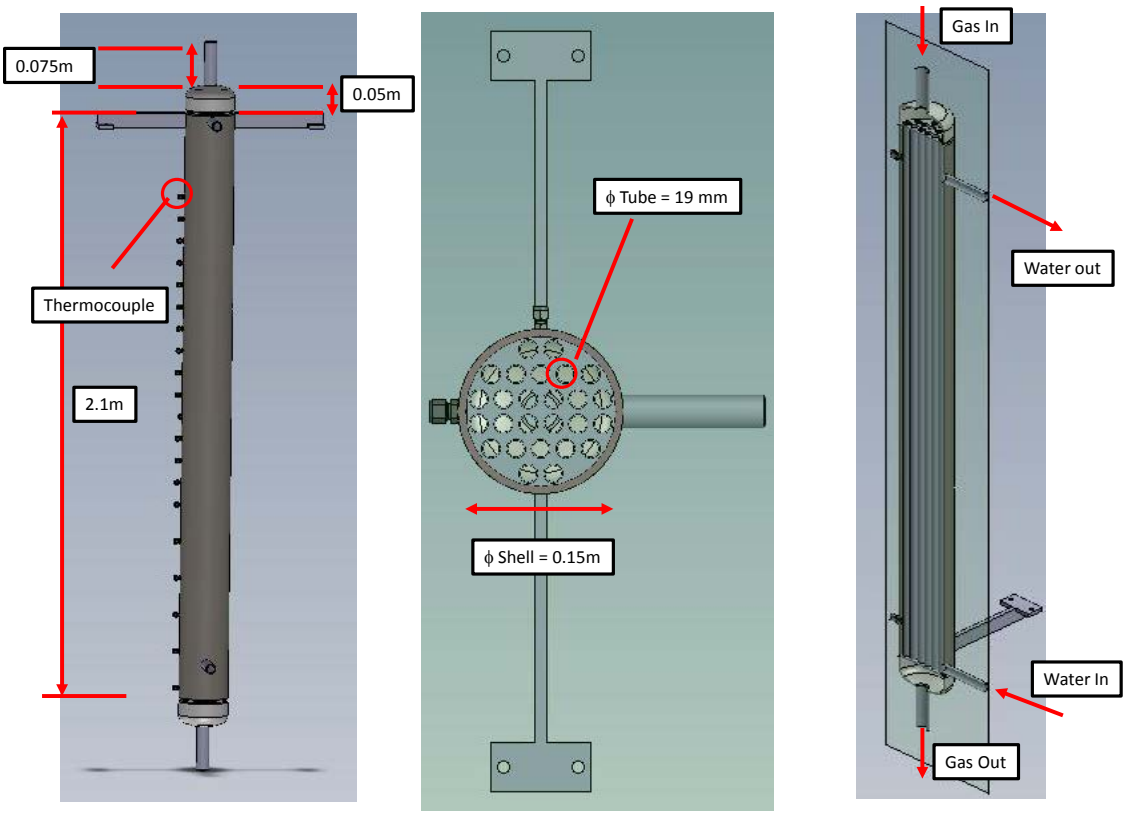

Figure 3.8. *Boiler -2 Dimensions*

Water Gas Shift Reactor

Generating high yields of CO_2 and H_2 is important for improving the efficiency of the CO_2/H_2 gas separation and EOR processes. To accomplish this, a CO-shift catalyst was used to convert CO and H_2O byproducts into valuable CO_2 and H_2O through the Water Gas Shift (WGS) reaction:

$$CO + H_2O \leftrightarrow CO_2 + H_2,\ \Delta H = -41\ kJ/mol. \tag{3.13}$$

A single bed packed reactor was constructed out of a 20 cm (6 inch) diameter x 1.8 m (6 ft) tall stainless steel pipe, which provides about 60L of bed volume. The reactor bed was located downstream of the auxiliary steam generator (Boiler-2) and upstream of the condenser. In this manner, the heat is pulled from the product stream by Boiler-2, which reduces the gas temperature to an optimal range between 190^0C to 310^0C for shift catalyst operation. Three 500 W electrical heaters were externally connected to the reactor wall to provide preheating during reduction cycles and startup operation of the reformer. The temperature of the catalyst bed was monitored with four thermocouples that were vertically spaced every 30 cm. These were installed to help prevent thermal conditions that may give rise to catalyst sintering (> 330^oC), and to determine the presence of temperature gradients inside the bed. The reactor was packed with a Medium Temperature shift catalyst provided by Unicat Catalyst Technologies, Inc. The catalyst consists of >42% CuO, >40% ZnO, 2 % graphite with an alumina balance. The catalyst pellets were cylindrically shaped with a 5 mm x 2.5 mm nominal dimension. The catalyst was reduced at 165^oC with1% hydrogen in nitrogen, total flow rate 400 SLPM, before use with the reformer. During reformer testing, the catalyst typically was operated at about 200^oC at the inlet, 260^oC at the outlet, and with an hourly space velocity between 3,000 – 4,000 h^{-1} (dry basis).

Condenser

A vertical shell and tube condenser was used to condense water from the product gas flow before passing the gas downstream to the CO_2/H_2 separator. A drawing of the apparatus is shown in Figure 3.9. The design of the unit followed the approach given for the Steam Generator-2. The gas from the water Gas Shift reactor is split and manifolded into eighteen 48 inch long x 1 inch diameter tubes. The gas flows down the tube array and into 24 inch long x 11 inch diameter reservoir. The gas is then turned up and exits the condenser through a single 3.5 inch O.D. tube. Water flows into the condenser at the bottom of the shell and out the top. Condensate is collected and vented out through control valve into a holding tank.

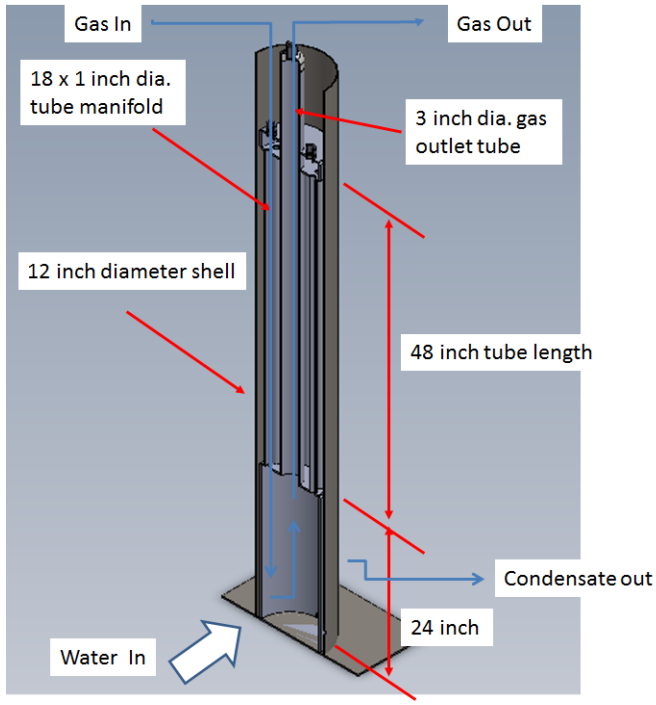

Figure 3.9. *Cut away model view of the water condenser*

Backpressure Control Valve

A backpressure control valve was designed to control the upstream pressure of the gasifier system to the design point of 10 bar (150 psia). Control of the system back pressure is achieved by opening the control valve to lower the upstream pressure, and closing it to increase the upstream pressure. In this design, real time automated control was achieved by using a computer software with a PID algorithm. A pressure transducer upstream of the back pressure valve records and sends the process pressure (4-20mA signal) to the computer, and the computer sends a variable output signal back (4-20mA) to an electronic controlled pneumatic regulator. The pneumatic regular then sends a pressurized slug of air (e.g., 3-15 psig) to activate the control valve so that the design set point is achieved. The computer software is programmed to react as faster than the valve actuator response time. However, in larger volume systems, as presented here, there can be a prolonged time delay of several seconds if the flow rate through the piping and vessels changes abruptly. One solution was the use of a gas ballast tank to dampen out the abrupt changes in flow rate.

The design of the backpressure control valve involved determining the flow coefficient, C_v or K_v, for a desired flow rate. The design equation used is:

$$C_v = Q_{SCFH}\sqrt{(460 + T_{in})SG}\left(\frac{1}{1360\sqrt{P_1 \Delta P}}\right), \quad (3.14)$$

$$K_v = 0.862 C_v \quad (3.15)$$

where Q is the flow rate in SCFH, SG is the specific gravity relative to air, P_1 is the upstream pressure (psia), and ΔP is the pressure drop, psia. The specific gravity is proportional to the ratio the gas molecular weight of the product gas to air, ρ_{PG}/ρ_{air}. To determine the product gas density, an average molecular weight of 19 kg/kmole is assumed based on the product gas mole fractions Table 3.10 summarizes the design assumptions, inputs, and calculated values for the valve C_v (K_v). For margin, the backpressure control valve is upsized by 1.5x.

Table 3.10. Design Summary for Backpressure Control Valve

Assumptions	**Value**	**Unit**
Molecular Weight of Product Gas	19.06	kg/kmole (lb/lbmole)
Inputs	**Value**	**Unit**
Volume flow rate, Q	8333	SCFH
Specific Gravity, SG (relative to air)	0.593	
Gas temperature, T_{in}	70	^oF
Upstream Pressure	150	psia
Downstream Pressure	35	psia
Pressure Differential	115	psia
Calculation	**Value**	**Unit**
C_v	0.883	gpm psi
K_v	0.761	m^3/s atm
C_v x 1.5 Margin	1.25	

Control Software Design

A computerized Data Acquisition and Control (DAC) system was designed to enable automated, rapid, real-time control and monitoring of the GO device operations. The DAC system is used for automatic process startup, operation and shut down, and to minimize the risk of design excursions. The DAC system reads, acquires and controls a whole host of process instrumentation including thermocouples, pressure transducers, differential pressure transducers, mass flow controllers, and valves, and chemical sensors. To interface the computer DAC software with GO hardware, a graphical real-time controller interface was developed

The graphical interface program was based on the system architecture and the Process and Instrumentation Diagram (P&ID) described above. The user interface is organized into four main process tabs that match the process subsystem architecture: The Feed Gas, the Reformer, the Tail Gas, and the Sensor systems. For example, Figure 3.10 shows a screen shot of the Reformer tab that displays all the process instrumentation including the two boilers, the super heater, the reformer, and the water gas shift reactor (WGS).

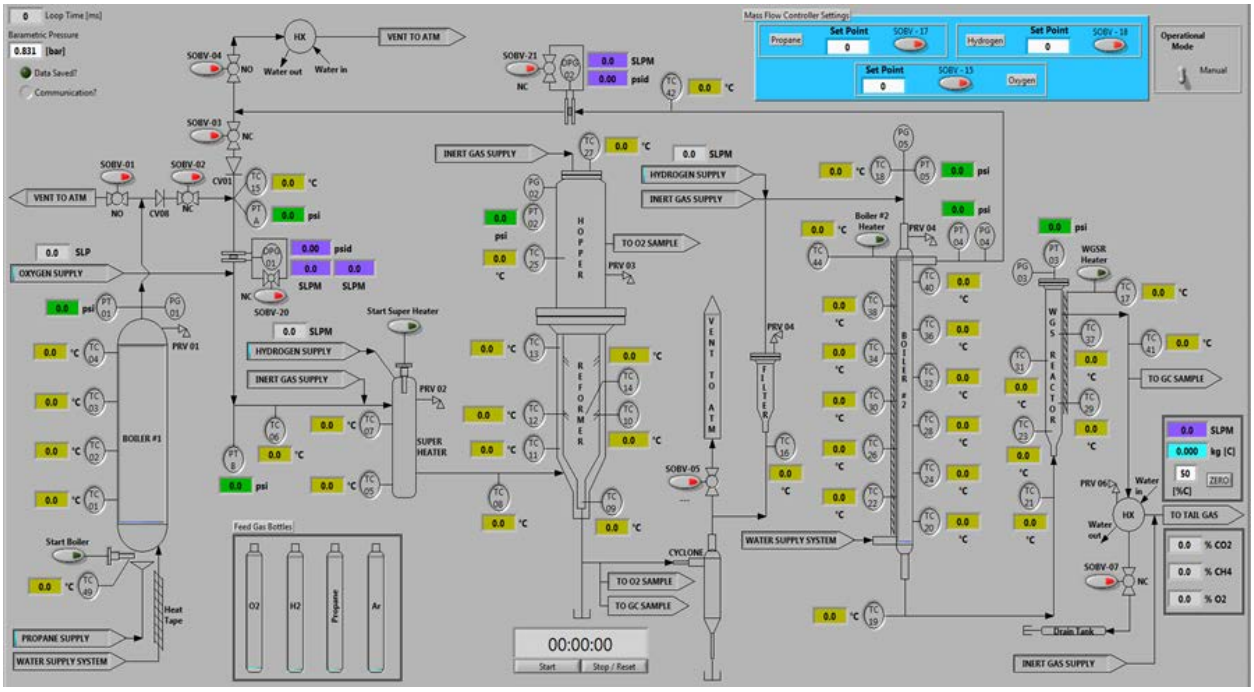

Figure 3.10. *Screen shot of the Reformer tab user interface*

As the primary screen interface for the entire system, the Reformer tab contains numerous thermocouple and pressure transducer readings, solenoid control valve actuation, and fluid level monitoring on the screen to allow for rapid and accurate read and control of the system. These are continuously read or maintained at a specified control state. When a process component is activated (e.g., solenoid activated ball valve), the component symbol is lighted to indicate operation. As the process instrumentation changes state in another process tab, the indicator arrows on the currently open tab will light up to indicate its present state of operation. In this manner, the user will always have indication of the current state of operation all main subsystems.

There are specific operational conditions for achieving the desired product gas composition. Deviating from an operational condition could result in poor product gas quality, or even create unsafe operating conditions. This is especially true during system start up and shut down where the potential for developing an explosive gas mixture is highest. To that end, the control software is designed with a PID loop control to manage reformer temperature, oxygen and steam flow, auxiliary steam flow, and tail gas flow rate during system startup, operation and shutdown. The control system is designed to alert the operator with a staged visual alarm system when process excursions occur. If a condition goes beyond a predetermine alarm limit, the program will initiate an automatic shutdown sequence and return the system to a safe system state.

The program is capable of both manual and automatic control of the system operation. The manual control software was developed to perform system checkouts and ensure all device instrumentation meet design specifications prior to product gas generation. The manual control

software will eventually be linked to an automatic controller that is presently in development. However, the user will still have direct access to each control output.

Instrumentation

The device was fully instrumented with mass flow controllers, flow orifice meters, pressure and temperature transducers. These devices enable the measurement of compositional data, mass and energy balances for the GO system. The key flow measurements and instruments used in this study are shown in Table 3.11.

Table 3.11. Flow Measurement Instrumentation

Stream	Instrument
Oxygen Feed	Mass Flow Controller
Hydrogen Feed	Mass Flow Controller
Propane Feed	Mass Flow Controller
Steam Feed	Flow Orifice
Nitrogen Purge	Flow Orifice
Biomass Feed	Optical Level Measurement
Product Gas	Flow Orifice, Gas Chromatograph
Feed Water	Flow Meter
Residual Product Char, Ash	Electronic Balance
Temperature	Thermocouples
Pressure	Pressure Transducers

During the device operation a sample flow was continuously sampled from the main gas stream for product gas composition. A Varian (Agilent) Model CP-4900 PRO Micro Gas Chromatograph equipped with multiple columns (10m PPQ, 20m Molecular Sieve and 6 m CP-Sil CB columns) and thermal conductivity detection (TCD) was used for the compositional analysis of CO, CO_2, CH_4, O_2, N_2, H_2, and C_2 and C_3 hydrocarbons in the product gas stream. Table 3.12 presents a summary of the analysis methods used in this study.

Table 3.12. Gas Chromatograph Analysis Method

Channel	Detector	Column	Carrier Gas	Sampling	Components Detected	Accuracy	Relative Standard Deviation
1	Thermal Conductivity	Molecular Sieve, 20m	N_2	On-line	H_2	98%	± 1%
2	Thermal Conductivity	Molecular Sieve, 20m	N_2	On-line	O_2, N_2, CO	98%	± 1%
3	Thermal Conductivity	PPQ, 10 m	He	On-line	CO_2, CH_4	98%	± 1%
4	Thermal Conductivity	CP-Sil CB, 6 m	He	On-line	C_2, C_3, C_4	98%	± 1%

On-line measurement of the gas constituents was made by sampling two slipstreams off the main process line- one port before the Water Gas Shift reactor, and one port downstream of the condenser. From each port the product gas passes through a gas conditioning assembly that includes pressure regulator, particle filter, ice water condensers, calcium sulfate desiccant, rotameters, and gas sampling valves before entering the GC. The GC flow conditioning schematic and instrumentation is presented in Figure 3.11. The run time is 4 minutes, and the chromatograms and product concentration (volume %) are electronically recorded by the GC data acquisition system. The GC detector response to the gas species is externally calibrated using vendor analyzed gas samples.

An electrochemical-based oxygen sensor (AMI model P-3) with a sensitivity range of 100 ppm - 25 vol. % was used to measure oxygen in the biomass magazine and product gas downstream of the reformer. The oxygen sensor serves two purposes: 1) to monitor the consumption of O_2 in the reformer and 2) to detect potentially unsafe O_2 levels in the system that may lead to an unsafe explosive flow conditions during operation. The sample gas was passed through a water conditioning system (water and particle traps) similar to that used in the GC system. A non-dispersive IR detector (e2V, IR15TT-R) was also used for detecting biomass ignition by monitoring the presence of CO_2 and CH_4 in the gas product stream.

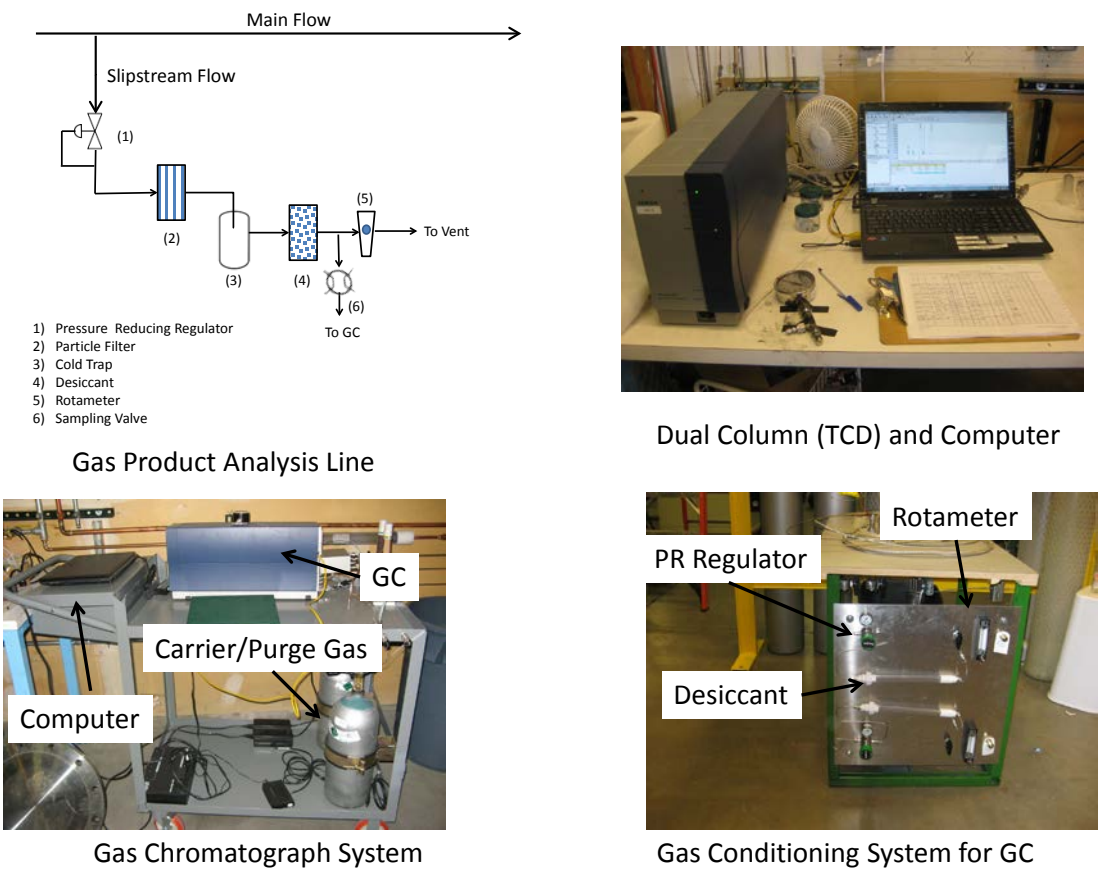

Figure 3.11. *Gas Sampling Line Schematic and GC Instrumentation*

3.1.2. Fabrication and Integration

The reformer system was fabricated with suitable materials that are compatible with the process conditions for the duration of the test. In general, 304-stainless steel was used for providing a suitable, reliable test platform for shakedown, improvements, and subsequent scale-up of the reformer components. However, some carbon steel piping was used to channel the blow-off in the pressure relief valves and in the tail gas and flare piping sections. Outdoor enclosures for the flow control instruments, electrical cables, switches and relays, data I/O chassis, and sensors are NEMA 4 rated. Electric wiring for supplying power to the test device was run through ¾ inch EMT conduit. Water was delivered to the water feed pump using ¾ inch copper pipe at 90 psi. Air for valve actuation was supplied at 120 psi through ½ inch EMT conduit. Feed gases were passed to the gasifier using 316 stainless steel tubing. Tubing, regulators, valves and fittings for oxygen flow were cleaned for oxygen service (CFOS). Oxygen compatible materials such as Teflon (PTFE) or Viton were used in locations where pure, high pressure oxygen flowed. Table 3.13 lists the material specification for the boiler, gasifier, super heater, WGS reactor, condenser, flange connections and pipe schedule for the system fabrication.

Table 3.13. System Material Specifications

Component	Specification
Boilers	Schedule 40 304 stainless steel
Gasifier	Schedule 40 304 stainless steel
Super Heater	Schedule 40 304 stainless steel
WGS Reactor	Schedule 40 304 stainless steel
Condenser	Schedule 40 304 stainless steel
Flow Orifice Flange- Tail Gas	150 pound 304 stainless steel raised face weld neck flange, 1.25 inch Schedule 40 bore
Flow Orifice Flange- Steam	150 pound 304 stainless steel raised face weld neck flange, 1.0 inch Schedule 40 bore
Gasifier Flange	150 pound 304 stainless steel raised face weld neck flange, 12 inch Schedule 40 bore
Piping	1 inch and 1.25 inch schedule 40 304 stainless steel; 1.25 inch schedule 40 carbon steel
Water Gas Shift Reactor	150 pound 304 stainless steel raised face weld neck flange, 6 inch Schedule 40 bore
Magazine Flange	150 pound 304 stainless steel raised face weld neck flange, 10 inch Schedule 40 bore

The test bed was initially assembled on two skids as shown in for preparation of the final assembly (Figure 3.12). Each skid was physically separated and put on a mobile platform for transporting to an outside laboratory area or even to an off-site location. The skids were roughly organized into gasification operations- boiler-1, magazine, gasifier, cyclone); and gas conditioning- WGS reactor, boiler-2, and condenser. A detailed view of the Feed Gas module

and Backpressure Control module is shown in Figure 3.13. The integration and placement of the computer automated DAC system is shown in Figures 3.14 and 3.15. The system was leak checked, and cold flow experiments including the computer DAC system were performed in this configuration to verify operation prior to the final assembly outside.

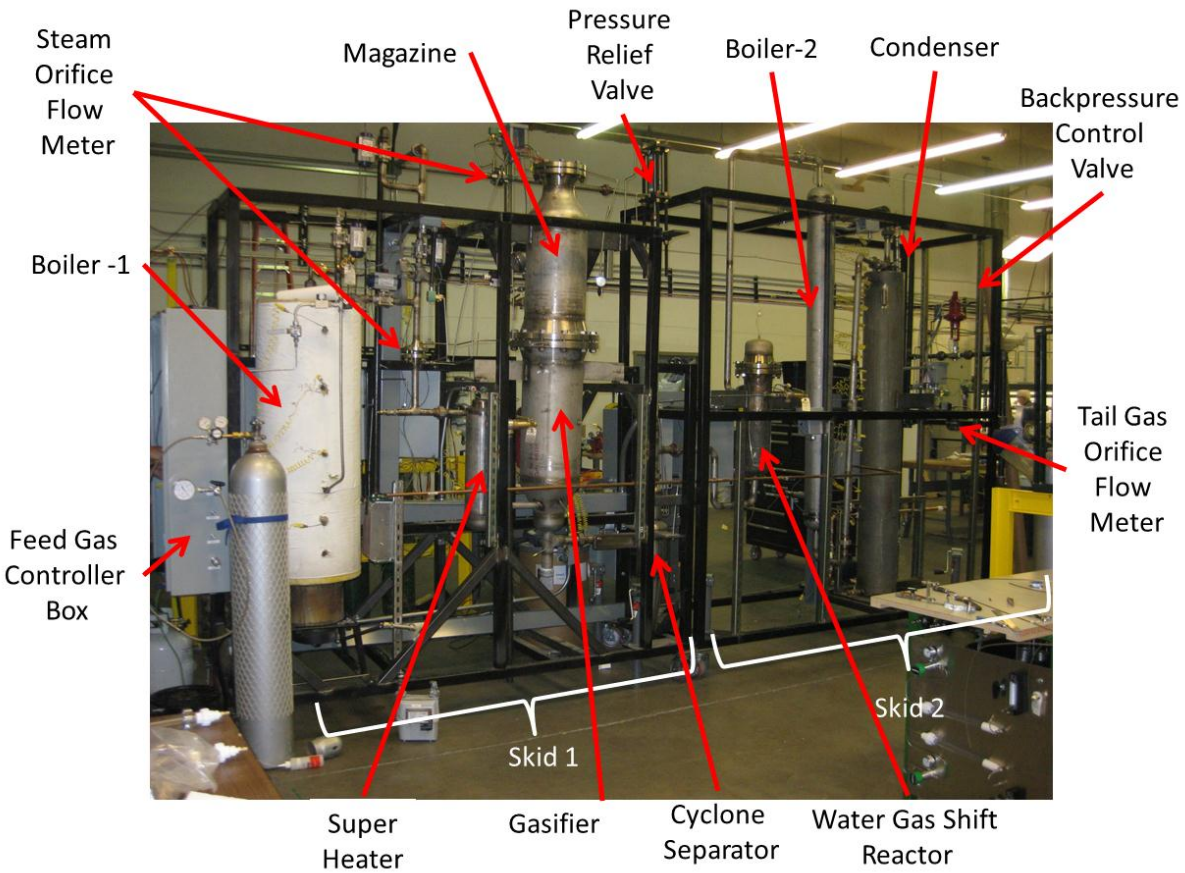

Figure 3.12. *The integrated gasifier system showing the main system components including feed gas controller module, flow orifices, steam generators, super heater, gasifier, fuel magazine, water gas shift reactor, condenser, and backpressure control valve.*

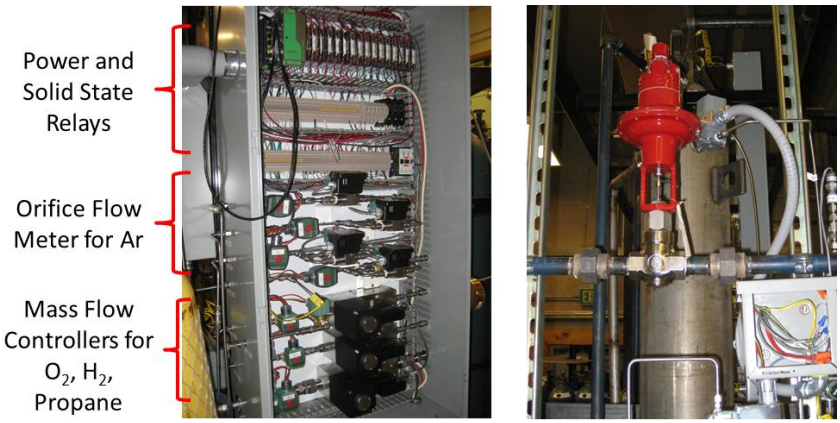

Figure 3.13. *Feed Gas Flow and Back Pressure Control Modules. Left: Feed Gas Flow Control Module. Right: Back Pressure Control Valve*

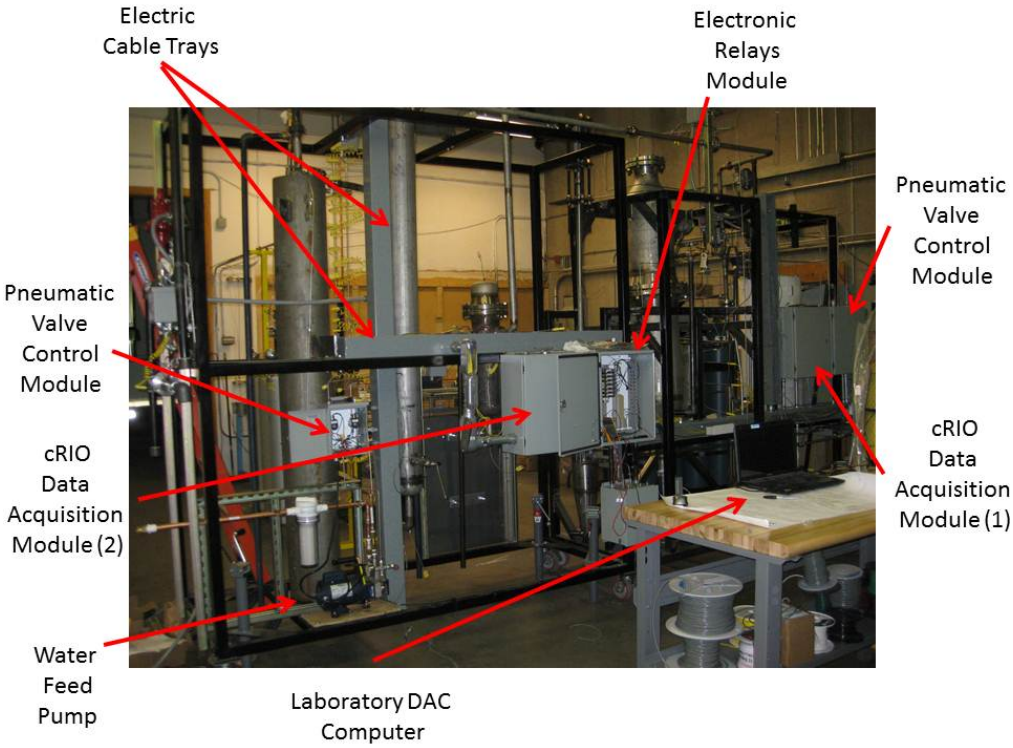

Figure 3.14. *Integrated Computer and Data Acquisition Control System.*

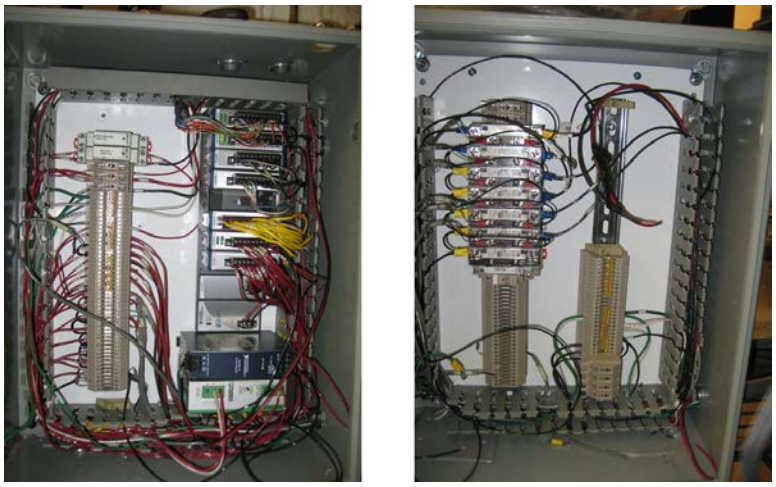

Figure 3.15. *Data Acquisition I/O chassis (Left) and Solid State Relay Module (Right)*

After the initial assembly and checkouts, the system was moved outside into a 25' x 25' x 8' fenced area for final assembly and remote test operations (Figure 3.16). The fence contained a main and side gate for equipment access and transport. Inside the enclosed area, the test bed was isolated from personnel by a 22' (L) x 10' (H) cement L-wall. Site interfacing of electricity, air, water, and the feed gas supply system plumbing was completed. A flare gas system was designed, fabricated and integrated to the gasifier system to exhaust product gas. Final checkout tests of the system components were performed including the computer DAC system, boiler, super heater, feed gas supply system, back pressure control valve, and tail gas flare to ensure operability before proceeding to hot fire.

Figure 3.16. *Final integration and assembly of the Phase IIIA system test bed. Left: gasifier system. Right: tail gas flare system*

3.1.3. Methodology

Process Parameter Definitions

The primary operating parameters that influence the product composition are the gasification medium (i.e., steam, oxidant and fuel), temperature, space velocity. To examine the interplay between operating conditions and product composition, a set of characteristic process parameters that describe hydrogen, oxygen, and carbon addition during operation are used. These include the Equivalence Ratio (ER), Steam to Oxygen ratio (S/O), and the Gasification Ratio (GR). The equivalence ratio is a useful quantity that identifies the oxidation regime present in the fuel reforming process. A value of ER = 0 indicates pyrolysis conditions, 0 < ER < 1, gasification, and ER > 1 combustion (Reed, T., et al., 1994). In steam-oxygen media the gasification ratio (GR), the steam to oxygen ratio (S/O), and the steam to biomass ratio (S/B) are typically used to evaluate the process (Wang, Y. and Kinoshita, C. M., 1992; Gil, J., et al., 1997; Turn, S., et al., 1998; Aznar, M. P., et al., 1998; Aznar, M. P., et al., 2006,; Lv, P., et al., 2007; Meng, X., et al., 2011; Siedlecki, M., and de Jong, W., 2011). The gasification ratio is similar to the steam to biomass ratio in steam reforming except that it accounts for the combined effect of steam, oxygen and biomass feed rate on product composition. Parametric variations of these process variables are performed to determine how these affect the reforming process and downstream gas composition. Table 3.14 summarizes the suite of process parameters and performance metrics used in these studies to evaluate the GO^{TM} process.

Table 3.14. Process and Performance Variables

Parameter	Definition	Remarks
Equivalence Ratio, ER	$ER = \frac{\left[\frac{\dot{m}_{O2}}{\dot{m}_{bio}}\right]_{Act}}{\left[\frac{\dot{m}_{O2}}{\dot{m}_{bio}}\right]_{Stoich}}$ where $\left[\frac{\dot{m}_{O2}}{\dot{m}_{bio}}\right]_{Stoich} = \frac{32}{12}m_C + 8m_H + m_S - m_O$	$\dot{m}_{O2}$ = mass flow rate of oxygen feed, in kg/min $\dot{m}_{bio}$ = mass flow rate of biomass feed, dry ash-free basis, in kg/min *Act* = actual run condition *Stoich* = stoichiometric condition m_C = C mass fraction in fuel, daf m_H = H mass fraction in fuel, daf m_S = S mass fraction in fuel, daf m_O = O mass fraction in fuel, daf ER is unitless
Gasification Ratio, GR	$GR = \left[\frac{(\dot{m}_{H2O} + \dot{m}_{O2})}{\dot{m}_{bio}}\right]$	$\dot{m}_{H2O}$ = mass flow rate of steam, kg/min $\dot{m}_{O2}$ = mass flow rate of oxygen feed, in kg/min $\dot{m}_{bio}$ = mass flow rate of biomass feed, dry ash-free basis, in kg/min GR in units of kg/kg, dry ash-free biomass
Steam to Oxygen		$\dot{n}_{H2O}$ = molar flow rate of steam feed, in mol/min

Ratio, S/O	$S/O = \left[\frac{\dot{n}_{H2O}}{\dot{n}_{O2}}\right]$	$\dot{n}_{O2}$ = molar flow rate of oxygen feed, in mol/min S/O in units of mol/mol
Steam to Biomass Ratio, S/B	$S/B = \left[\frac{\dot{m}_{H2O}}{\dot{m}_{bio}}\right]$	$\dot{m}_{H2O}$ = mass flow rate of steam, kg/min $\dot{m}_{bio}$ = mass flow rate of biomass feed, dry ash-free basis, in kg/min S/B in units of kg/kg, dry ash-free biomass
Superficial Gas Velocity, SV	$SV = \left[\frac{\dot{Q}_{PG}}{A_c}\right]$	$\dot{Q}_{PG}$= Product gas volumetric flow rate, Nm^3/min A_c = Reactor area cross section, m^2 SV in units of $m^3/sec/m^2$
Residence Time, τ_R	$\tau_R = \left[\frac{V}{\dot{Q}_{PG} \div 60}\right]$	V = reactor bed volume, m^3 $\dot{Q}_a$= Actual gas volumetric flow rate, m^3/min t_R is in units of seconds

Carbon Conversion Efficiency, CCE	$CCE = \frac{Total\ C\ reacted\ in\ the\ system}{Total\ C\ fed\ in\ the\ system}$ $= \left[\frac{V_{PG} x_C \left(\frac{12}{22.4}\right)}{(m_C)\left(m_{bio}(1 - m_{ash})\right)}\right] \times 100\%$	V_{PG} = total volume of product gas, Nm^3 x_C = mole fraction of carbon in the product gas m_{bio}= total mass of the biomass fuel added, kg m_C = C mass fraction in the biomass m_{ash} = Ash mass fraction in the biomass
Gas Yield, GY	$GY = \left[\frac{V_{PG}}{m_{bio}}\right]$	V_{PG} = total volume of product gas, Nm^3 m_{bio} = total mass of the biomass fuel added, kg GY is in units Nm^3 gas/kg biomass
Cold Gas Efficiency, η_{CG}	$\eta_{CG} =$ $\left[\frac{(\sum x_i LHV_i)\ GY}{LHV_{bio}}\right] \times 100\%$	x_i = mole fraction of gas species i LHV_i = Lower Heating Value of gas species i, MJ/Nm^3 GY = gas yield, Nm^3 gas/kg biomass LHV_{bio} = Lower Heating Value of biomass, MJ/kg

Test Protocol

A pre-test protocol was developed and followed prior to starting the reformer for each experiment to ensure that the system hardware was properly functioning, and in a safe operating condition. These included operational checks of the system valves, pressure transducers, fluid flow meters and controllers, and temperature transducers; performing system pressurization and

leak checks; boiler filling and firing; Water Gas Shift reactor pre-heating; super heater and flare igniter checks; gas chromatograph and other chemical sensor operation.

At the beginning of each test run, the amount of fuel is weighed and loaded into the reformer until the magazine is filled and covers both sets of nozzle banks. In cases where wood pellets are used, charcoal is added first to cover the lower reformer nozzles followed by a known quantity of wood pellets. The Water Gas Shift reactor is pre-reduced before testing and is kept isolated from air exposure. Prior to testing, the Water Gas Shift reactor is heated with external heaters to its operating temperature. Boiler-1 is heated to generate steam and vented until the time steam is diverted to the Super Heater. The entire system downstream of the boiler is purged with a small flow of nitrogen to remove stagnant pockets of air before fuel ignition.

The process is comprised of three steps: startup, operation and shutdown. The reformer is started by passing steam-oxygen mixtures into the Super Heater. A small flow of hydrogen is added to the flow, and then ignited using a cartridge heater. The superheated steam-oxygen mixture is then sent to the reformer. Before the fuel is ignited, the outflow from the reformer is vented to atmosphere upstream of the Tar Destruction, Boiler-2 and Water Gas Shift units. Once the fuel is ignited, the flow is diverted to these downstream to these units. At this point, measurements of the product gas flow rate, fuel feed rate, gas composition are begun. The data collection rate for temperature, pressure and flow rate was once every four seconds. The product gas composition was analyzed by GC at a rate of once every five minutes.

The lock-hopper system and upper reformer magazine was kept free of oxygen, steam and other gasification gases by a small continuous nitrogen purge. Biomass feeding to the gasifier was started when the biomass in the upper magazine dropped below a predetermined level as detected with an optical level sensor. The number and frequency of biomass injections is logged and thus the mass addition recorded. The carbon feed rate of the biomass is automatically matched to the production rate of carbon in the product gas so as to keep the reformer system in steady and stable operation.

Once the product gas temperature exiting the reformer heated the Tar Destructor to 450°C, a small oxygen flow of about 20 SPLM was admitted to the Tar Destruction reactor. This quickly raised the temperature above 800°C in the reactor and shortly afterwards, steam from the Boiler-2 was subsequently diverted back to the reformer. Liquid level sensors in both primary and secondary boilers automatically triggered a water pump that maintained a proper water level in each boiler depending on the unit demand. Generally, the system reached steady operation in 30 minutes after ignition. Each operational event such as the biomass ignition, flow diversion, and shutdown are recorded.

The system is shut down by terminating the oxidizer flows and starting a nitrogen purge flow. The nitrogen purge helps cool the system and prevents of continued combustion of char inside the reactor. Emergency shutdown procedures are also in place. In this event, the gasifier agent (steam and oxygen) and biomass feed are automatically stopped. The high pressure gas is then diverted to a safe exit in the flare and inert gas then flushes the system.

At the end of the test, the residual char and ash is weighed and used in the determination of the carbon conversion and mass balance. The time history of flow, temperature, pressure, and gas composition is recorded and used to optimize the system operation and determine the system performance.

Biomass Fuel Properties

An easy-to-feed and gasify feedstock was chosen for this effort which included commercially available natural hardwood lump charcoal (Frontier Charcoal) and pine wood pellets (New Earth Wood Pellets). Pine wood is an attractive fuel as there are vast supplies of beetle kill across the western regions of the U. S. Photographs of these fuels are shown in Figure 3.17. The charcoal consisted of a wide variety of irregular sizes, which ranged from one-half centimeter to nearly fifteen centimeters in length (Figure 3.17, top panel). Larger particles sizes tend to cause bridging and channeling, which may lead to uneven mass flow and localized high temperatures. Excessively high temperatures may also contribute slag and clinker formation, which can foul the reformer and other downstream unit operations. Therefore, the larger pieces of charcoal were crushed into smaller sizes less than five cm in length (Figure 3.17, left panel). The dust and fines generated from tamping was estimated to be <15% of the total mass. The wood pellets were nominally 7mm in diameter, and variable in length with up to 1.5 cm in length. The wood pellets were used in the reformer as received and with no pre-processing. The proximate and ultimate analysis of the biomass is summarized in Table 3.15. The full analysis report is given in Table A.3.1 of Section A.3 in the Appendix. The formula for the wood pellet biomass is $CH_{1.3}O_{0.6}$ based on the ultimate analysis.

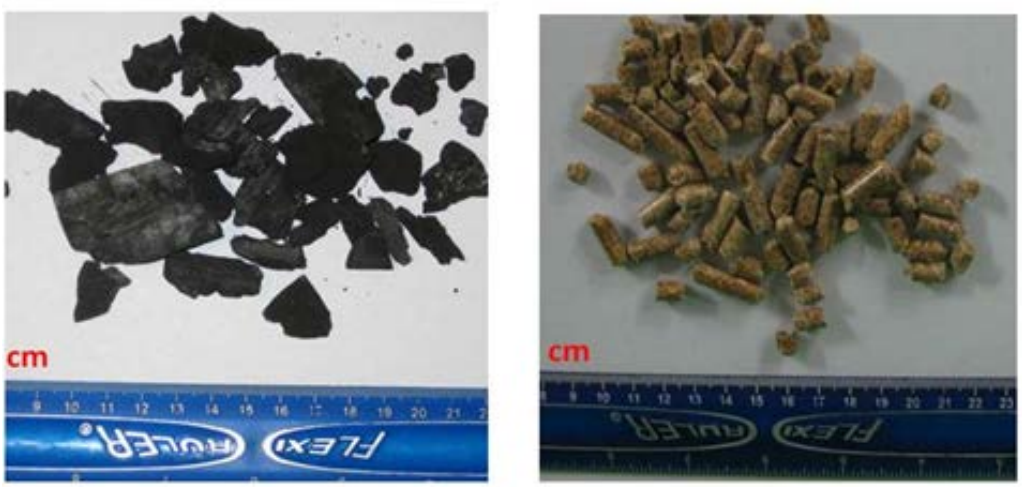

Figure 3.17. *Biomass fuel types. Left: Lump charcoal. Right: Wood pellets as received and used in reformer operation.*

Table 3.15. Biomass Fuel Properties

Parameter	Charcoal (As Received)	Wood Pellet (As Received)	Wood Pellet (Dry, Ash Free)
Type	Hardwood	Processed Pine	
Physical Properties			
Diameter, mm	Variable, < 25 mm	Variable, 6 - 8 mm	
Length, mm	Variable, < 50 mm	Variable, 6 - 38 mm	
Bulk Density, kg/m^3	200	750	
Actual Density, kg/m^3	400	1100	
Proximate Analysis			
Moisture Content, wt. %	3.54	6.20	
Ash Content, wt. %	3.91	0.58	
Volatile Matter, wt. %	30.38	76.94	
Fixed Carbon, wt. %	62.17	16.28	
Total	100.0	100.0	
Ultimate Analysis			
H		5.39	5.78
C		50.50	54.17
O		37.01	39.71
N		0.25	0.27
S		.07	0.07
Ash, wt.%		0.58	-
Moisture Content, wt. %		6.20	-
Total		100.00	100.00
HHV, MJ/kg		18.48	19.83

Notes: Ultimate and Proximate Analysis performed by Wyoming Analytical Laboratories, Laramie, WY. Complete analysis results are given in the Appendix.

3.2. Results and Discussion

This section summarizes our test campaign and results, which was highlighted by the system scale up from 1000 to 6000 SLPM of product gas, 10 bar product gas generation, the generation high CO_2 and H_2 yield, and the demonstration of several hours of continuous system operation. In parallel, reservoir characterization, geo-model development, reservoir simulation, and economic modeling was performed for the CO_2-EOR of a small producer field in Cheyenne, County, CO. The following sections detail the key results that led to the successful demonstration of the GO reformer system, and field site selection.

3.2.1. System Checkout

System checkout tests were performed using charcoal to establish a reliable startup and shutdown procedure, and to ensure that key subsystem components and instrumentation met design and operational specifications. These tests included the boiler, feed gas control, super heater, reformer, product gas flow meter, and the gas analysis subsystems. Charcoal was chosen due to its low ash and tar content, which avoids the potential operational complexity encountered

with wood or other biomass materials. Any operational excursions from expected performance were identified and fixed. Once these operations were corrected, the entire system with the full suite of operations including the Tar Destruction reactor, Steam Generator-2, Water Gas Shift reactor, and Continuous Feed System was performed.

3.2.1.1 System Start-Up, Operation and Shutdown

The reformer was first fired on January 5th, 2012, and several test runs were conducted over a wide range of conditions to achieve reliable system start-up, operation and shutdown. The test cases are identified by a three digit calendar date which enumerates the day of the year, followed by the test number. For example, the first-fire test number is recorded as 005-01. The system was performance tested over a wide range of conditions with over forty test runs conducted. Table A.4.1 in Appendix A.4 summarizes the project test runs.

The base reformer was typically charged with about 13 kg of charcoal, which filled the reformer to its capacity of 36 L as shown in Figure 3.18. System pressure and operational checks were performed prior to ignition to ensure the safe operating status of the system. The boiler was then filled to its nominal operating level of about 36 L with feed water. At start-up the boiler was typically heated with a propane flow rate between 10 and 20 SLPM. The boiler was heated until the steam pressure registered just above one atmosphere and was vented until the firing of the superheater. The super heater was ignited using a flow mixture consisting of 100 SLPM O_2 and 30 SLPM H_2. Once it was ignited and a stable temperature achieved, steam flow was brought into the super heater. The hot H_2O-O_2 mixture then flowed into the reformer where it heated and ultimately ignited the charcoal in the reformer. The time to charcoal ignition was approximately 30 - 45 minutes. At the moment of charcoal ignition, the H_2 was turned off and the reformer product gas was diverted downstream. The system pressure was controlled through adjustment of a backpressure control valve. An orifice flow meter downstream of the back pressure control valve was used for measurement of the product gas flow rate. Periodic adjustments in the propane and water feed rate were performed to keep the steam flow at a desired level. The steam and oxygen flow rates were then adjusted to give a desired product gas flow rate.

During the reformer operation measurements of temperature, flow rate, gas composition, and pressure were recorded. Figure 3.19 shows a typical reformer temperature time history, and shows the events where charcoal ignition and reformer shutdown have occurred. The charcoal ignition was indicated by a sudden rise in the temperature as registered by the thermocouples placed inside the reformer. The bed combustion temperature is measured at the nozzle exit plane by three thermocouples. A true bed temperature is probably not registered since the thermocouples extend only a short distance from the nozzle exit, and oxygen and steam flow directly over the probe which cools the thermocouple surface. A second thermocouple measures the reformer exit gas temperature 25 cm downstream from the grate, and this temperature reading was used mostly in data analysis. The charcoal is gravity fed from the top of the reformer magazine and falls down to the lower row of nozzles as it is consumed. The temperature as read by the thermocouples at the nozzle exit fluctuated widely during operation as

compared to the reformer exit temperature. Presumably, this arises from hot, glowing coals falling onto the thermocouple surface followed by pockets of cooler bed voids as the fuel bed moves downward. Once the reformer outlet temperature rises above 800°C the reformer system is shut down to avoid thermal runaway and possible damage to the reformer. The system shutdown events involved sequentially shutting off oxygen flow, isolating the steam generator from the reformer, venting its steam, purging the reformer system with nitrogen, and opening the system to atmospheric pressure.

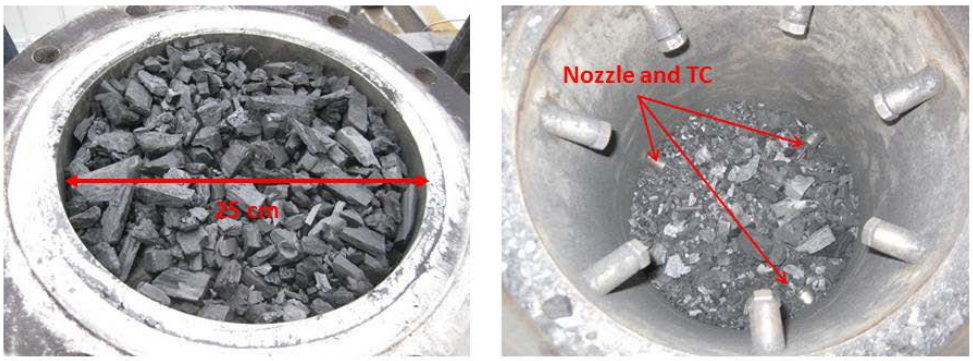

Figure 3.18. *Reformer fuel load before and after testing. Left: Initial load of 13 kg of charcoal. Right: The level of spent char after testing. The three gas reactant nozzles with their thermocouples extending into the biomass are identified. The upper nozzle bank is also shown but was not used in these tests.*

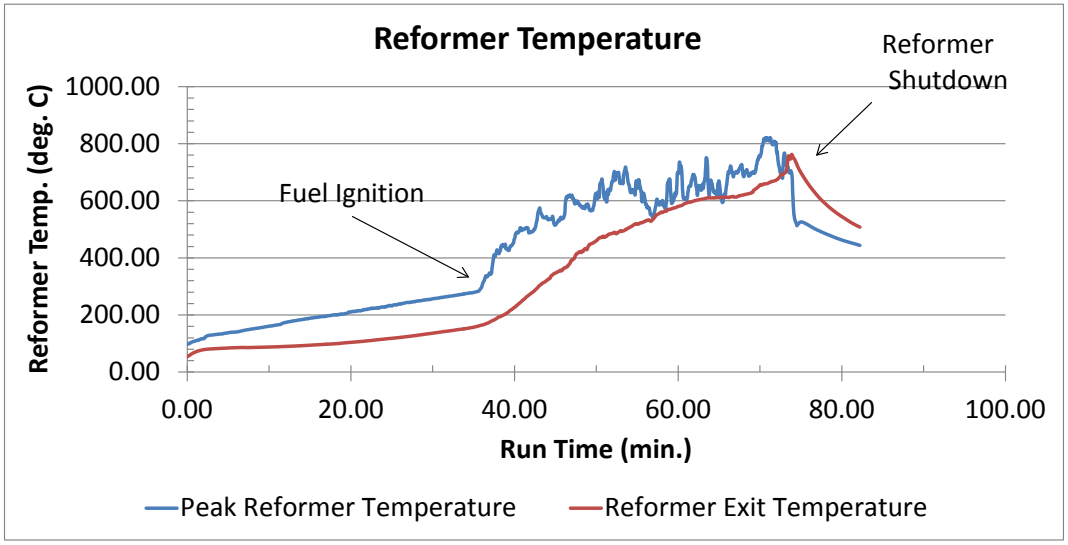

Figure 3.19. *The reformer bed and gas exit temperature profile. The bed temperature is plotted as the peak temperature of three thermocouples at the nozzle exit. Reformer ignition and shutdown are indicated by arrows. (Test 018-04).*

A typical product gas flow rate in batch mode using charcoal as the fuel is shown in Figure 3.20. Steady reformer product outflow was demonstrated for about ½ hour through adjustment in the steam and oxygen flow rates. A goal of about a 3:1 steam to oxygen mole ratio was desired, and a general downward adjustment of steam flow rate with concurrent increases in oxygen flow rate were made to achieve this ratio. This resulted in a peak product gas flow rate of near 800 SLPM.

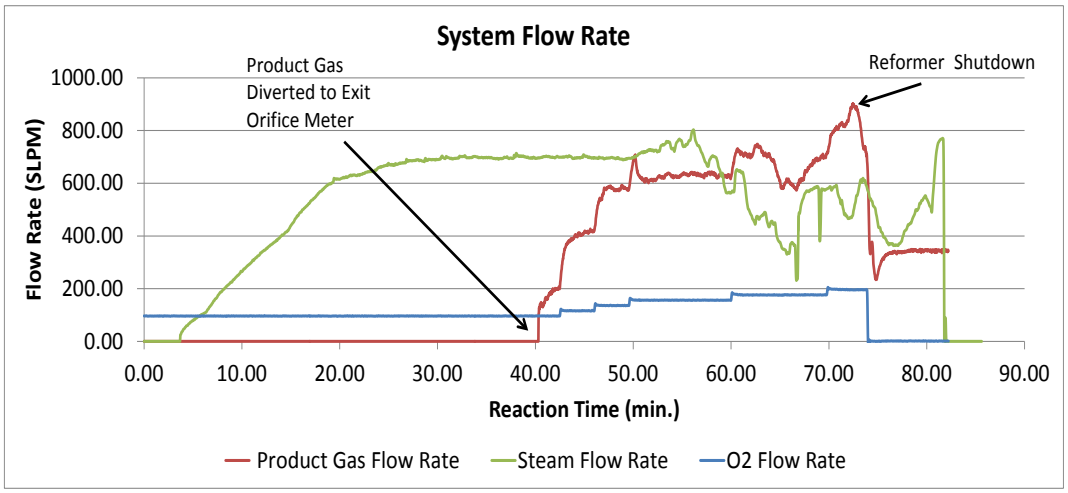

Figure 3.20. *The product gas flow rate. Steady product gas flow was achieved for about one-half hour until the fuel was spent. (Test 018-04).*

Compositional analysis of the product gas was determined by sampling a small gas slipstream and analyzing the constituents by gas chromatography. The product gas was sampled at two pull-off points, one between the reformer and cyclone, and the other downstream of the Water Gas Shift reactor between the condenser and back-pressure control valve. The latter sample point was sampled most often as it determined the quality and performance of the entire reformer operation. A typical gas chromatograph analysis summary of the product gas stream from the reformer is shown in Table 3.16, which quantifies the production of carbon dioxide and hydrogen from the reformer operation. Note that Table 3.16 data were collected without the Water Gas Shift catalyst in the reactor.

Table 3.16. Product Gas Composition

		Product gas Composition (volume %)						
Elapsed Time (Min.) [1]	Sample Location	H_2	O_2	N_2	CH_4	CO	CO_2	Total
0	Reformer	16.26	37.87	14.44	0.5	7.39	18.83	95.29
2	Tail Gas	36.77	0.59	1.01	2.59	19.4	37.81	98.17
13	Tail Gas	43.14	0.21	0.36	1.25	28.49	26.76	100.21
21	Tail Gas	41.74	0.12	0.27	0.64	36.26	22.07	101.10

28	Tail Gas	36.74	0.13	0.31	0.51	40.5	23.05	101.24
32	Tail Gas	36.47	0.15	0.34	0.27	41.11	22.86	101.2

1. Elapsed time is taken from the time the flow is diverted downstream

Several factors affect the pressure drop and product gas flow rate of the reformer. These include the bed cross section and depth, biomass and char particle size, the void fraction of the bed material, and the gas temperature and composition. A bed with high porosity gives rise to low pressure drop and efficient downstream volumetric flow. High temperature increases the gas viscosity and velocity, leading to larger pressure drop. The gas volume during biomass gasification will increase, which leads to higher velocity. Biomass and char produced during reaction also tend to contract or fracture to smaller particles, which increases the gas flow resistance. During these checkout tests, the pressure drop in the reformer was measured. A typical system pressure measurement is shown in Figure 3.21 at three locations: downstream of the boiler, in the reformer, and downstream of the Water Gas Shift (WGS) reactor. Under these conditions, the pressure drop measured from the reformer downstream to the WGS reactor was modest, with a ΔP of < .05 atm., and indicates efficient gas flow through the system is achieved. In addition, the low pressure drop shows that the grate is efficiently passing spent biomass, ash without clogging.

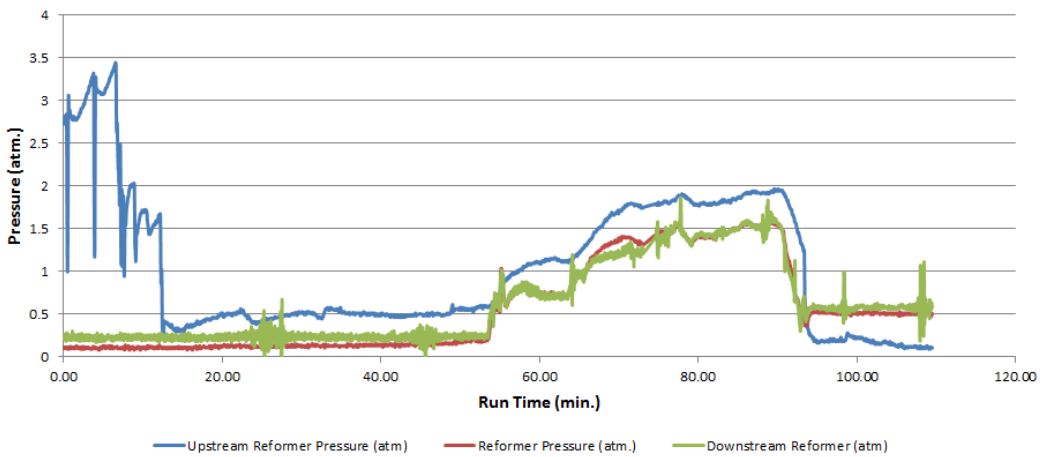

Figure 3.21. *Reformer System Pressure. The pressure drop from the outlet of Steam Generator-1 across the steam orifice meter to the reformer inlet is about 0.5 atm., and from inside the reformer bed to the outlet of the reformer is < 0.05 atm. Flow Conditions: Steam = 300-400 SLPM, Oxygen = 100-200 SLPM, Product Gas = 600-800 SLPM. (Test 018-04).*

Operational Challenges Encountered

During the system checkout tests various operational challenges were uncovered and resolved. One such problem was the observation of an asymmetric radial temperature profile at the nozzle exit (Figure 3.22, Left panel). Here Thermocouple – 12 (TC-12) registers a temperature twice as high as the other two thermocouples. This is not uncommon with nozzle-based (tuyere) reactant injection; however, it can potentially lead to bridging, channeling, local slag, and clinkering problems. The unbalanced temperature distribution at the nozzle exit is

presumably caused by an uneven gas flow distribution through the steam-oxygen injector bank. This was corrected by reducing the exit area of the injectors from 1.27 cm (1/2 inch) to .64 cm (1/4 inch). The area reduction at the nozzle exit causes an increase in the upstream plenum pressure which causes the gas to evenly distribute across the steam-oxygen injectors.

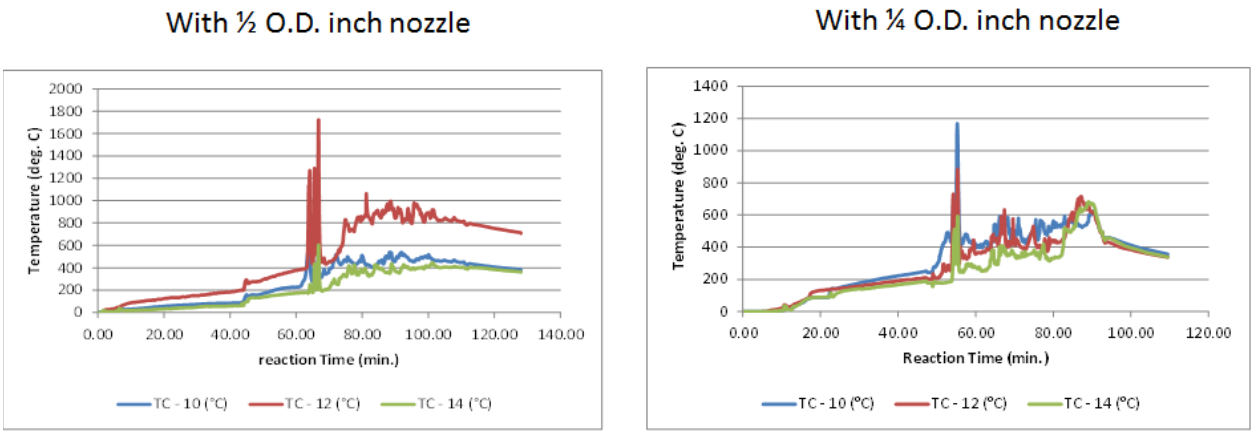

Figure 3.22. *Radial temperature in the reformer bed. Left: Asymmetric reformer heating with a ½ inch nozzle diameter (Test 010-2). Right: Reformer temperature with a reduced ¼ inch nozzle diameter (Test 018-4).*

The reformer exit temperature typically was between 600 and 700^{0}C. However, during operations there were occasional temperature excursions which resulted in reformer gas exit temperatures above 800°C. At this point the reformer operation was shut down as a precautionary measure to avoid potential damage to the reformer. In some cases when the exit temperature exceeded 800°C for prolonged periods a post run examination revealed that the grate and pipe was, indeed, thermally damaged (Figure 3.23). Apparently as the fuel is consumed and drops below the nozzle bank, a channel is formed which allows hot O_2-H_2O gas to flow down to the grate without undergoing the endothermic reduction reactions. In this case, the hot O_2-H_2O gas impinges upon the grate and pipe surfaces, oxidizes the steel, and eventually causes it to burn.

It was also observed that small lumps and slabs of slag usually formed at the charcoal – reactant interface inside the reformer when temperature excursions occurred. The slag mass was typically less than 100 grams, and visually appeared porous with small isolated pockets of shiny, glassy fragments imbedded in the slag. No slag was observed in downstream piping or units. To prevent the thermal excursions from occurring, operational changes were made in the control program that automatically shuts down the reformer when the exit temperature exceeds 800°C.

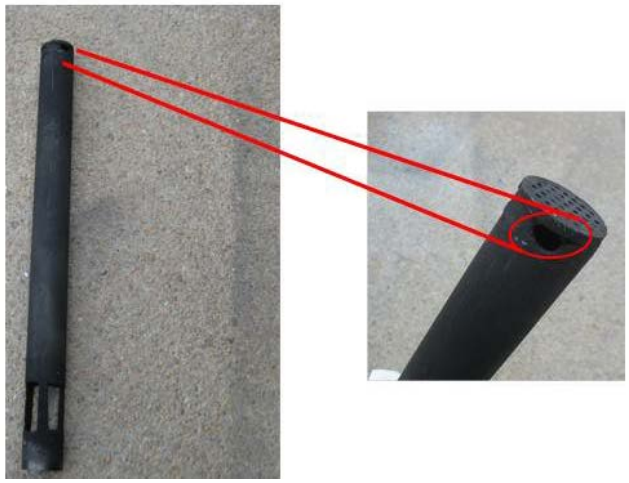

Figure 3.23. *Post-run photographs of thermal damage to pipe and grate. Note the 3/8 inch burn hole in the pipe at the interface between the grate and pipe.*

In summary, successful small scale checkout tests were conducted for the purpose of measuring and verifying system flow, pressure, temperature, data acquisition and instrument control operation. The checkout tests were performed in batch mode with charcoal. The super heater and reformer were ignited reliably, which resulted in the measurement of 600-800 SLPM of product gas at 3-4 atm pressure. Measurements of H_2, CO_2, CO, and CH_4 concentrations were quantified with an on-line gas chromatograph. The reformer peak temperature at the nozzle exit was typically between 600-800°C with an exit temperature of 600-700°C. Reformer exit temperature excursions above 800°C were periodically observed during these tests. These occurred at the end of the run when the fuel level dropped below the gasifier nozzle bank and when fuel channeling occurred. This resulted in the immediate shutdown of the reformer as it was discovered that thermal damage to the grate can occur.

3.2.2. Phase IIIA System Testing

Following the successful reformer checkout testing, the GO^{TM} system was performance tested over a wide range of operating conditions with respect to steam and oxygen flow rate, temperature and pressure. Our approach first involved scale-up tests with charcoal in batch mode to quickly reach the design goals of 4,000 SLPM and 10 bar operation while minimizing operational difficulties. Once these goals were obtained, tests were conducted with pine wood pellets to demonstrate gas generation from a more representative biomass feed stock. The Water Gas Shift reactor was brought on-line and its performance evaluated for enrichment of the CO_2 and H_2 yield in the product gas. Following these tests, a continuous biomass feed system was designed and constructed to demonstrate longer duration test runs at the preferred operating condition. Tests of the Tar Destructor were also performed. A preferred set of operating conditions were established based on the results from these tests. The test results for the key experiments leading to the achievement of our objectives are presented below.

3.2.2.1. Batch Operation with Charcoal: 4000 SLPM

Using procedures developed in the checkout tests, the reformer was loaded with 36 kg of charcoal and ignited with superheated Steam-O_2-H_2 mixtures. Ignition was typically achieved

using a super heater reactant mixture of 640 SLPM steam, 150 SLPM oxygen, and 58 SLPM hydrogen. Once ignited, the hydrogen was turned off and the product gas was then diverted downstream. The system temperature, product flow rate, system pressure drop and fuel consumption were subsequently measured for the duration of the reformer operation.

A typical steam-oxygen gasification test using charcoal is presented in Figure 3.24. Fuel ignition was achieved near the 60 minute mark from the super heater firing as indicated by the arrow in the upper left panel in Figure 3.24. The average temperature inside the reformer, measured at the exit of the tuyeres, was about 800^0C. The reformer exhaust temperature varied from 650-700 ^{o}C during the test. Shortly after ignition the product gas was diverted to the tail gas exit and its flow measured. Steam Generator-2 was filled with water during this test and the waste heat in the product gas stream was recovered to generate additional steam flow. This amounted to about 30% of the total steam used in the experiment. Through adjustment of steam and oxygen flow rate, the system outflow reached our design goal of 4,000 SLPM as seen in the lower panel of Figure 3.24. The system pressure was also monitored during the course of the reaction and peaked near 8.4 bar (8.3 atm.), which is close the design point of 10 bar, 150 PSI (Figure 3.25, Upper panel). The pressure drop from the reformer downstream to the back pressure control valve was small, on average $\Delta P < .5$ atm., and indicates good gas throughput through the reformer and downstream piping (Figure 3.25, Lower panel). The test results for this run is summarized in Table 3.17.

The reformer operated for about 55 minutes until the fuel was exhausted as indicated by the sudden reformer exit temperature jump from 700^0C to 770^oC. During this period the product gas was sampled in the tail gas about once every five minutes and its composition analyzed by gas chromatography (Table 3.17). On average, the measured concentration in volume % for the species H_2, CO_2, CO and CH_4 during the run were 46 %, 28 %, 27 %, and 1.3 %, respectively. We note that the Water Gas Shift reactor was not operated at this time.

A carbon conversion efficiency (CCE) of the system based on the carbon mass generated in the gas flow and the carbon consumed in the reformer was determined and summarized in Table 3.18. The carbon generated in the gas flow is calculated from the time integrated cumulative volume of 85 Nm^3 and an average product gas fractional carbon composition of 0.55. The total carbon reacted at the end of the run was 25.0 kg. At the conclusion of the test about 3.8 kg of residual mass was measured, which indicates 32.8 kg of the charcoal fuel was burned. Charcoal typically has a carbon mass fraction in the range of 0.7 – 0.8. Taking a charcoal mass fraction of 0.75, and an ash mass fraction of 0.039, the total carbon fed to the system was 23.6 kg. The carbon conversion efficiency is thus:

$$CCE = \frac{Total\ C\ reacted\ in\ the\ system}{Total\ C\ fed\ in\ the\ system} = \left[\frac{V_{PG} x_C \left(\frac{12}{22.4}\right)}{(m_C)\left(m_{bio}(1-m_{ash})\right)}\right] \times 100\% \tag{3.16}$$

$$CCE = \frac{85 Nm^3 (0.55) \frac{12\ kg}{22.4 Nm^3}}{\left((0.75)(32.8kg)(1-0.039)\right)} \times 100\% = \frac{25.0kg}{23.6kg} = 106\% \tag{3.17}$$

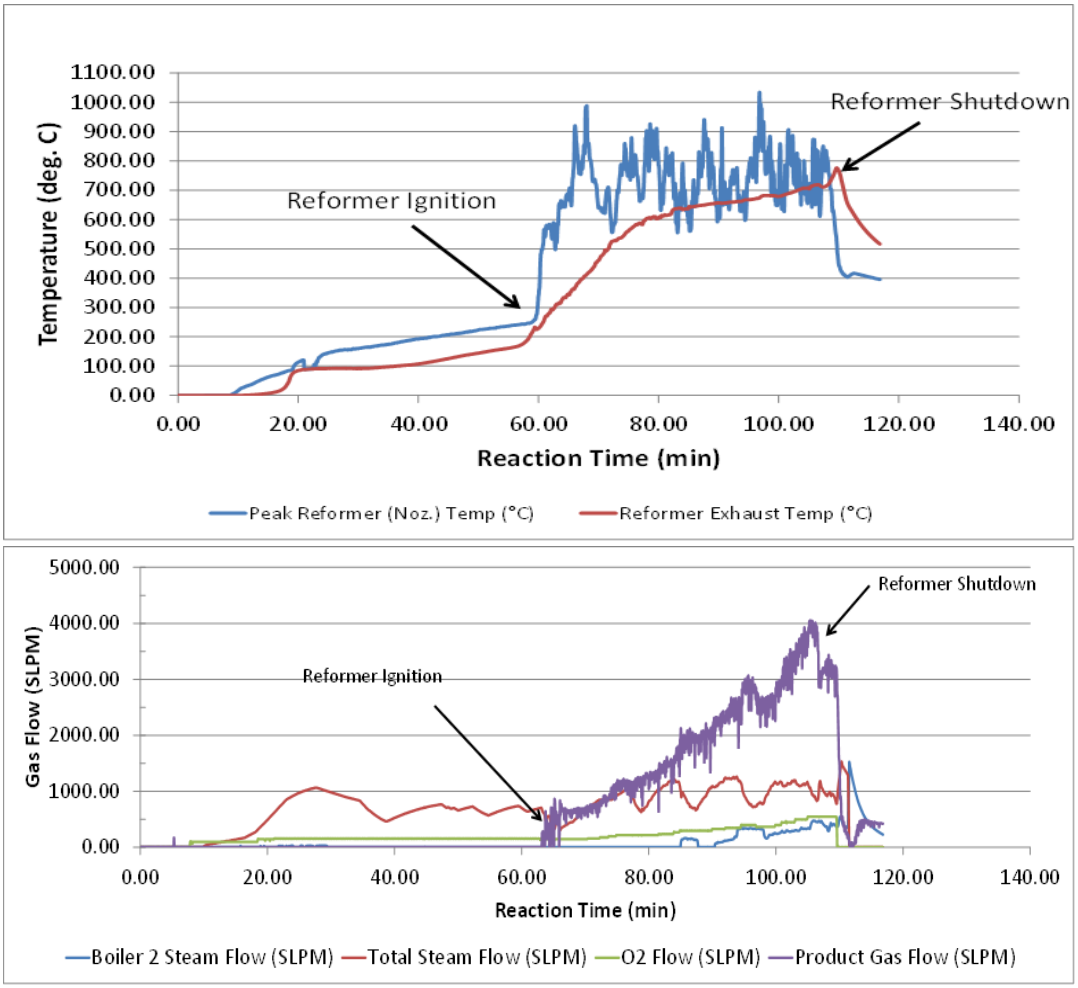

Figure 3.24. *Reformer performance data with charcoal. The arrows indicate main reactor events. Upper: System temperature measured in the reformer. Lower: System flow rate for steam, oxygen, and product gas output. (Test 055-12)*

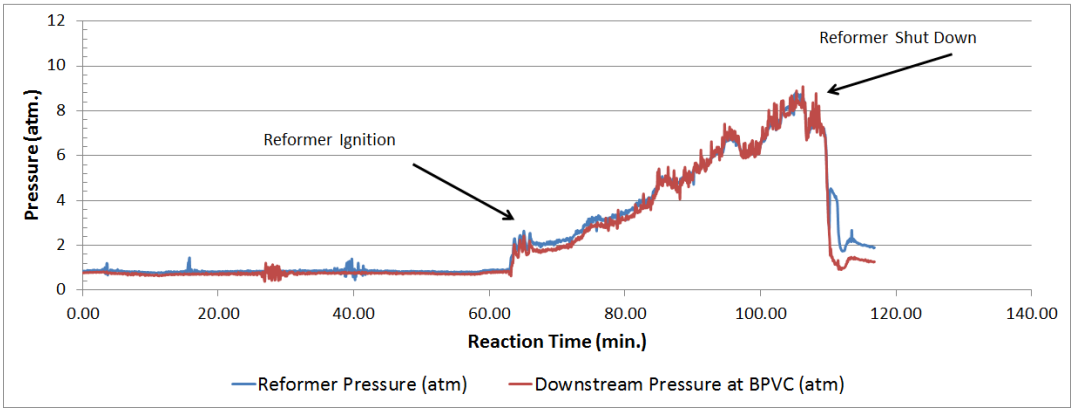

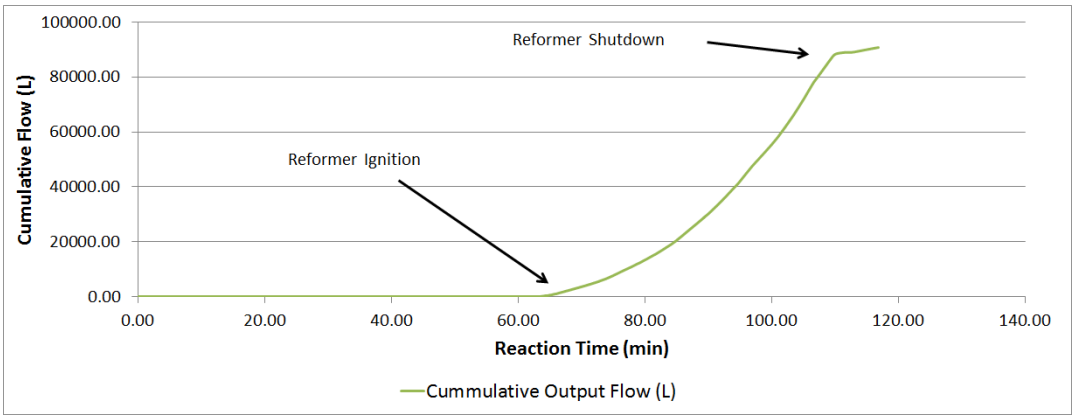

Figure 3.25. *Reformer performance data with charcoal. Upper: System pressure drop measured between the reformer and upstream of the backpressure control valve. Lower: Total product gas volume generated during run. (Test 055-12).*

Table 3.17. Product Gas Composition with Charcoal (Test 055-12, dry gas basis)

Elapsed Time (Min)	H_2 (vol. %)	O_2 (vol. %)	N_2 (vol. %)	CH_4 (vol. %)	CO (vol. %)	CO_2 (vol. %)	Total	Fractional C in PG	Gas MW
0:08	44.64	1.84	0.38		23.09	28.49	98.44	0.51	20.59
0:15	46.98	0.22	0.18	2.11	27.27	27.26	104.02	0.54	21.03
0:22	47.7	0.18	0.18	2.02	26.56	27.34	103.98	0.54	20.85
0:29	46.05	0.16	0.25	1.53	34.09	22.69	104.77	0.56	20.82
0:36	49.73	0.12	0.21	1.35	20.93	31.24	103.58	0.52	20.91
0:43	46.7	0.06	0.18	1.29	31.17	25.01	104.41	0.55	20.94
0:50	43.99	0.06	0.23	0.65	29.39	30.51	104.83	0.58	22.72
0:51	42.72	0.12	0.41	0.48	34.3	26.4	104.43	0.59	22.30
							Avg.	0.55	21.27

Table 3.18. Test 055-12 Data Summary

Parameter	Value
Maximum Product Gas Flow Rate, SLPM	**4000**
System Pressure, bar	**8.4**
Exit Gas Temperature, °C	**650-700**
Carbon Conversion Efficiency, %	**106**
Total Product Gas Volume, Nm^3	84.6
Volume fraction of C in PG	.55
Total C Reacted, kg	24.9
Amt. Fuel Loaded in Reformer, kg	36.1
Residual Fuel After Run, kg	3.8
Fuel Fed in System, kg	32.3

Fractional C content in Fuel	0.75
Fractional Ash Content in Fuel	.039
Total Carbon Fed in System, kg	23.3

3.2.2.2. Batch Operation with Pine Pellets: 4000 SLPM, 10 Bar Demonstration

Following the successful operation with charcoal, several reformer tests were conducted in batch mode with pine wood pellets as the fuel source. The variation of temperature, product gas flow rate, pressure, and product gas volume is presented for Test 102-19 in Figures 3.26 and 3.27. In this test the reformer bed was first loaded with 13.0 kg of charcoal, followed by 41.4 kg of pine wood pellets. Biomass ignition was achieved using a 100 SLPM steam and 30 SLPM of oxygen mixture in about 25 minutes after the super heater ignited. Once the fuel ignited, the product gas was diverted downstream and the reformer was parametrically tested with variations of steam and oxygen flow rate for about 58 minutes until the fuel was exhausted.

A relatively stable temperature and product gas flow rate profile was established in about 30 minutes after ignition. Note that the exit gas temperature is higher than the bed temperature. However, recall that the bed temperature here is actually the temperature measured at the nozzle exit plane. Here the steam and oxygen flow pass over the thermocouples which keeps them relatively cool compared to the combustion temperature further inside the bed. The product gas flow rate typically operated above 2,500 SLPM with an occasional spike in gas flow rate near 3,500 SLPM. The steam and oxygen flow rates were periodically adjusted that gave a S/O ratio in the range of 3 to 6 (mol/mol). The reformer pressure averaged about 11 atm (11.1 bar) during the test which met the operational pressure requirement. In total, the reformer was operated for 58 minutes and a total of 110 Nm^3 of product gas was generated until the unit was shut down. The residual biomass after the run was 1.5 kg, which gave a total gasifier biomass mass addition of 53 kg, and a biomass feed rate of 0.91 kg/min. The product gas was sampled and its component concentration measured by gas chromatography. An average carbon mole fraction of 0.49 was measured in the gas stream, which gave a total of 28.9 kg of C reacted in the system. Using these data, the carbon conversion efficiency was 99%. A test summary of Test 102-19 is presented in Table x.

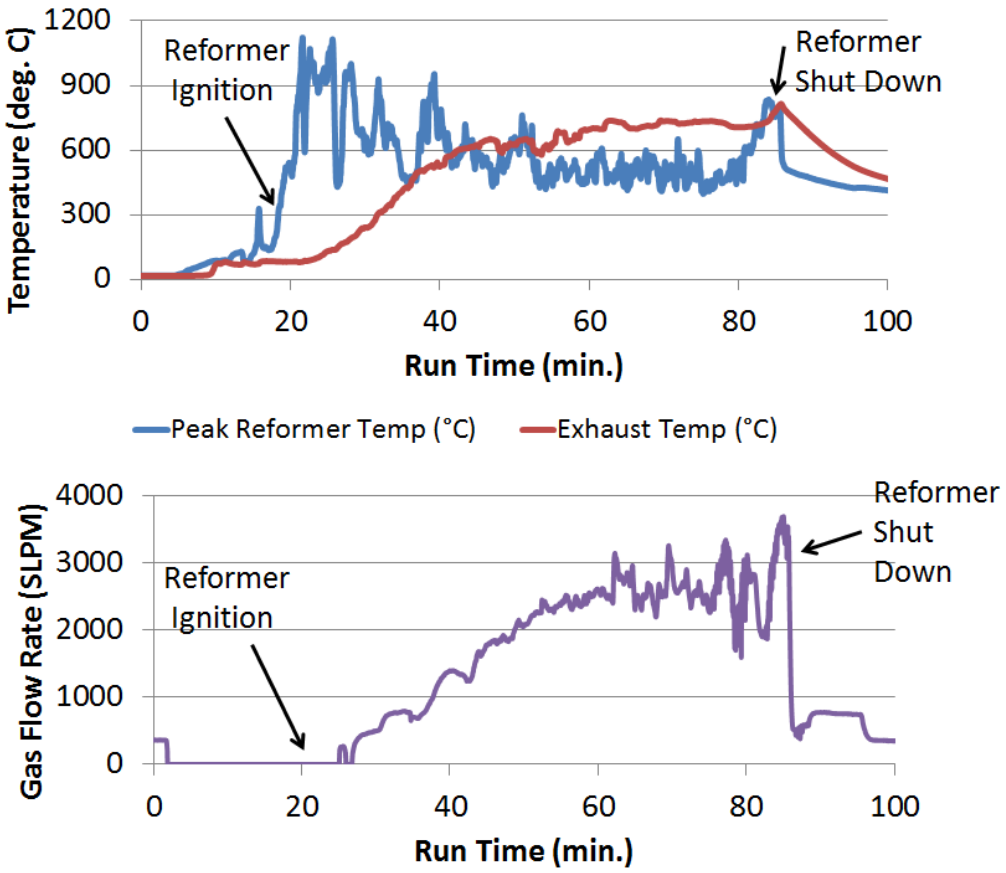

Figure 3.26. *Reformer operation with wood pellets. Top: Temperature profile of the reformer and reformer exit. Bottom: Product gas flow rate. The product gas flow rate peaked near 3500 SLPM before shutdown. (Test 102-19)*

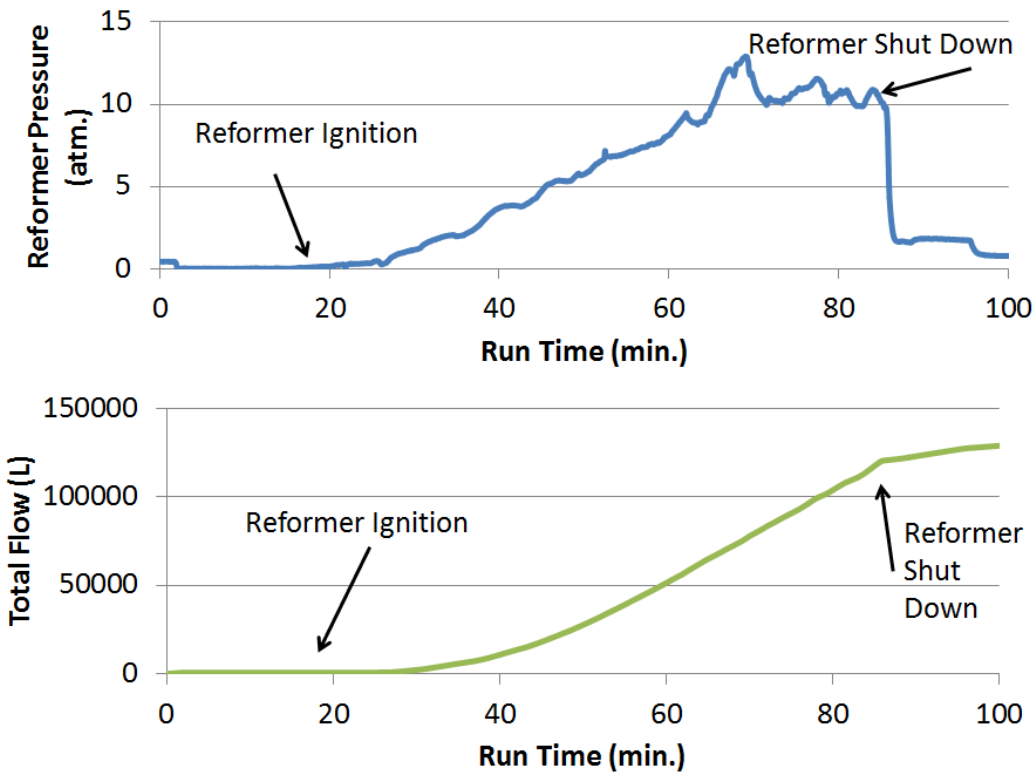

Figure 3.27. *Reformer operation with wood pellets. Top: Reformer pressure in atmospheres. Bottom: Cumulative product gas volume in liters. The total gas volume generated was about 110 Nm^3 at the reformer shutdown. (Test 102-19).*

Table 3.19. Test 102-19 Data Summary

Parameter	Value
Maximum Product Gas Flow Rate, SLPM	**3600**
System Pressure, bar	**11**
Exit Gas Temperature, ^{o}C	**700**
Carbon Conversion Efficiency, %	**98.9**
Total Product Gas Volume, Nm^3	110
Volume fraction of C in PG	0.49
Total C Reacted, kg	28.9
Amt. Fuel Loaded in Reformer, kg	54.4
Residual Fuel After Run, kg	1.5
Fuel Fed in System, kg	52.9
Fractional C content in Fuel	0.56
Fractional Ash Content in Fuel	.014
Total Carbon Fed in System, kg	29.2
Gas Yield, Nm^3/kg	**2.1**

In summary, the batch operation test results show that the present gasifier design performs as designed, and is suitable for generating useful quantities and pressures of product gas for CO_2-EOR. Having achieved the design flow rate and pressure goals of 4000 SLPM and 10 bar, the next set of test objectives were to enrich the CO_2 and H_2 yield in the product gas using the Water Gas Shift catalytic reactor. These results are discussed in the following section.

3.2.2.3. Water Gas Shift Reactor: Enrichment of the CO_2 and H_2 Yield

A Water Gas Shift (WGS) Reactor was placed into service downstream of Steam Generator-2 to increase the concentration of CO_2 and H_2 in the product gas. The 60 L WGS reactor was packed with about 70 kg of a copper-zinc oxide Medium Temperature Shift Catalyst (MTS-401, Unicat Catalyst Technologies). The Gas Hourly Space Velocity (GHSV) for the reactor at 4000 SLPM was about 4000 h^{-1}. For efficient conversion the WGS reactor was located downstream of the auxiliary boiler. In this manner, heat is extracted from the stream flow to generate steam while the gas is concurrently cooled as it enters the reactor. This enables the inlet temperature to the WGS reactor to be kept in the range of 200-250°C, which is within the manufactures' recommended operating temperature. The stream temperatures at outlet of the shift reactor varied between 260-300°C, respectively.

The performance of the Water Gas Shift reactor in the enhancement of the CO_2 and H_2 product yield was examined by Gas Chromatographic analysis of the gas downstream of the shift reactor. An example comparison of the gas composition with and without the Water Gas Shift reactor is shown in Figure 3.28. These data show a 1.4X increase in the CO_2 concentration in the product gas with the WGS reactor. Additionally, efficient conversion (removal) of up to 90% of the inlet CO concentration was achieved with the shift catalyst.

The H_2O/CO ratio at the reactor inlet is an important parameter for optimum conversion of CO and H_2O into CO_2 and H_2 by the shift catalyst. The CO was determined directly by gas chromatography analysis of the product gas upstream of the inlet to the Water Gas Shift reactor. However, the water concentration upstream of the Water Gas Shift reactor is determined indirectly from mass balance considerations of the hydrogen inflow to the reformer, and the hydrogen outflow of the product gas. Hydrogen enters the gasifier as steam, and water from the biomass. Hydrogen leaves the gasifier as H_2, CH_4, C_3H_8, char and tar. The hydrogen content in the char and tar is small compared to the other products and is excluded from the calculation. Thus the steam conversion becomes:

$$Steam\ Conversion, \% = \frac{\left[100 \times \dot{V}_{PG}\,(4C_3H_8 + 2CH_4 + H_2)\frac{18}{22.4}\right]}{\dot{m}_{H2O} + \dot{m}_{Bio}(x_{MC})} \tag{3.18}$$

where $\dot{V_{PG}}$ is the volumetric flow rate of the product gas in Nm^3/min, CH_4, C_3H_8, H_2 are the mole fractions of the respective product gas species, $\dot{m}_{H2O}$ is the steam feed rate (kg/min), $\dot{m}_{Bio}$ is the biomass feed rate (kg/min), and x_{MC} is the fractional moisture content of the biomass feed. Given a volumetric flow rate of 1.5Nm^3/min; product gas mole fractions of CH_4 = 0.032, C_3H_8 = 0.004, H_2 = 0.39; a steam feed rate of 0.81 kg/min, a biomass feed rate of 0.89 kg/min, and a

biomass moisture content of 0.062, the steam conversion was about 67 %. Accordingly, the unused water content downstream of the gasifier was 33%.

Typical water concentrations in the product gas flow upstream of the WGS reactor were determined to be in the range of 10 - 40 %. The relationship between the Steam/O_2 ratio, the WGS reactor inlet H_2O gas concentration, and the WGS reactor inlet H_2O/CO ratio is shown in Figure 3.29.

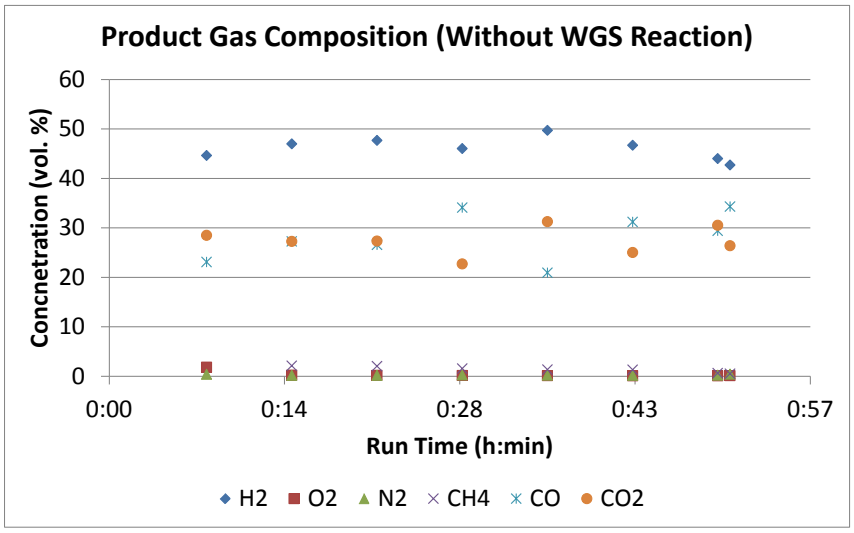

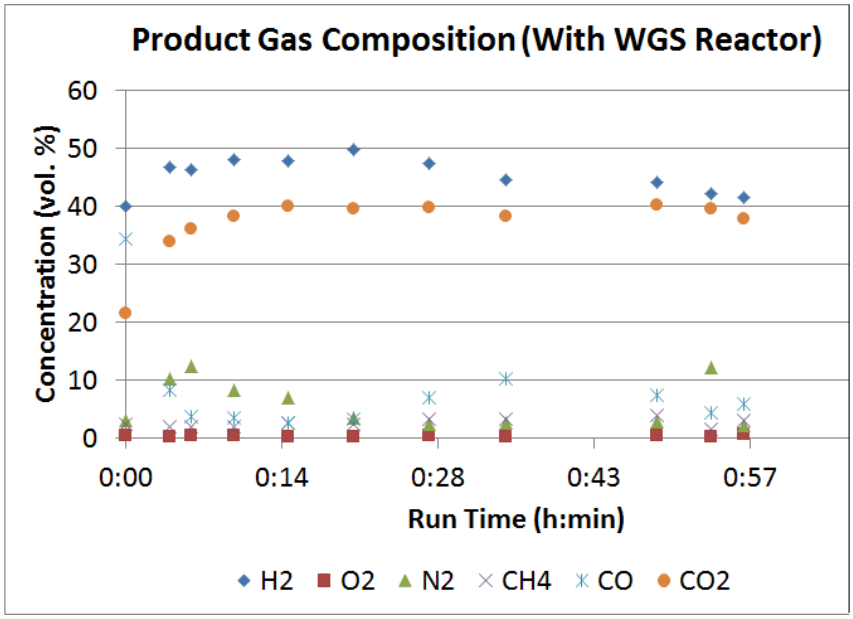

Figure 3.28. *Comparison of Product Gas Composition, dry gas basis. Left: Without use of the WGS reactor (Test). Right: Product gas composition from the exit WGS reactor. The CO_2 concentration increased from 28 vol % to 40 vol %, and the H_2 concentration exceeded 45 vol % with the Water Gas Shift reactor. (Test 102-19)*

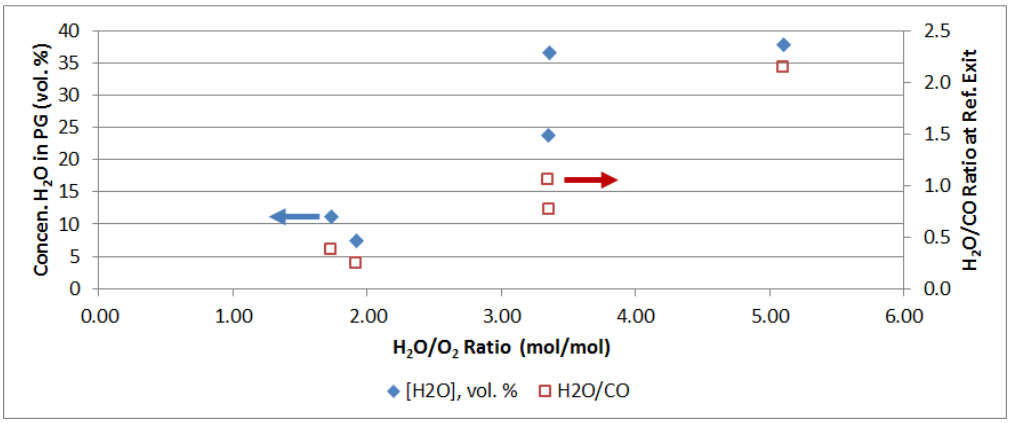

Figure 3.29. *Water vapor concentration and H_2O/CO ratio at the WGS reactor inlet as a function of the Steam/O_2 ratio.*

Using data in Figure 3.29, the interplay between the inlet shift reactor H_2O/CO ratio and product gas composition is shown in Figure 3.30. These data suggest the H_2O/CO ratio at the inlet of the Water Gas Shift reactor should be kept above 2 or for maximum yield of CO_2 and H_2. A H_2O/CO ratio of approximately 2 corresponds to a reformer (H_2O+O_2)/ biomass ratio of about 1.5, and a H_2O/O_2 ratio of 5. The H_2O/CO ratio presented here is consistent with the data reported by Aznar and co-workers in their study of H_2 production by biomass gasification with steam-O_2 mixtures using a water gas shift reactor (Aznar, M., et al., 2006).

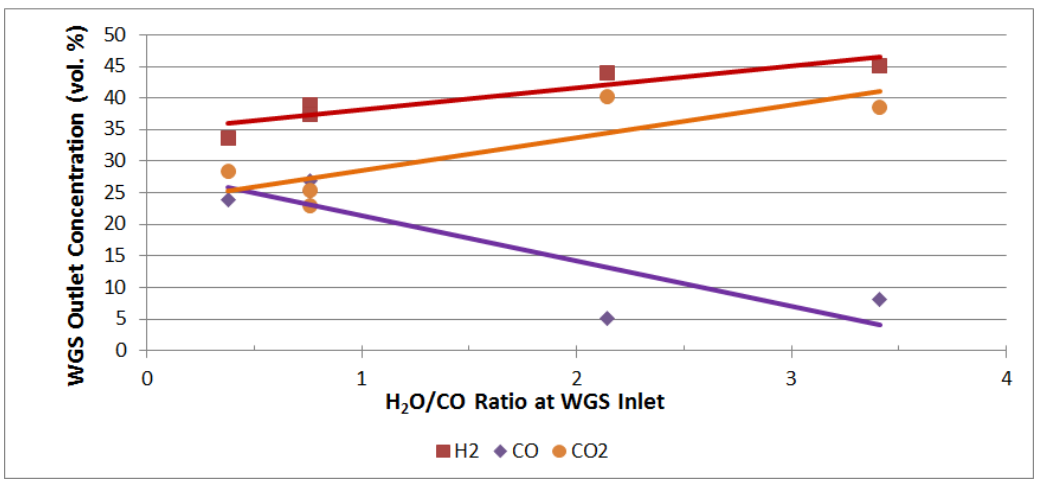

Figure 3.30. *CO_2, H_2, and CO gas outlet concentration as a function of the H_2O/CO ratio at the Water Gas Shift reactor inlet.*

A comparison of the product gas composition with the calculated thermodynamic equilibrium can provide additional insight into the WGS reactor performance. The temperature dependent equilibrium constant K_{eq} for the WGS reaction is given by (Moe, 1962):

$$K_{WGS} = \frac{[CO_2][H_2]}{[CO][H_2O]} = \exp\left(-4.33 + \frac{4577.8}{T(K)}\right) \tag{3.19}$$

The Water Gas Shift reaction is exothermic, and therefore the equilibrium constant decreases with increasing temperature. Using the product gas composition data above and a mole fraction of 0.1 for H_2O based on the process model calculations, a value of 40 for K_{WGS} corresponding to 298°C is estimated. In comparison, the exit temperature of the WGS reactor averaged about 275°C, which gives an equilibrium constant of about 55. Comparing these two values suggest that the gas composition is still significantly far from equilibrium and improvements in CO_2 and H_2 gas yield may be possible to the WGS reactor system.

WGS Reactor Operational Challenges

During the course of testing we encountered periodic temperature spikes in the WGS reactor that exceeded the catalyst operating limit of 325°C. An example of the thermal excursion is shown in Figure 3.31. These temperature excursions appeared to cause reduced WGS activity as indicated by lower than expected CO_2 yield and CO conversion efficiency during these periods. Presumably, the high temperatures may have sintered the catalyst causing it to lose its activity. We then replaced the spent reactor catalyst with fresh, reduced catalyst and resumed testing which resulted in the WGS reactor returning to its previous conversion efficiency.

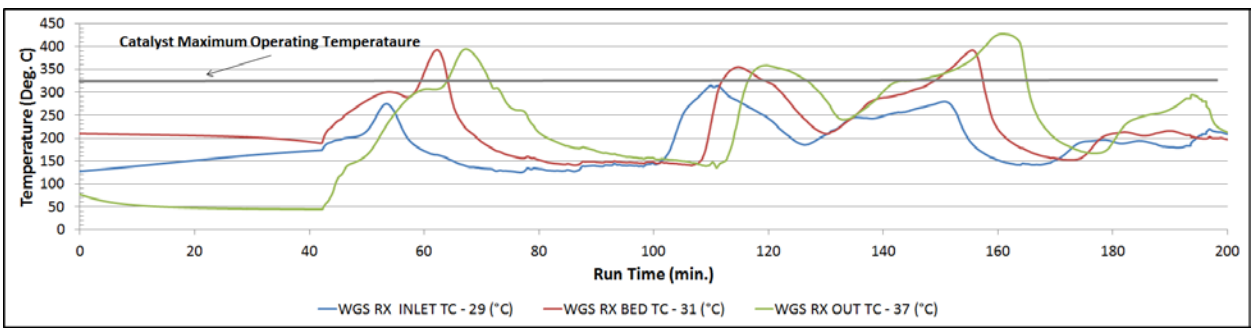

Figure 3.31. *Example temperature excursion in the Water Gas Shift Reactor.*

During the course of several tests we also observed a gradual increase in pressure drop across the WGS reactor bed, which was several times over that expected from just flow rate and catalyst bed considerations. An examination of the reactor inlet and bed showed that fine coke-like particles and some tar had deposited on the surfaces of the reactor inlet. These contaminants may have also contributed to the reduced activity by blinding the catalyst surfaces and preventing efficient contact of the reactant gases with the catalyst surface.

Future WGS Reactor Optimization

One approach to improve the gas yield is to water cool the reactor bed with a shell and tube heat exchanger coupled to the WGS reactor. In this configuration the heat exchanger extracts heat from the exothermic WGS reaction keeping the reactor bed operating at a steady temperature. Furthermore, this heat recovery approach is especially beneficial as the water can be converted to steam for use in the reformer. In addition, an extra gas clean-up chamber such as a high temperature candle filter is desirable for removing the small particles that escape the cyclone and the tar destruction catalyst.

In summary, the WGS reactor significantly improved the gas yield of the CO_2 and H_2 while reducing the CO content of the product gas. The H_2O/CO ratio upstream of the reactor

inlet is an important parameter, and to get good CO conversions a ratio > 2 is needed. By optimizing the temperature profile of the reactor and reducing particle deposition, it is expected that higher WGS conversion performance can be achieved while generating additional amounts of steam for the reformer.

3.2.2.4. Effect of Operating Parameters on Product Gas Composition

The goal of these tests is to determine the effects of the reformer operating conditions on the product gas composition, and determine a preferred operating condition for the reformer in longer duration testing. There are various operational parameters that suitably describe the steam-oxygen biomass gasification process including the Equivalence Ratio (ER), the Gasification Ratio (GR), and the Steam to Oxygen Ratio (S/O):

$$Equivalence\ Ratio, ER = \frac{\left[\frac{\dot{m}_{O2}}{\dot{m}_{bio}}\right]_{Act}}{\left[\frac{\dot{m}_{O2}}{\dot{m}_{bio}}\right]_{Stoich}}, (in\ units\ of\ \ kg/kg) \tag{3.20}$$

$$Gasification\ Ratio, GR = \left[\frac{(\dot{m}_{H2O} + \dot{m}_{O2})}{\dot{m}_{bio}}\right], (in\ units\ of\ \ kg/kg) \tag{3.21}$$

$$Steam\ to\ Oxygen\ Ratio, S/O = \left[\frac{\dot{n}_{H2O}}{\dot{n}_{O2}}\right], (in\ units\ of\ mol/mol) \tag{3.22}$$

We note that the GR is a term defined by Gil and co-workers to characterize the combined effects of reactant steam, oxygen and biomass on product gas composition in steam-oxygen driven biomass gasification (Gil., J., et al., 1997, 1999). The effects of these operating parameters on the gasification performance as defined by the CO_2, H_2, and CO product gas concentration and the reaction temperature are evaluated over a relatively wide range of operating conditions. These data were collected downstream of the gasifier exit and without any gas conditioning operations such as the Water Gas Shift and Tar Destruction reactors. The results of these tests are presented in the following sections.

Effect of ER, GR, and S/O on Temperature and Product Gas Composition

The Equivalence Ratio and Gasification Ratio affects the product gas temperature in a nonlinear manner as shown in Figure 3.32. The temperature initially rises as the ER increases from 0.15 to 0.25, and then levels off as the ER is increased to 0.33. The effect of the Equivalence Ratio (ER), Gasification Ratio (GR) and Steam to Oxygen ratio (S/O) on gas composition is presented in Figures 3.33 – 3.35. The CO_2 content gradually increases from about 20% (vol.) to over 30% (vol.) as the GR and S/O increases. The H_2 content is between 35 and 40% (vol.), and somewhat surprisingly, is constant or even shows a slight decrease in concentration over the ER, GR and S/O ranges studied. The variation of CO concentration with GR and S/O ranges between 15 and 30 % (vol.) for these conditions, and decreases with increasing GR and S/O. Methane concentration remains reasonably constant over the 3- 5% (vol.) range for the GR and S/O values studied.

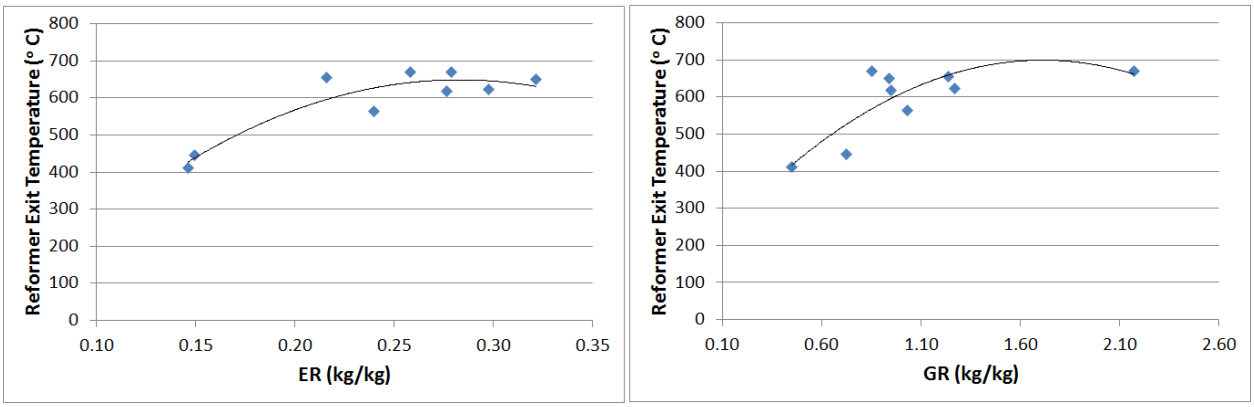

Figure 3.32. Reformer exit temperature as a function of the Equivalence Ratio and Gasification Ratio. A simple second-order polynomial fit to the data is performed to show trending. (Tests 138-21, 143-22, 205-30, 215-32)

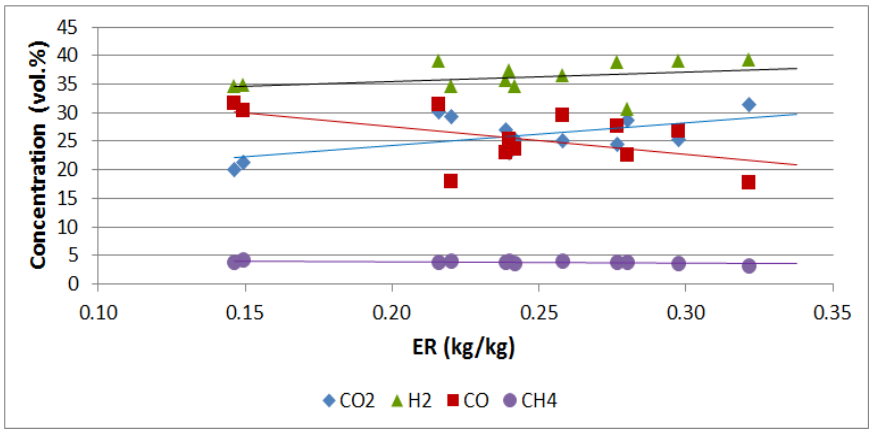

Figure 3.33. *Effect of the Equivalence Ratio (ER) on the product gas (dry gas basis) composition (Tests 138-21, 143-22, 205-30, 215-32)*

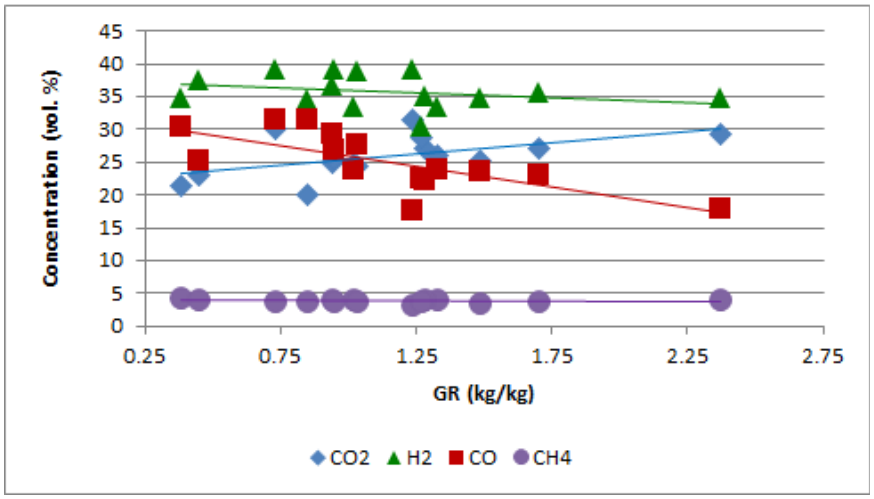

Figure 3.34. *Effect of the Gasification Ratio (GR) on the product gas (dry gas basis) composition (Tests 138-21, 143-22, 205-30, 215-32)*

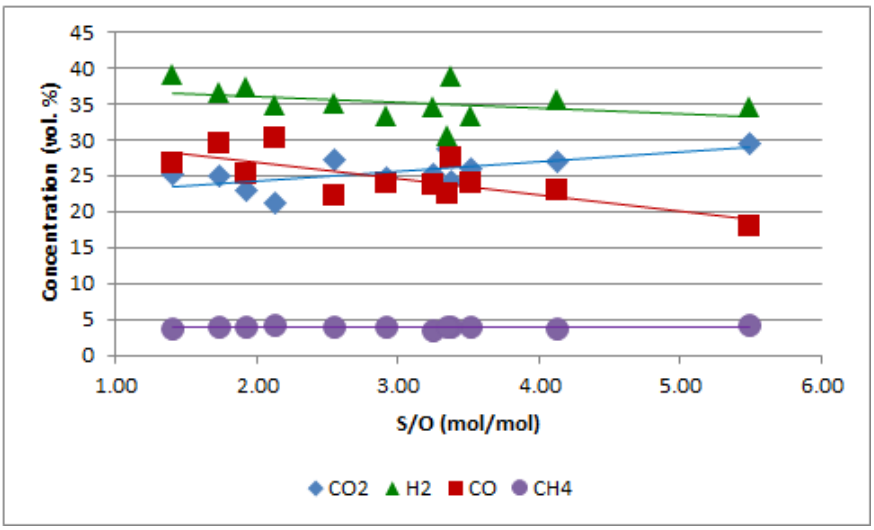

Figure 3.35. *Effect of the Steam to Oxygen ratio (S/O) on the product gas (dry gas basis) composition (Tests 138-21, 143-22, 205-30, 215-32)*

The behavior of the H_2/CO and CO/CO_2 ratios is shown in Figure 3.36 for various GR and S/O conditions. The H_2/CO ratio increases with GR and S/O, and conversely, the CO/CO_2 ratio decreases with higher GR and S/O values.

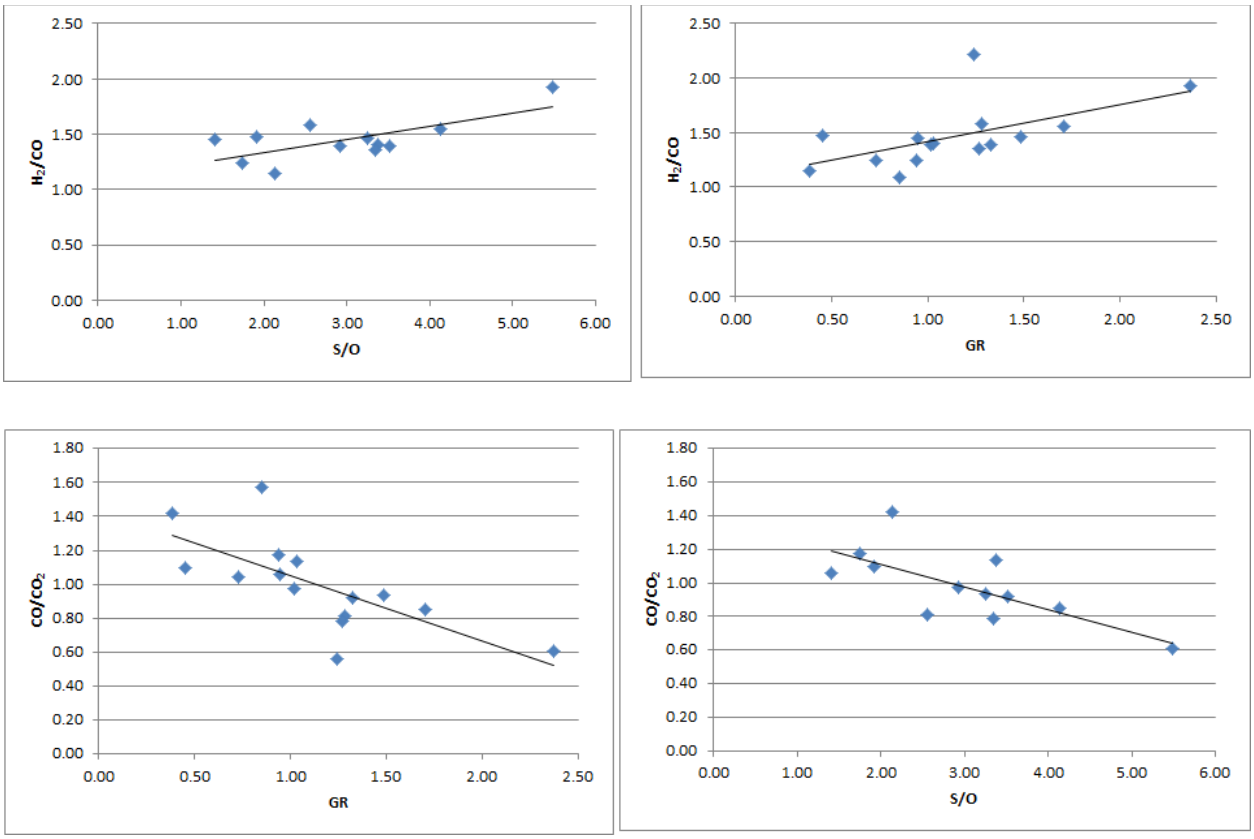

Figure 3.36. *H_2/CO and CO/CO_2 ratio for various S/O and GR values (Tests 138-21, 143-22, 205-30, 215-32)*

The effect of the GR and ER on product gas flow rate and product gas yield is shown in Figure 3.37. A linear dependence of the product gas flow rate and gas yield with GR and ER is observed, respectively.

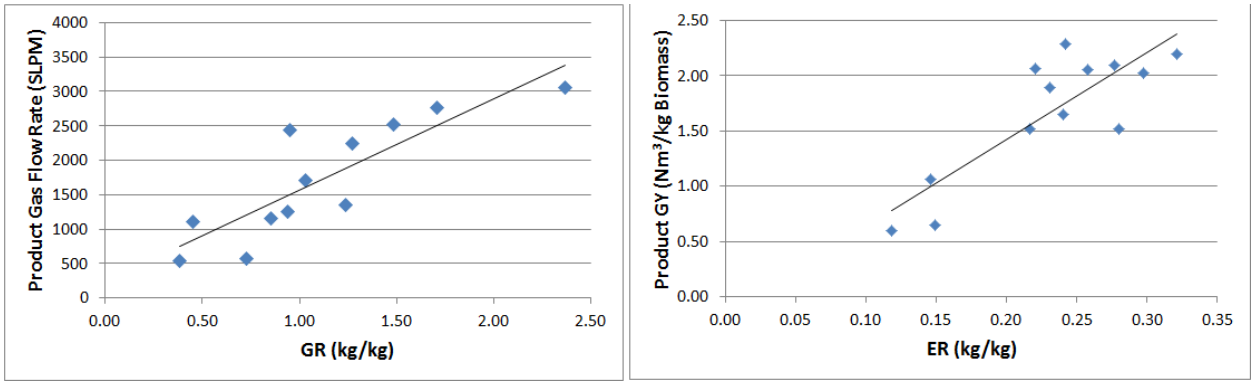

Figure 3.37. *Effect of the product was flow rate and gas yield on the GR and ER. The gas yield, GY, is the volume of product gas generated per kg of biomass added. (Tests 138-21, 143-22, 205-30, 215-32)*

The temperature and compositional trending of the product gas in Figures x-x can be interpreted within the framework of the reforming, oxidation, water gas shift reactions:

Reforming:

Boudouard: $C_{(s)} + CO_2 \leftrightarrow 2CO$, $\Delta H = +172$ kJ/mol (3.23)

Steam Reforming: $C_{(s)} + H_2O \leftrightarrow CO + H_2$ $\Delta H = +131$ kJ/mol (3.24)*

Methanation:

$CO + 3H_2 \leftrightarrow CH_4 + H_2O$ $\Delta H = -206$ kJ/mol (3.25)

$C_{(s)} + H_2 \leftrightarrow CH_4$ $\Delta H = -87.4$ kJ/mol (3.26)

Oxidation:

$C_{(s)} + 1/2O_2 \leftrightarrow CO$ $\Delta H = -111$ kJ/mol (3.27)*

$C_{(s)} + O_2 \leftrightarrow CO_2$ $\Delta H = -408.8$ kJ/mol (3.28)*

Water Gas Shift Reaction:

$CO + H_2O \leftrightarrow CO_2 + H_2$ $\Delta H = -40$ kJ/mol (3.29)*

where * denotes the primary reactions.

Starting with Figure 3.32, the exit gas temperature initially increases with increasing ER and GR. This behavior is suggestive of an increase in the amount of oxygen added to the system. The addition of oxygen promotes the exothermic oxidation reactions and heat release to the system. As more heat is generated, the temperature continues to rise which then promotes the endothermic Boudouard reaction and the steam reforming reactions. Since these reactions absorb heat, any further increase in the gas temperature is inhibited and the temperature rise flattens with increasing ER and GR. The increase in ER and GR also increases the flow rate which may increase the sensible heat loss in the system.

The increase in CO_2 concentration with the ER, GR and S/O is probably due to a combination of effects of oxygen, steam and product gas flow rate. As the GR increases, the

amount of oxygen fed to the reactor increases which promotes the combustion reaction resulting in increased CO_2 yield. At higher GR, a larger H_2O concentration is also introduced to the reactor which absorbs more heat and lowers the temperature. This promotes the water gas shift reaction at the expense of the Boudouard reaction resulting in the enhancement of CO_2 concentration, and a reduction in the CO yield. As noted above, the increase in GR increases the product gas flow rate which increases could increase the sensible heat loss of the reactor.

In pure steam reforming, the H_2 concentration increases on increasing steam to biomass ratio. In contrast, the H_2 concentration in these data slightly decreases due the presence of oxygen and steam. This may result from a self-balance of exothermic and endothermic reactions in the reactor. For example, as higher amounts of oxygen are added to the system an increase in the oxidation reactions occur. This generates greater heat release and a temperature increase. The increase in temperature enhances the rate of steam reforming reactions, which then consume the heat in the generation of H_2. As more heat is consumed the hydrogen rate of production is slowed and, on balance, the production of H_2 is relatively constant. Hydrogen may react with oxygen which would cause a decrease in its outlet concentration.

The downward trend of CO with increasing GR, ER, and S/O ratios is presumably due to increased steam flow and reduced temperature. A higher steam concentration promotes the water gas shift reaction at the expense of the Boudouard and steam reforming reactions, which are source reactions for the generation of CO. These trends are in general agreement with other researchers who have gasified biomass with steam and oxygen (Wang and Kinoshita, 1992; Gil, J., et al., 1997, 1999; Lv, P., et al., 2007; Kitzler, H., et al., 2011; Meng, X, et al., 2011; Ran, J. and Li, C., 2012). A comparison to other steam-oxygen gasification experiments are presented in Table 3.20.

Table 3.20. Comparison of GO Operating Conditions and Gas Composition with Literature Data

Parameter	Test: 205-30	Literature[1]	Literature[2]
Reformer Type	DD	FB	DD
Operating Conditions			
Steam Flow Rate (kg/min)	1.21	0.05	0.069
O_2 Flow Rate (kg/min)	0.29	0.019	0.036
Biomass Feed Rate (kg/min)	0.88	0.075	0.11
S/O (mol/mol)	4.13	4.7	3.4
GR (kg/kg)	1.70	0.92	0.95
ER (kg/kg)	0.22	0.2	0.22
S/B (kg/kg)	1.37	0.72	0.63
Pressure (bar)	10	3	1
Product Gas Composition (vol.%, dry basis, N_2 free)			
H_2	38.99	33.5	26.42

O_2	0.11		.97
CH_4	4.14	8.0	3.52
CO	25.14	18.6	36.85
CO_2	29.61	28.0	31.96
C_2+	0.6		0.25

DD = Downdraft gasifier, FB = Fluidized Bed, [1]Kitzler, H., et al., (2011), [2]Lv., P., et al., (2007)

3.2.2.5. Tar Destruction Reactor

Tar condensation presents significant operational challenges to downstream machinery including plugging downstream piping, filters, heat exchangers, and catalyst pores. There are two basic strategies to tar removal: 1) internal gasifier treatments and 2) hot gas cleaning external to the gasifier. The internal treatment includes the selection of a suitable operating condition (e.g., temperature, ER, biomass type), the use of bed additives and catalysts, and gasifier design (e.g., downdraft configuration). . The external downstream approach uses physical separation, thermal cracking and catalysts for reducing the tar concentration in the product gas stream. There are a variety of catalysts available in which to crack and destroy the tar including nickel, dolomite, olivine, and silicates. In both cases, sufficient gas residence is necessary to allow the reaction to go to completion.

Simple thermal cracking of tars requires temperatures in excess of 1250°C, which could induce thermal stresses and deformation in the steel reactor wall, especially at the 10 bar operating pressures encountered in this study. Thus we selected an external catalytic approach using olivine, $(Mg,Fe)_2SiO_4$, whose activity occurs in the temperature range from about 850°C to 900°C. Although there are more active catalysts such as nickel and dolomite, the olivine was chosen because of its combined performance of structural robustness at high pressure, inexpensive cost, wide spread availability, and activity.

Tar destruction by olivine in an external reactor was studied by Reed and co-workers who developed a simple first order kinetic expression for tar removal (Reed, T. B., et al, 1994):

$$C = C_0 e^{-k\tau_R} \tag{3.30}$$

where C is the concentration of the tar after a residence time τ_R in the reactor bed, C_0 is the initial tar concentration, and k is the first order rate coefficient, k = 4.37 s^{-1}. At 850°C and a reactor residence time of 0.51 seconds, 90% tar destruction by 1 mm diameter olivine particles was observed. Similar results were obtained by Devi and co-workers, although a calcination time of several hours with air at 900°C was needed to achieve this level of conversion (Devi, et al., 2005).

The gas temperature exiting the Reformer is nominally 700°C; therefore some method of gas heating is needed. A relatively simple approach to gas heating is to add small amounts oxygen to the product gas stream, and react it with the hydrogen in the product gas stream:

$$O_2 + 2H_2 \rightarrow 2H_2O, \Delta H_c = -286 \text{ kJ/mol} \tag{3.31}$$

The estimated oxygen flow rate to achieve the olivine operating temperature is calculated by an enthalpy balance approach where adiabatic temperature and composition at constant pressure is assumed. In this process it is assumed that hydrogen is in excess of oxygen, that oxygen is completely consumed, and that the gas flow components are just O_2, H_2, N_2 (purge), and H_2O. The mole amounts of the reactants are taken from the experimental gas flow rate inputs for a 4000 SLPM test. The results of this calculation is shown in Figure 3.38, which indicate an added oxygen flow rate of 50 SLPM is sufficient to generate a product gas temperature of 850°C.

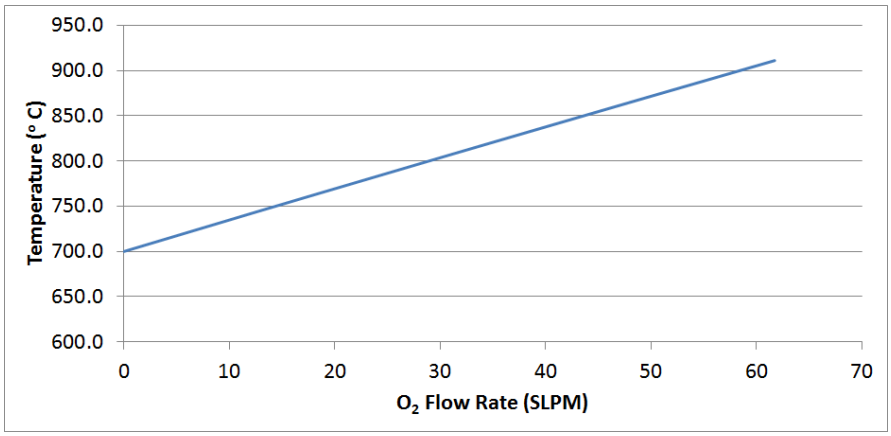

Figure 3.38. *A plot of temperature vs. oxygen flow rate for product gas heating.* Reaction Conditions: *Flow Rate: 4000 SLPM; Initial Temperature: 700°C.*

The Tar Destruction Reactor was tested under operating conditions at flow conditions between 2500-4000 SLPM, and 10 bar pressure. An example of the gas heating is shown in Figure 3.39 and indicates successful gas heating to 850°C was accomplished with an oxygen flow rate of about 25 SLPM, about half what we initially calculated. Steady oxygen flow rate and temperature was achieved over the duration of the test. The reactor was easily driven to temperatures near 950°C with higher oxygen flow rates.

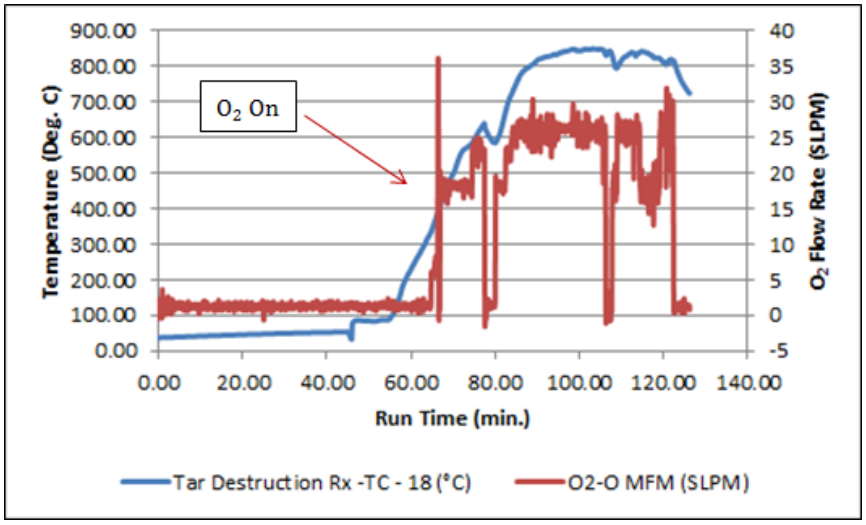

Figure 3.39. *Exit temperature profile for the Tar Destruction Reactor. The oxygen flow rate was turned on at an exit gas temperature of about 450°C. Adjustments in the oxygen flow led to outlet temperature near 850°C. Product Gas Conditions: 4000 SLPM, 10 bar. Reactor: 15 cm diameter x 30 cm depth, 9.5 kg olivine.*

We can estimate the efficiency of tar conversion using the rate coefficient k given by Reed and co-workers, and the gas residence time τ_r of 0.2 seconds in the reactor under our operating conditions. The tar conversion efficiency, CE_{tar}, is given by

$$CE_{tar} = (1 - \exp(-k\tau_r) \quad (3.32)$$

The performance of this reactor is limited by the reactor residence time. For the test conditions here we expect about 60% tar conversion using the kinetic parameters given Reed and co-workers. For a conversion efficiency > 90%, a reactor with a residence time exceeding 0.5 seconds is required.

3.2.2.6. Preferred Operating Conditions

The batch fed GO™ downdraft reactor using pine wood pellets with an steam-oxygen gasification agent generated stable product gas flow rate above 3500 SLPM at 10 bar. The addition of a single packed bed Water Gas Shift Reactor with a Medium Temperature Shift catalyst (CuO-ZnO) generated high yields of CO_2 and H_2 with concentrations routinely exceeding 35 vol. % and 40 vol. %, respectively. Improved thermal control and particle reduction into the reactor bed can enhance the performance and operability of the WGS reactor.

An external Tar Destruction Reactor was demonstrated using olivine as the tar removal catalyst. An oxygen feed system was developed to generate *in situ* gas heating for reaching the olivine operating temperatures of 850 to 900°C. This was accomplished by adding a small flow of 25 -30 SLPM of oxygen just upstream of the Tar Destruction Reactor. It is estimated that about 60% of the tar is destroyed in the reactor based on kinetic conditions given by Reed and co-workers (Reed, T. et al., 1994). The reactor performance was limited by a small residence

time of about 0.2 seconds, which is 2.5 times less than that given by Reed. Future reactors will be designed with a sufficient residence time to enable >90% tar conversion.

Various operating parameters such as the Equivalence Ratio, the Gasification Ratio, and the Steam to Oxygen ratio were analyzed over a wide range of operating conditions to determine their effect on product gas composition. These results show that the steam-oxygen gasification agent generates a very different product gas composition compared to just oxygen (air) or just steam gasification. Through adjustment of these operating parameters, the CO_2 and H_2 product concentration are preferentially formed over CO and CH_4 content. These results provide a set of operating conditions going forward for demonstrating longer-duration test runs and are presented in Table 3.21.

Table 3.21. Preferred Operating Conditions (4000 SLPM, 10 bar Operation)

Parameter	Value
Gasification Agent	
Medium	Steam-Oxygen
Steam/Oxygen Ratio	4-5 (mol/mol)
Gasification Ratio	1-2 (kg/kg)
Equivalence Ratio	0.25-0.33 (kg/kg)
Fuel	
Type	Pine Pellets
Feed Rate	1.7-1.9 kg/min
Tar Destruction Reactor	
Bed	Olivine
O_2 Flow Rate	25-30 SLPM
Temperature	850-900°C
Water Gas Shift Reactor	
Catalyst	MTS CuO-ZnO
H_2O/CO	2-3
Operating Temperature	200-300°C

3.2.2.7. Extended Duration Testing

The objective for this set of experiments was to benchmark the GO^{TM} system performance under conditions of continuous fuel feeding and extended test operation at 4000 SLPM, 10 bar operation. To demonstrate longer duration reformer operation, a continuous biomass feed assembly was designed, fabricated and tested. These results are discussed in the following sections.

Design of Continuous Biomass Feed System

The continuous biomass feed system consisted of two assemblies, a fuel transport system and a fuel injection system. The fuel transport system uses an air-blown pneumatic conveyance for delivering feed to the injector. The fuel injection system consists of hopper and lock-hopper configuration, which includes a storage hopper, a cup valve assembly to collect a biomass

sample, a sequentially timed three-valve lock-hopper for purging, pressurizing and injecting pine wood pellets into the reformer at operating pressure. A schematic diagram of the feed system apparatus is shown in Figure 3.40.

Biomass is fed to the feed hopper using a dilute phase conveyance approach through a 2 inch PVC pipe. In this mode, the material is transported at high velocities and low pressure through the system while being suspended in air. To keep the material in suspension, it is necessary to maintain a minimum conveying air velocity that, for most materials, is on the order of 2500 – 6000 feet/minute. Initially, two in-house laboratory air compressors were connected in parallel to supply the air flow. This was later upgraded to a single regenerative air blower (Busch Vacuum, 4.5 hp, 206 CFM) to provide the conveying air velocity. The volumetric air flow output is adjusted to about 100 CFM to give a velocity of about 4600 fpm. A 30 L feed storage silo was used to store the wood pellets during operation. The outflow of the silo connects to the 2 inch PVC conveyance pipe through a ball valve and tee. A pneumatic vibrator is used to shake lose any feed bound inside the pipe. The wood pellets are delivered to the feed hopper by pneumatic or dilute phase conveyance in a 2 inch pipe. To convey the biomass, the outflow of the air blower is powered up and the air sent into the 2 inch conveyance pipe. The ball valve is opened, and wood pellets drop down from the storage silo into the conveyance pipe. The pellets are entrained in the air flow and carried to the feed hopper. To check that the feed is being fed to the reformer, a camera is mounted in the feed hopper to periodically view the feed level during the course of the test.

The feed hopper operates through a timed multi-step valve opening and closing sequence between a rotating feeder cup valve and two solenoid ball valves. The sequence consists of loading, purging, pressurizing, and injecting the biomass into a collection chamber, and injecting the pressurized fuel into the gasifier magazine. Using Figure x as a guide, the basic procedure is as follows. The rotating cup valve (SOBV-F4) in its upward position is filled with slug of biomass from the hopper into its reservoir. The cup valve rotates down and drops the biomass into a feed chamber (C-1). The feed chamber consists of three solenoid valves. The top (SOBV-F1) and bottom (SOBV-F3) valves serve to isolate the biomass from the system for pressurization. A middle valve (SOBV-F2) is kept open all the time and serves as a redundant isolation valve. The top solenoid operating ball valve opens and receives the biomass from the cup valve. The bottom valve is closed until which time the biomass is injected into the reformer. After the biomass is delivered into the chamber, both solenoid ball valves close and the chamber is pressurized by opening SOBV-5 with nitrogen to a value equal to the reformer pressure. The bottom solenoid valve then opens and drops the biomass into the reformer and then closes and the process then repeats.

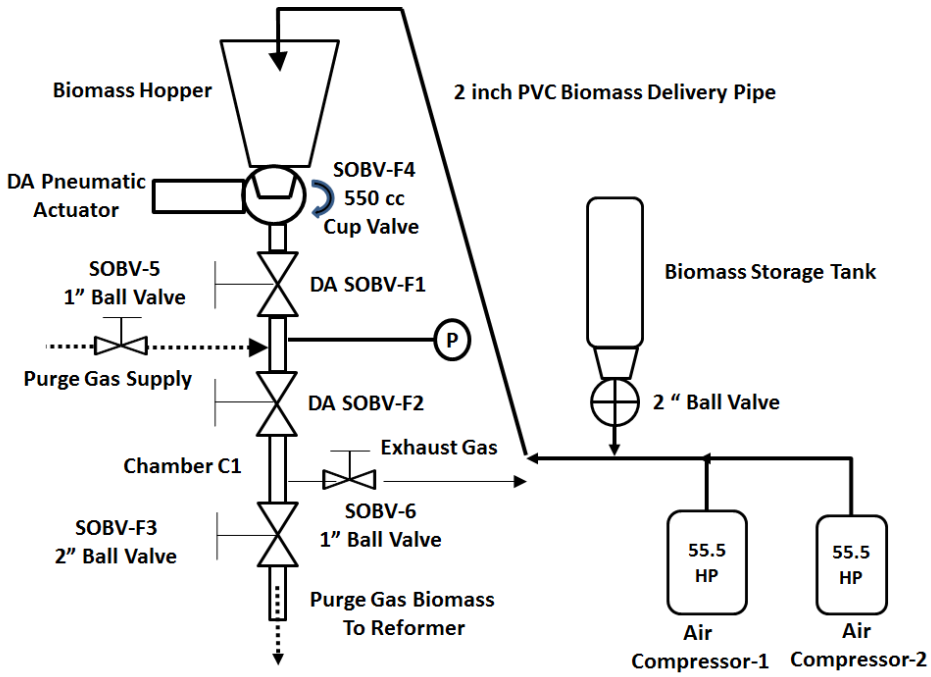

Figure 3.40. *Continuous biomass feeder assembly for the 4000 SLPM Product Gas demonstration. DA = Double Acting, SOBV = Solenoid Operating Ball Valve, P = Pressure transducer. Position switches were placed on each SOBV to determine the open/shut status of the valve.*

The feed system is designed to deliver biomass fuel at a rate equal to its burn rate. Following the approach given in Section 3.1.1.2, the biomass feed rate to the reformer is 1.5 kg/min. Using a 0.6 L cup volume, and a fuel bulk density of 0.7 kg/L, the mass addition to the reformer is 0.42 kg. Thus, the frequency of addition to match the burn rate is thus (0.42 kg)/(1.5 kg/min), or one injection every 17 seconds. A similar approach for the full sized 20,000 SLPM system gives a feed rate of 7.5 kg/min. The calculated feed system delivery rate for a 4,000 and 20,000 SLPM system is summarized in Table 3.22.

Table 3.22. Nominal Biomass Feed Rate to Reformer

Product Gas Flow Rate (SLPM)	Oxygen Mass Flow Rate (kg/min)	Biomass to O_2 Mass Ratio	Biomass Feed Rate (kg/min)	Biomass Bulk Density (kg/L)	Feeder Cup Volume (L)	Mass Addition (kg)	Biomass Injection Rate
4,000	0.37	4.0	1.5	0.7	0.6	0.42	1 every 17 seconds
20,000	1.85	4.0	7.5	0.7	7.5	5.2	1 every 40 seconds

The biomass addition frequency is controlled automatically by the data control system so that during operation the fuel delivery rate can be adjusted to match the biomass burn rate. An example of the valve timing sequence for loading and delivering the biomass to the reformer is given in Table 3.23. Photographs of the fabricated continuous feed assembly and the final system integration are presented in Figures 3.41 -3.42.

Table 3.23. Feed Control Program Sequence

Step	Action	SOBV F1	SOBV F2	SOBV F3	SOBV F4	SOBV 5	SOBV 6	Nominal Step Time (sec)
1	System initialized to starting positions	Closed	Closed	Open	Closed	Closed	Closed	3
2	Vent Chambers 2 and 3	Open	Closed	Open	Closed	Closed	Closed	2
3	Load fuel into Chamber 2	Open	Closed	Open	Open	Closed	Closed	2
4	Lock fuel in place in Chambers 2 and 3	Closed	Closed	Open	Closed	Closed	Open	2
5	Pressurize fuel in Chambers 2 and 3	Closed	Closed	Open	Closed	Open	Closed	2
6	Inject fuel into reformer	Closed	Open	Open	Closed	Closed	Closed	3
7	Return to Starting positions	Closed	Closed	Open	Closed	Closed	Closed	3

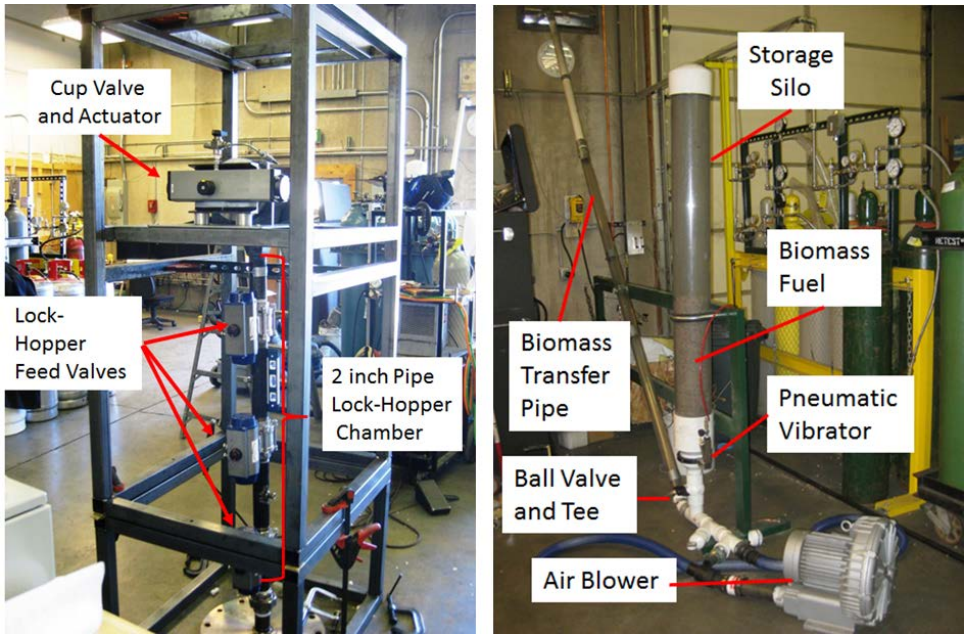

Figure 3.41. *Constructed continuous biomass feed system for the 4000 SLPM product gas demonstration. Left: Pressurized Lock-hopper (prior to integration). Right: Pneumatic conveyance system*

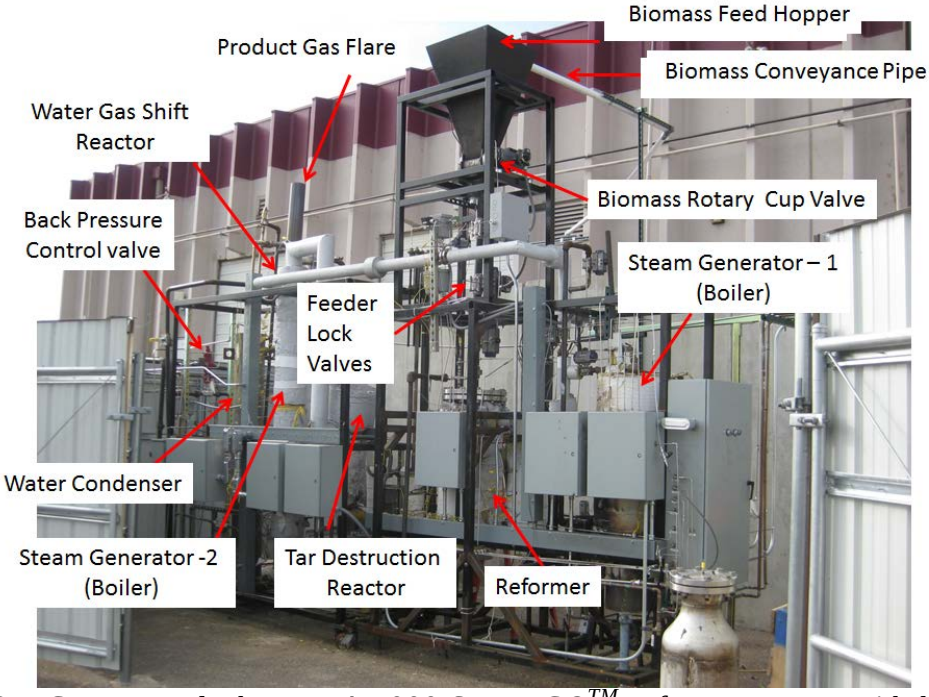

Figure 3.42. *Constructed Phase IIIA 4000 SLPM GO^{TM} reformer system with biomass feed system.*

Design Verification Testing

Several verification tests and modifications were conducted on the feed system to ensure it performed to its design specifications. These tests included optimization of the valve sequence

and timing, feed level in reformer, inert gas pressurization and purge flow, and the mass of biomass delivered to the reformer. One of the key challenges overcame was the blockage of the biomass flow from the feed pipe into the reformer (Figure 3.43).

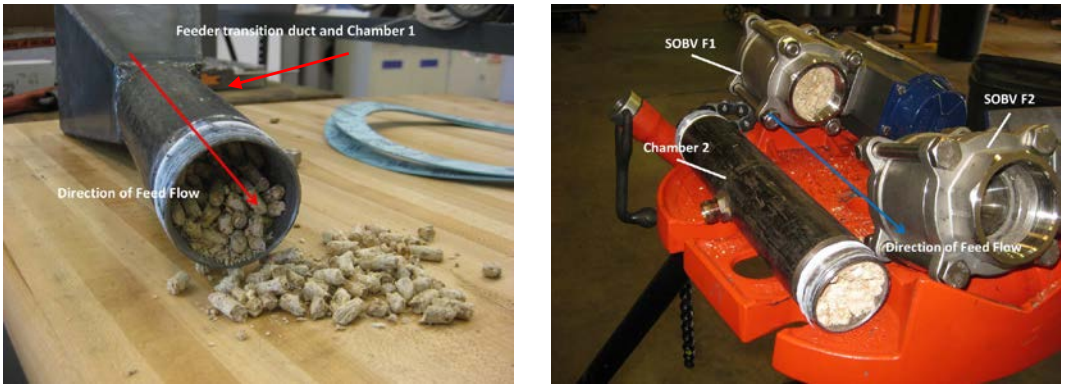

Figure 3.43. *Biomass Feed Assembly Blockage. Chambers 1 and 2, and SOBV F1 and SOBV F2 were hard-packed with wood pellets preventing the downward flow of the biomass from the hopper. The direction of the wood pellet flow is indicated by the arrows.*

Various factors contributed to the biomass blockage into the reformer. In one case it was observed during testing that the ball valves for the feed delivery system were not closing completely. This allowed moisture to rise up into the feed source which caused the wood pellets to dissolve into a sticky, hard-packed mass. This eventually prevented the pellets from flowing down into the reformer which starved the reformer of fuel. In another instance, the wood pellet feed rate was too high into the reformer which caused the pellet feed flow in the pipe to backup and choke until it stopped. In both cases, once the reformer was starved of its fuel the reformer climbed to excessive temperatures and the test was shut-down.

The biomass feed blockage in the feed chamber was corrected with three actions- inserting a higher torque double-acting actuators on SOBV F1 and SOBV F3 to ensure valve closure, inserting a nitrogen purge gas flow system from Chamber 2 down into the reformer to prevent unwanted steam rising up into the feed system, and implementing a computer controlled valve control algorithm that matched the biomass (i.e., carbon) input from the wood pellets to the carbon output as measured by the flow system diagnostics.

Extended Run Test 163-26

Having corrected the fuel plugging in the feeder, a series of extended run tests with the continuous feed system was performed with the goal of achieving 4000 SLPM, 10 bar product gas production. The extended run tests were performed under the operating conditions established in previous batch mode tests.

Initial tests were run at reduced steam-oxygen and biomass feed rate to ensure the system configuration was operating properly before pushing the system to the 4000 SLPM design goal. The test began by loading the gasifier bed with charcoal and pine wood pellets in the manner described in previous batch experiments. This was followed by loading fuel into the feed system hopper above the gasifier bed using the pneumatic conveyor. In total about 36 kg of pine pellets

was transferred to the hopper. Following the fuel loading, the super heater was ignited and a steady flow of steam-oxygen at 475°C was injected into the reformer. The reformer was ignited near the 45 minute mark.

The results of Test 163-26 are shown in Figure 3.44 with the key test and operational events identified. As the biomass burned down in the reformer magazine the fuel was replenished by the activation of the pneumatic fuel conveyance and lock-hopper injection systems. The fuel in the reformer was burned for about 30 minutes before the automated feed system was activated. The amount of biomass added to the reactor was registered so that the carbon feed rate could be matched to the carbon present in the product gas. The trigger for activating the fuel addition was accomplished by monitoring the temperature rise at three vertical points in the upper biomass reformer bed. This was later replaced with an optical level sensor which proved to be more accurate and reliable. Over the course of the experiment, the biomass, H_2O and O_2 flow rates were adjusted until the product gas flow rate steadied near 2000 SLPM, or about half our target flow rate (Figure 3.44, bottom panel). To achieve this flow rate, an operating condition with an average biomass feed rate of 1.1 kg/min (as received basis), a GR of 1.15 (kg/kg), an ER of 0.26 (kg/kg), and a S/O ratio of 3.6 (mol/mol) was used. With the continuous feed system in operation, the run time was extended about twice as long as the previous batch test runs.

.

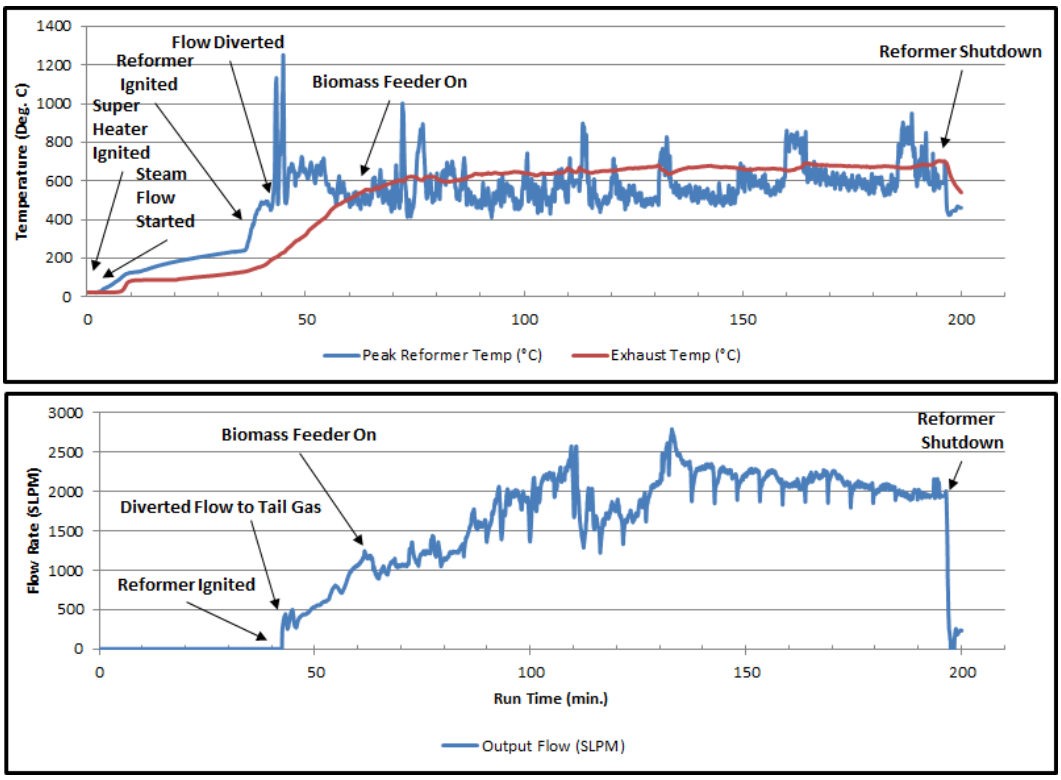

Figure 3.44. Reformer Time History. Top: Reformer bed and exit temperature. Bottom: Product gas flow rate. (Test 163-26)

Extended Run Test 171-28

After demonstrating successful extended run operation of the system at lower feed rates, the system feed rate was pushed with the goal of achieving 4000 SLPM and 10 bar pressure operation in extended operation. The result of this test is shown in Figures 3.45-3.47. The temperature profile at the reformer exit reveals steady operation and its temperature is characteristic of the values encountered in the reduction reaction zone. Through adjustment of the steam and oxygen flow rates, a steady flow product gas flow rate above 3500 SLPM was achieved. Periodic peak flow rates above 4000 SLPM were recorded. The steadiest flow occurred over the last 30 minutes of the run. Here the S/O ratio in this interval averaged about 4.2, while the biomass feed rate was delivered at a rate of 1.9 kg/min (as received). The Gasifier Ratio and Equivalence Ratio were 1.2 and 0.25, respectively. The Gas Yield for this experiment was 1.9 Nm^3/kg biomass.

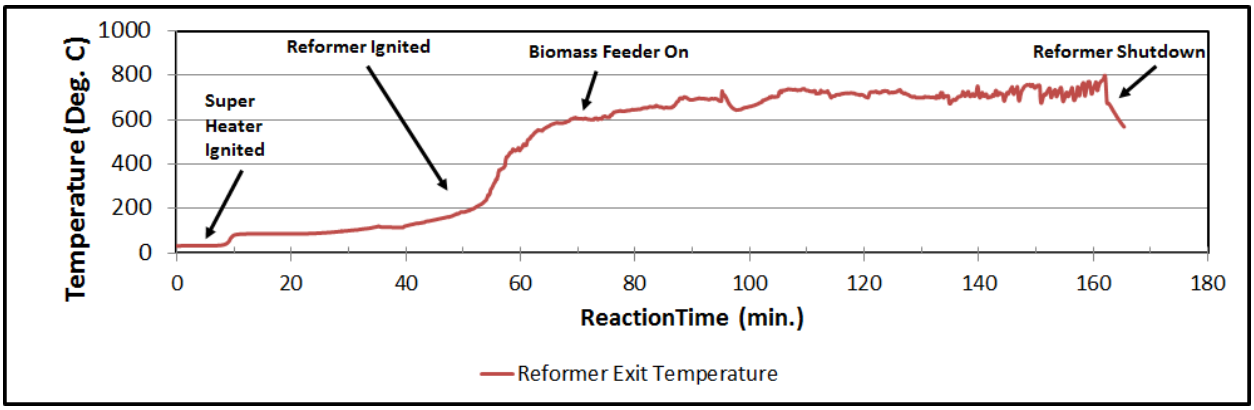

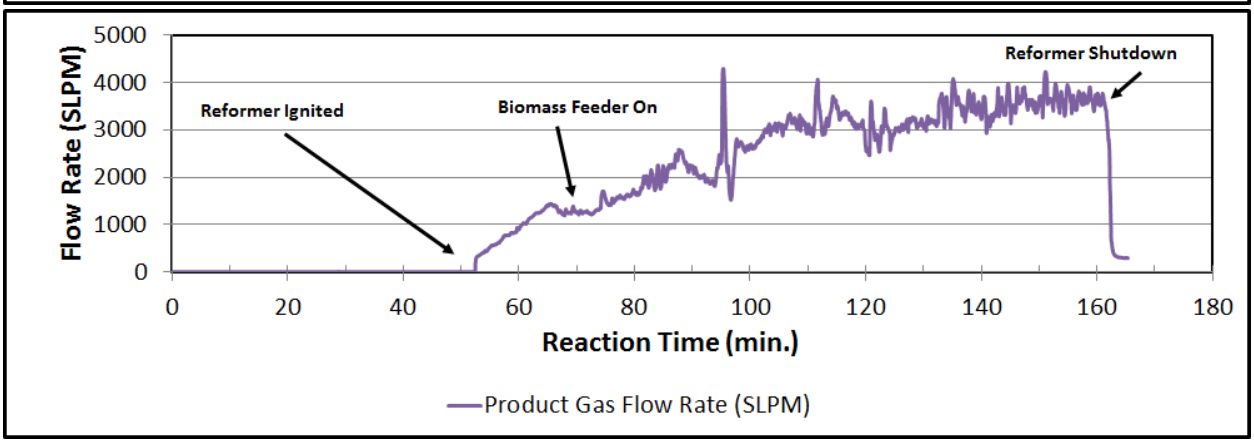

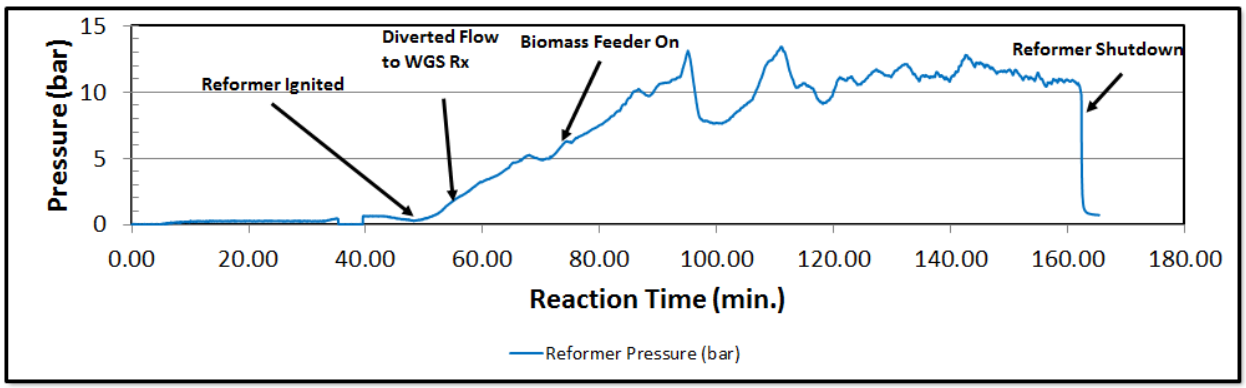

Figure 3.45. *Reformer Time History. Top: Reformer exit temperature. Middle: Product gas flow rate. Bottom: Reformer pressure. (Test 171-28)*

Product Gas Composition

The Water Gas Shift product gas composition and reactor temperature profile for Test 171-28 is shown in Figures 3.46 and 3.47. The gas analysis data was initiated just after the gas was diverted downstream to the Water Gas Shift Reactor. The thermal profile of the Water Gas Shift reactor in Figure 3.47 shows the inlet temperature averaged around 225°C, while the outlet temperature rose to 300°C, which are within the operating temperature of the catalyst. Once the Water Gas Shift reactor temperature equilibrated, the CO_2 concentrations climbed from 20 to near 40 vol. %. Similarly, the H_2 content rose from a low of 30 vol. % to over 40 vol. %. Concurrently, the CO dropped from 30 vol. % to about 4.5 vol. % giving a conversion efficiency of about 85%.

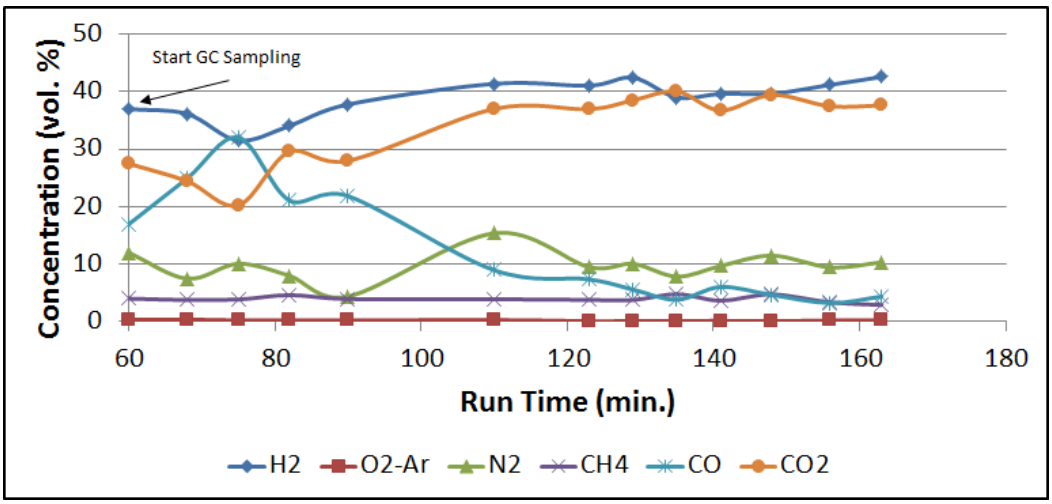

Figure 3.46. *Product Gas Composition (dry basis). The nitrogen purge gas is also shown. (Test 171-28).*

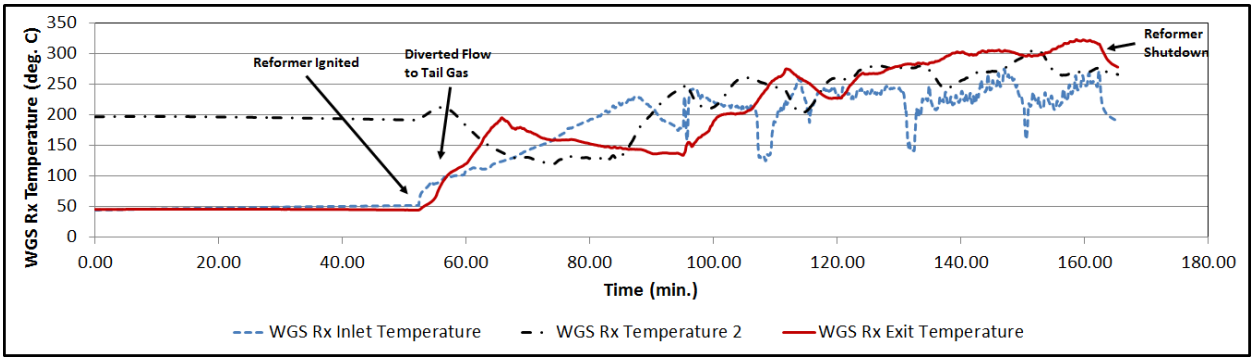

Figure 3.47. *Water Gas Shift Reactor temperatures. Stable WGS reactor conditions were obtained during the test duration (Test 171-28).*

Mass Balance

The mass balance for these test runs is summarized in Table 3.24. The total mass input is comprised of the steam, oxygen and biomass feed rates while the mass output includes the product gas and char flow rates. The char flow rate is determined by measuring the residual mass over the time duration of the test run. The char mass is corrected for an assumed carbon content of 85 wt% on dry, ash-free basis, and the ash content of the biomass.

Table 3.24. Material Balance[1]

Test Run	Total Input				Total Output			Balance
	Steam (kg/min)	Oxygen (kg/min)	Biomass (kg/min)	Total Input (kg/min)	Prod. Gas (kg/min)	Char (kg/min)	Total Output (kg/min)	$Mass_{Out} - Mass_{In}$
163-26	0.68	0.34	1.14	2.16	2.02	0.048	2.07	.048
171-28	1.18	0.49	1.95	3.62	3.54	0.067	3.61	-0.013

[1] Flow rates are averaged values taken after the system reached steady operation

Energy Balance

An energy balance summary for the reformer, defined as Energy Output/Energy Input, for Tests 163-97 and 171-28 is presented in Table 3.25. The enthalpy at temperature T is calculated from the following equation:

$$H(T) = H_f(298.15K) + \int_{298}^{T} C_P dT \tag{3.33}$$

where T is the experimental temperature and C_P is the heat capacity at constant pressure, and 298.15K is the reference temperature. The reformer heat balance is constrained by input/output conditions taken from experimental data including temperature, mass flow rate, pressure, and the biomass ultimate analysis. The steam – oxygen gasification agent, biomass, and product gas inlet and outlet temperatures are listed in Table 3.25. The feed rates are based on a kg per hour

basis. The heat loss through the reactor wall, radiation from the reactor surface, and ash outflow is assumed to be 10% of the heat from the input stream.

Table 3.25. Reformer Energy Balance

Test	Stream	Conditions	Amount (kg)	Total H (MJ)
163-97	Input	$T_{(H2O+O2)}$: 280°C $T_{(Biomass)}$: 25°C	140.97	-593.09
	Output	$T_{(PG)}$: 670°C	124.37	-598.86
	Balance		-16.60	-5.77
171-28	Input	$T_{(H2O+O2)}$: 300°C $T_{(Biomass)}$: 25°C	228.54	-1021.92
	Output	$T_{(PG)}$: 750°C	216.75	-1225.36
	Balance		-11.79	-203.45

To achieve energy balance the output temperature for Test 171-28 the product gas temperature would have to be 950°C, which suggests a significant larger heat loss occurs at the higher rate flow conditions.

Steam Generator-2 Operation

At steady state, the energy requirement for heating the gasification agents (steam and oxygen) and the biomass (with moisture) could be met by heat recovery of the product gas. Thus, one goal of the system tests is to evaluate the efficiency of the Steam Generator-2 operation and energy integration. A plot of the total steam flow rate, (combined Steam Generator-1 and Steam Generator-2 flow rate) and that generated from just Steam Generator-2 is presented in Figure 3.48. Here, Steam Generator-2 generates about 50% of the total flow in the reformer test.

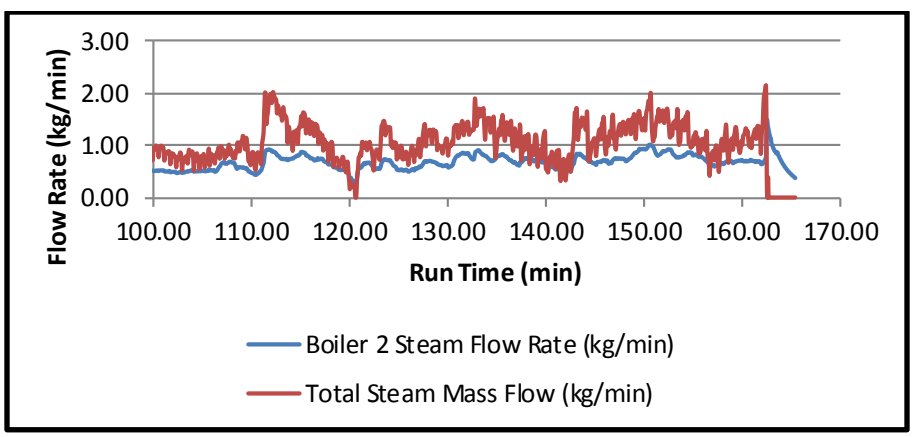

Figure 3.48. *Comparison of the Total Steam Flow Rate (Steam Generator-1 and Steam Generator-2 flow rate) and Steam Generator-2 flow rate (Test 171-28).*

Interestingly, our process model calculations indicate that the heat recovery by Steam Generator-2 should be capable of generating substantially more steam flow than that observed in Figure 3.48. We would expect Steam Generator-2 to produce nearly all of the steam supplied to the reformer based on energy integration (see Process Model Stream Table Summary Appendix A.4). The lower than expected steam flow experienced in actual operation may have resulted from a variety of conditions including thermal losses, failure to reach steady state in the Steam Generator-2 unit, operating an undersized heat exchanger in the Steam Generator-2 unit, and the occurrence of unbalanced steam pressure between Steam Generator-1 and Steam Generator-2 flow streams.

3.2.2.8. Phase IIIA Test Summary

The system testing of a 4000 SLPM (200,000 CFD) demonstrator was successfully carried out. All of the key GO^{TM} reformer system operations for a full scale, field portable CO_2-EOR field unit were successfully demonstrated including continuous fuel feeding, product gas cleanup, tar destruction, heat integration, and CO_2 and H_2 yield enhancement. The Phase IIIA GO system milestone of 4000 SLPM (200,000 SCFD) product gas generation at 10 bar was achieved using both charcoal and wood biomass fuels. Continuous reformer operation of over two hours was demonstrated using a high pressure lock-hopper system with pneumatic fuel conveyance. High yields of H_2 (>45 vol. %), CO_2 (>40 vol. %) product gas were established with the use of a Water Gas Shift reactor. These data demonstrate the viability of the GO^{TM} system for a portable CO_2-EOR system, and provide a scaling path forward for the Phase IIIB unit. The data for batch and continuous operation test runs are summarized in Table 3.25.

Table 3.25. Test Summary for the GO^{TM} Reformer

Parameter	Test: 102-19	Test: 163-26	Test: 171-28
Fuel	Pine Pellets	Pine Pellets	Pine Pellets
Operating Mode	Bach	Continuous	Continuous
Run Time (min.)	58	154	110
Operating Conditions[1]			
Steam Flow Rate (SLPM)	1377	842	1464
Steam Flow Rate (kg/min)	1.11	0.68	1.18
O_2 Flow Rate (SLPM)	313	236	346
O_2 Flow Rate (kg/min)	0.45	0.34	0.49
Biomass Feed Rate (kg/min)	0.91	1.14	1.95
S/O (mol/mol)	4.4	3.5	4.2
GR (kg/kg)	1.71	1.15	1.25
ER (kg/kg)	0.33	0.26	0.24
S/B (kg/kg)	1.21	0.60	0.60
Product Gas Conditions[1]			

PG Flow Rate (SLPM)	2576	2063	3565
PG Flow Rate (kg/min)	2.50	2.00	3.54
Reformer Pressure (bar)	11.0	6.1	11.0
Reformer Exit Temperature (^oC)	710	668	719
Product Gas Composition Downstream WGS (vol.%, dry basis)			
H_2	45.68	48.06	40.06
O_2	0.32	0.06	0.11
N_2	5.60	2.49	9.74
CH_4	2.62	3.73	3.84
CO	7.40	4.72	4.59
CO_2	37.81	40.62	38.30
MW_{avg} (kg/kmol)	21.68	21.76	22.28
Gas Yield (Nm^3/kg Biomass)	2.07	1.27	1.94
Carbon Conversion Eff. (%)	94.85	96.74	94.03
SV (Nm^3/m^2-s)	0.87	0.70	1.21

[1] Averaged values reported after steady operation is achieved

3.2.3. Phase IIIB System Testing

Results from the operational conditions of the Phase III A reformer are used to design a 5X device scale-up to generate 20,000 SLPM (1million SCFD) of combined driver gas. The design criteria for the Phase IIIB system are summarized in Table 3.26.

Table 3.26. Phase IIIB Design Criteria

Parameter	Value	Units
Product Gas Volume Flow Rate	20,000	SLPM
Gasification Medium	Oxygen and Steam	
Operating Conditions		
Steam Feed Rate	7500	SLPM
Oxygen Feed Rate	1700	SLPM
Biomass Feed Rate	9.5	kg/min
S/O	4.5	(mol/mol)
ER	0.2	(kg/kg)
GR	0.9	(kg/kg)
S/B	0.6	(kg/kg)
Product Gas Pressure	10	Bar
Gas Yield	2.1	Nm^3/kg biomass

To operate the system at these higher flow conditions requires modification the biomass feed and steam delivery systems. The results of designing and fabricating these components, and the performance testing of the scaled-up GO^{TM} demonstrator are discussed in the following sections.

3.2.3.1. Continuous Feed System Design and Construction

Using the approach described in Section 3.2.2.7, the biomass feed rate for 20,000 SLPM operation was determined to be 7.5 kg/min (see Table 3.22). We note that at this rate the previous rotary cup valve design will lead to an unmanageable size, high torque operation, and long cycle time. Therefore, a new feed approach was undertaken to enable a high mass injection rate that is cost effective and reliable, and can meet cycle times that are within commercially available actuator specifications.

A linearly activated, two-cup valve approach was chosen as the mode of operation. The design of this valve is shown in Figure 3.49. The valve basically consists of three parts: feed cup slide, cup slide housing, and a linear actuator to move the feed cup slide forwards and backwards. The feed cup contains two 3.7 L cups, labeled as Cup-1 and Cup-2 (6 inch diameter each), and two sets of actuator mounts that attach the cup slide to the linear actuator. The housing has two 6 inch diameter inlet ports, a 6 inch diameter outlet port, and a slot through which the actuator mounts attach. A feed hopper containing the biomass is attached above the unit. As the valve actuator slides forward, biomass drops into Cup-1. Then cup slider reverses its direction and Cup-1 discharges the biomass into the lock-hopper as it traverses the exit port while Cup-2 is filled with biomass. Then the actuator once again moves the cup slide forward to fill Cup-1, while Cup-2 into discharges its contents into the lock-hopper, and fill cup-1. This process is repeated as needed to feed the reformer at the reformer burn rate. The sliding cup valve design dimensions are presented in Appendix A.5.

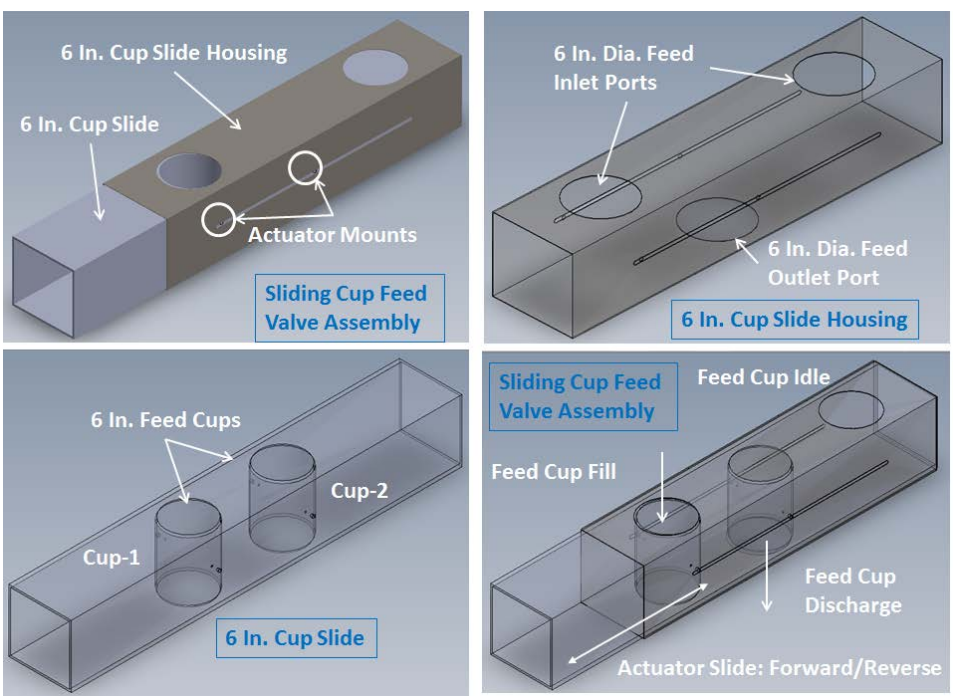

Figure 3.49. *Sliding cup feed valve design. Upper Left: Valve Assembly. Upper Right: Cup slide housing. Lower Left: Feed Cup Slide. Lower Right: Sliding cup feed valve illustrating fuel fill and discharge events.*

The sliding cup feeder valve is coupled to a pressurized lock-hopper system for injecting fuel to the reformer. The integrated design of the feed system including the feed hopper, sliding cup valve and lock-hopper is presented in Figure 3.50. The lock-hopper is constructed from two, 4 inch Solenoid Operated Ball Valves (SOBV). In-between the two valves is a 4-inch diameter pipe to collect the biomass from the cup feeder. The collected feed is pressurized and then injected into the reformer. A redundant 4-inch diameter isolation valve is placed downstream of the lock-hopper to isolate the feed system from the reformer in the event of a process malfunction.

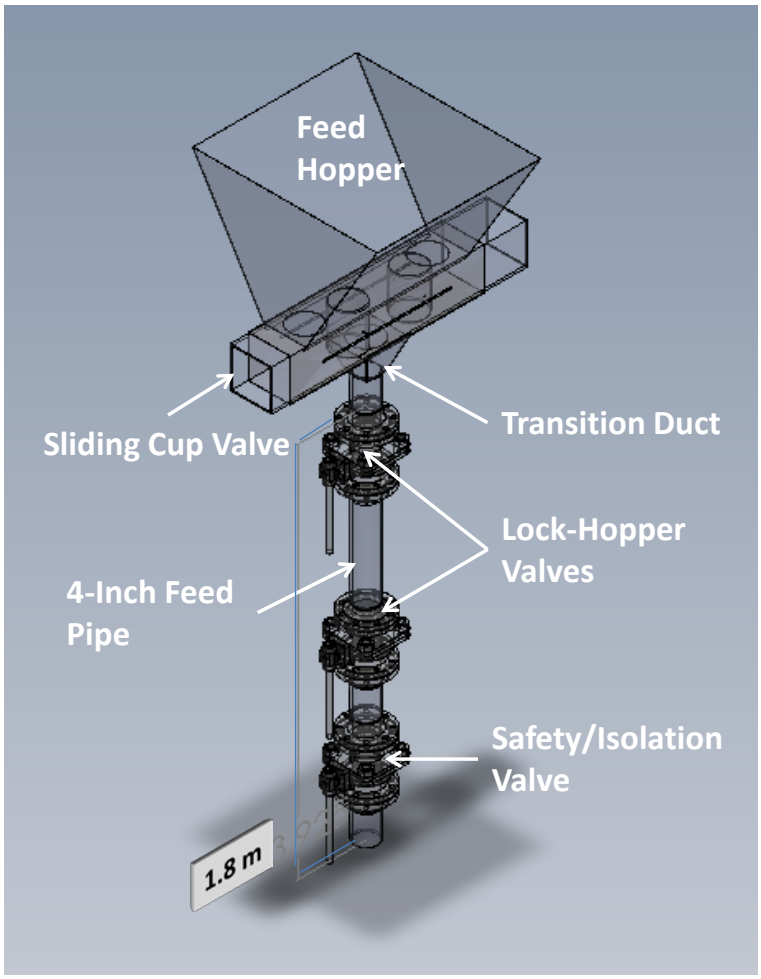

Figure 3.50. *Model drawing of the 450 kg/h feed system showing the integrated configuration of the feed hopper, slider cup valve, and the lock-hopper.*

The process diagram for the entire feed system is presented in Figure 3.51. The feed system operates basically in the same manner as the previous lock-hopper demonstrated for the 4000 SLPM system. In summary, a pneumatic conveyor transfer biomass from a storage silo to the feed system. The feed system then injects biomass intermittently across a small pressure

boundary between the feeder and the reformer. This is accomplished by the timed sequential opening and closing of the slider valve, and the pressurization of the top and bottom valves lock-hopper valves. In this manner, the top valve is opened to receive material from the sider valve and into the lock hopper, while the bottom valve is maintained in a closed position. The material discharges into a 5 L metering chamber, which is slightly oversized to provide surge capacity, flow leveling, and isolation from the process. The top valve is closed, the lock hopper is brought slightly above system pressure, 10 bar, with nitrogen. After the pressurization, the bottom valve is opened, and the material is discharged into the reformer. Following discharging and injection of the fuel from the lock hopper chamber, the bottom valve is closed and the vessel depressurized to allow another cycle.

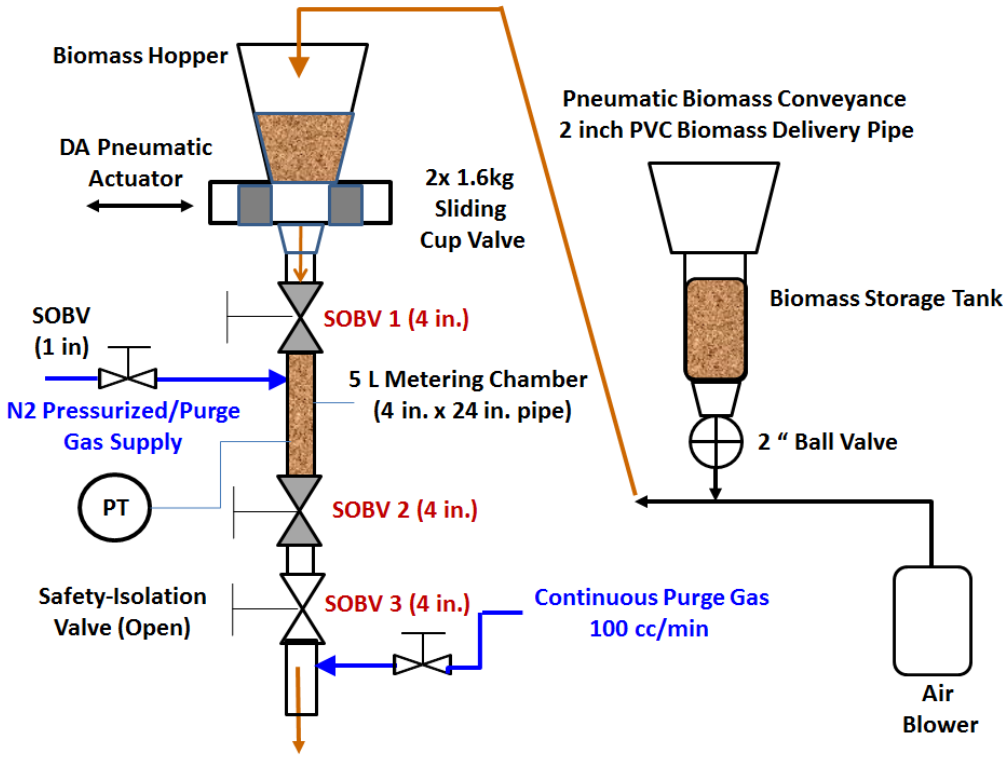

Figure 3.51. *Process schematic for 450 kg/h feed system*

Steam Enhancement

The maximum output for Steam Generator-1 in Phase IIIA was about 1000 SLPM of steam, which is not adequate for the high flow demonstration in Phase IIIB. Therefore, a larger steam generator was built to deliver steam at five times the previous test flow rate. The steam generator design is based on a shell and tube heat exchanger that was used successfully in another project (Figure 3.52). This boiler is capable of delivering 6000 SLPM of steam at 70% efficiency. Checkout tests indicated steam flow rates above 4000 SLPM were readily obtainable and indicated the boiler was suitable for the Phase IIIB tests.

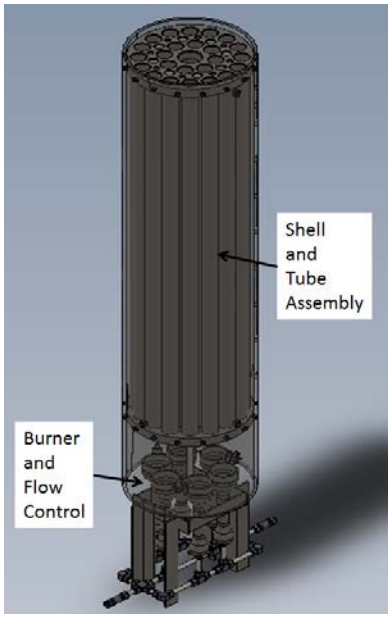

Figure 3.52. *Design of the new Steam Generator-1 unit*

Phase IIIB Construction and Integration

The feed and conveyance system components were assembled and final cold flow check out tests of the biomass feed rate were performed. Through control system adjustment of the valve cycle time, the feed system demonstrated a feed rate up to 9.5 kg/min. Figures 3.53-3.55 shows photographs of the new boiler and feed system construction and integration into the GO^{TM} reformer.

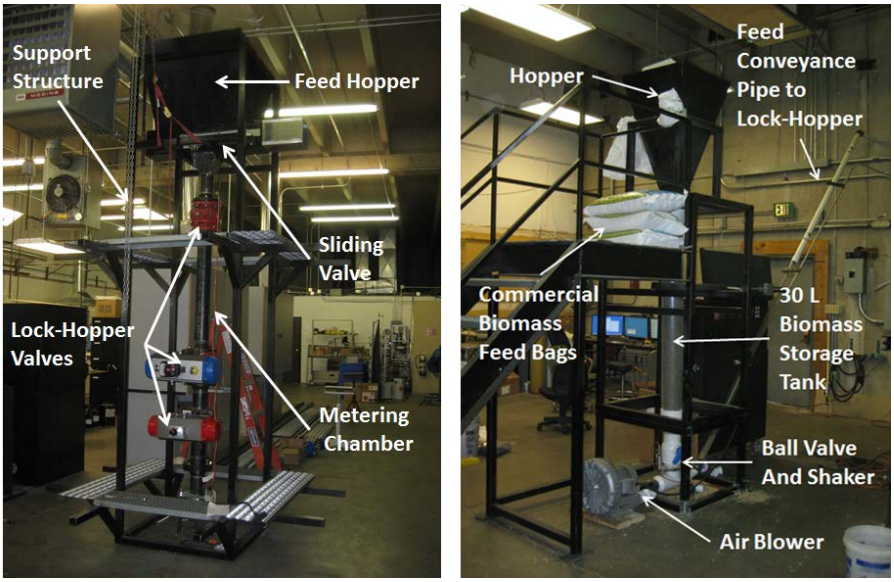

Figure 3.53. *New biomass feed system (450kg/h) in the Pioneer Astronautics' laboratory. Left: Constructed lock-hopper. Right: Pneumatic conveyance system*

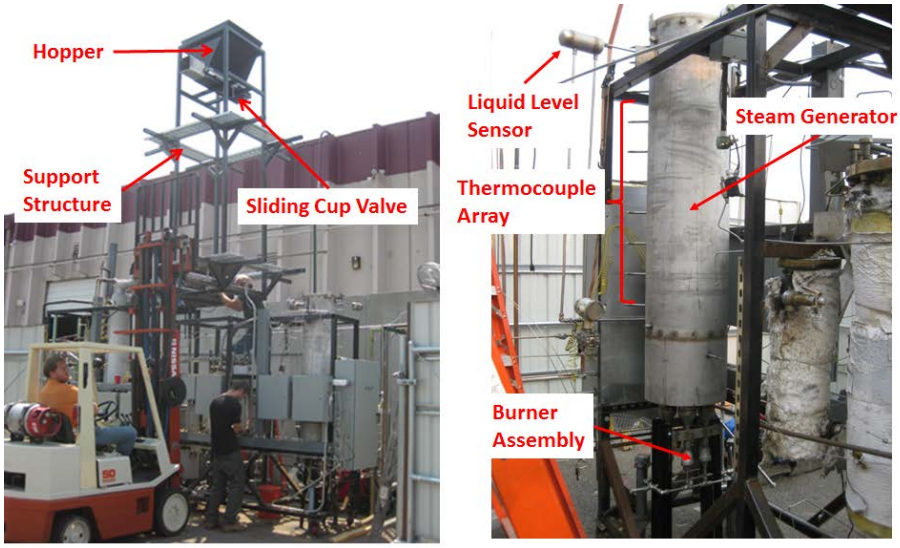

Figure 3.54. *Various stages of integration of the new biomass feed system and steam generator into the GO^{TM} reformer system. Left: New lock-hopper erection. Right: New Steam Generator-1 integration*

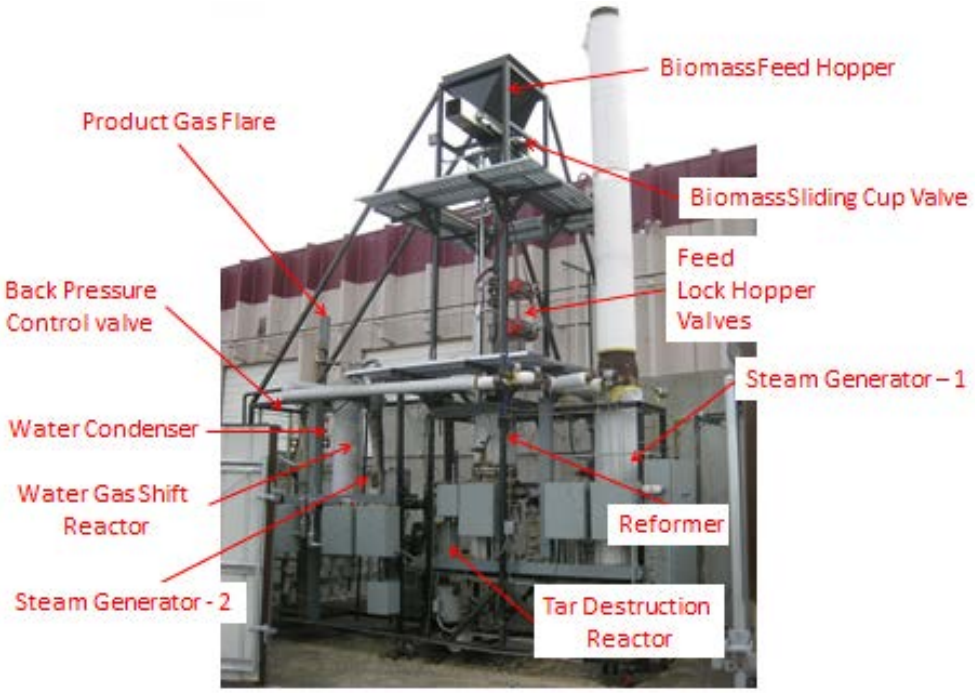

Figure 3.55. *Completed construction of the Phase IIIB reformer system at the Pioneer Astronautics facility. The system contains all the principal components to operate a transportable CO_2/H_2 generator for Enhanced Oil Recovery.*

3.2.3.2. Initial Testing

Following the checkout tests of the new fuel feed system and Steam Generator-1, initial testing of the Phase IIIB system was performed to establish baseline operability of the system and it's supporting diagnostic instrumentation. In addition, the grate drive was modified to prevent chain and sprocket slippage in view of long duration operation.

The full scale feed system was first fired on October 9, 2012, at a nominal flow condition of 0.7 kg/min biomass and an S/O of 4 (mol/mol). The system was operated according to previous methods and procedures developed in Phase IIIA. A product gas flow rate of about 3300 SLPM, and an H_2/CO of 1.6 and CO_2/CO of 1.4 at the reformer outlet was generated. These values compare well to previous test results in Phase IIIA. The results for product gas flow rate are presented in Table 3.27. We note this test and those that follow were conducted without the Water Gas Shift reactor in operation.

Table 3.27. Baseline Test Results for the Phase IIIB Reformer (Test 284-35)

Steam Flow Rate (SLPM)	Oxygen Flow Rate (SLPM)	Biomass Flow Rate (kg/min)	Average PG Flow Rate (SLPM)	H_2 (vol. %)	N_2 (vol. %)	CH_4 (vol. %)	CO (vol. %)	CO_2 (vol. %)	Total
1350	333	0.69	3262	34.39	9.6	3.99	21.06	29.69	98.73

3.2.3.3. Operational Testing

Following the initial baseline testing, the GO™ system was performance tested over a range of operating conditions to support 20,000 SLPM product gas. The results of these tests are presented below

<u>Test 290-36</u>

The first attempt at flow scaling the system was Test 290-36 on October 18, 2012. The test began with a Phase IIIA nominal operational condition of 1 kg/min biomass and an S/O ratio of 4. The steam, oxygen, and the biomass feed rates were then bootstrapped up to achieve higher product gas flow rate. However, the experiment was terminated just 25 minutes into the run due to a rapid run-up of the product gas exit temperature which exceeded 800°C. This was done according to operating procedures to avoid thermal damage to the reformer.

The test bed was examined after the experiment for causes of the temperature excursion. Figure 3.56 shows a photograph of the status of the post-test reformer bed and grate. Surprisingly, a fuel arch had developed that spans the entire inner diameter of the reformer. The hole in the bridge was created by test operators after the experiment to view the reactor volume below the arch. Inspection showed that the fuel was completely consumed down to the grate.

As the bridge developed in the bed it created a no-flow fuel condition. The reformer beneath the arch is therefore starved of fuel, and the excess oxygen causes the transition from gasification to full combustion. This causes a sudden increase in gas temperature to levels that can damage to reformer. Similar to bridging is fuel channeling, which arises from poor flow

patterns in the reformer bed and also leads to high gas temperatures. It should be noted these bridging events are not associated with the feed hopper but with the fuel flow inside the reformer.

(A) (B)

Figure 3.56. *Fuel plugging in reactor and thermal damage to grate. A). Biomass arch across the reformer. The hole was punctured after the test run for purposes of viewing into the reactor bed. B). A view of the hollowed-out reformer bed beneath the fuel arch. (Test 290-36)*

The bridge may have formed by introducing the steam too rapidly into the reformer. Therefore, modifications to the operating procedure and steam flow system were performed to produce a more stable and controlled steam addition to the reformer. This involved adding a Back Pressure Control Valve and a new flow orifice to the Steam Generator-1 and 2 lines, respectively. A nitrogen gas blast was also installed upstream of the reformer to bust through the bridge in the event a bridge forms.

Test 292-3

Test 292-37 was conducted shortly after these changes were implemented, and a much longer run time was initially achieved. A peak flow rate of 5000 SLPM was achieved as the flow rates were increased. However, as the run progressed high exit gas temperature (800°C) was again experienced in addition to the development of a high pressure drop across the reformer

bed (ΔP = 1 atm). Therefore the test was shut down after 90 minutes of operation despite instituting the steam flow adjustments and N_2 gas blast. A post-test examination revealed significant pluggage of the grate by char dust, and thermal grate damage. Presumably, in the event of a bridge/channel collapse a sudden on-rush of fuel quenches the flame, reduces the temperature, and causes the formation of fine char and particle-laden gas. The particles then flow down below the nozzles, and ultimately deposit on the grate causing a high pressure drop in the reformer. As a channel forms oxygen flows through it down to the char at the grate which may thermally damage the grate (Figure 3.56).

Figure 3.57. *Thermally damaged grate caused by fuel channel or bridge in reformer. Note the slag deposition on the surface of the grate indicating high temperature conditions were experienced.*

Tests 300-38 and 305-39

Two more tests were conducted, 300-38 and 305-39, this time with modifications to the rotating grate to enable operation in forward and reverse directions for bed agitation. Higher steam flow rates were also used during testing to moderate the temperature. The S/O ratio was varied between 6 and 7, although there were periods where the S/O was adjusted as high as 10 to keep the temperature under control. Product gas flow rates near 4500 SLPM were generated. However, thermal and pressure excursions persisted which caused premature system shut-down.

System Modifications

At this time a further evaluation of the causes of the temperature and pressure excursions were undertaken to identify and prevent their occurrence in future runs. Our examination of the reformer after a test run revealed that the bridge regularly formed just underneath the flange connection between upper fuel magazine and the lower reformer. Here an abrupt area reduction occurs as the biomass flow channel diameter reduces from 30 cm to 25 cm due to the presence of the upper steam-oxygen nozzle plenum. In such cases it is possible that a stagnant fuel zone

develops that traps fuel along the walls similar to funnel flow in silos which leads ultimately to the formation of a bridge and a no-flow condition. To alleviate the flow stagnation, a tapered duct with a 30 cm inlet diameter and 25 cm outlet diameter was constructed that made a smooth transition from the upper magazine to the lower reformer bed. We also made sure the reformer was well insulated and sufficient nitrogen purge gas was present so that steam condensation would not occur.

A bed stirrer was added the reformer by attaching a shaft to the rotating grate. This design allowed the simultaneous rotation of the grate and the agitation of the fuel bed allowing char and ash to be removed while disrupting the formation of a bridge. The design of the bed stirrer is shown in Figure 3.58. We note that with higher steam and oxygen flow rates the gas residence time may not be sufficient to allow endothermic reforming and reduction reactions to proceed fully. Therefore the steam and oxygen were injected through the upper nozzle bank to give longer reaction time and moderate the gas temperature. The lower bank was closed off during these runs.

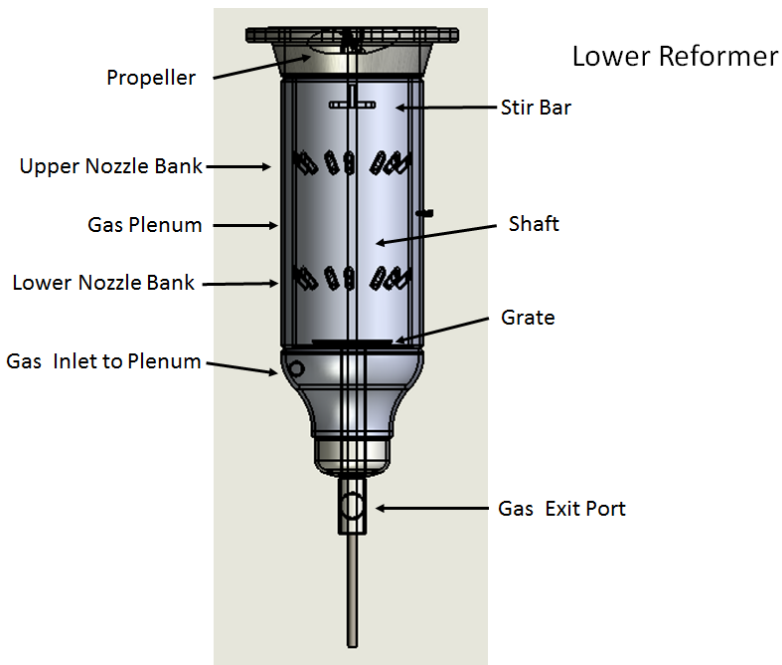

Figure 3.58. *Design of the reformer bed stirrer apparatus. Two propeller sizes, 5 an 9 inch, were used to agitate the bed.*

With these new hardware modifications and operating procedures implemented, the product gas scale-up tests resumed and the results summarized below.

Test 310-40

The steam oxygen flow was diverted to the upper nozzle bank to create longer residence time and reduce reformer temperature. The reformer was operated with a higher average S/O ratio = 6 to reduce temperature. Through adjustment of the steam, oxygen and biomass flow rate, the product gas flow rate was scaled to a peak flow of 4330 SLPM. A sudden drop in

product gas flow rate (ΔQ = 1000 SLPM) and increase in pressure drop (ΔP = 1 atm) in reformer was and the test was stopped 60 minutes into the run. A post-test analysis indicated that a particle blockage in the grate caused the test to be terminated.

Test 319-41

This test was performed with the transition duct between the upper reformer and lower reformer in place. The steam-oxygen mixture entered the upper nozzle ring, and an average S/O of 7 was used. An unusual product gas distribution formed: H_2 < 10%, CO < 10%, and CO_2> 45% O_2 > 30%, signifying a fuel channel had formed and forcing the stoppage of the test after 67 minutes of run time.

Test 325-42

The product gas flow scaling test was repeated this time with a newly fabricated, 5-inch propeller bed stirrer. A peak flow of 6000 SLPM was obtained. To achieve this flow rate the S/O ratio was adjusted to fall in the 8-12 range to moderate the reaction temperature. Nevertheless, the test was stopped after 67 minutes due to a temperature spike in the system due to the formation of bridge and rat hole that formed around the propeller blade.

Test 331-43

The reformer was fitted with a 9-inch propeller blade to stir a larger bed cross section. This resulted in the achievement of 5300 SLPM. However, the development of high pressure drop across the Tar Destruction reactor forced the test to be stopped after 55 minutes. Post-run examinations showed that the bed stirrer prevented bridge formation in the upper magazine and that particle dislodgement from the grate created the pressure drop. At this point the program drew to close and no further testing was conducted.

Phase IIIB Test Campaign Summary

The average product gas composition, operating condition, and product gas flow rate for the Phase IIIB campaign is summarized in Figure 3.58. In Figure 3.59, Test 284-35 is the initial baseline test, while Tests 292-331 summarizes the test results carried out with the large scale feed system, olivine tar destruction reactor, and the heat recovery/steam generator units described previously. The gas composition was sampled at the exit of the reformer and without treatment from the Water Gas Shift reactor.

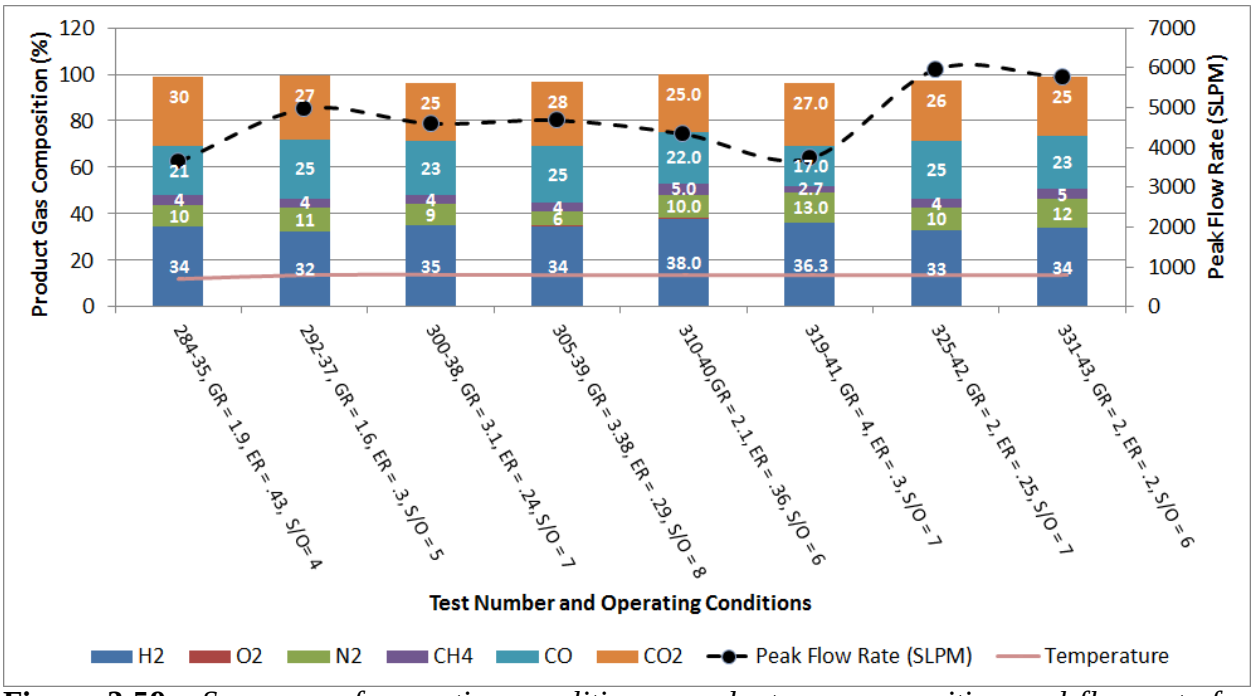

Figure 3.59. *Summary of operating conditions, product gas composition and flow rate for Phase IIIB testing*

Post Run Discussion

The pine wood pellets are a good choice for feeding since they are small and uniform in size and flow easily. However, they may not be an ideal fuel in the reformer for the following reasons. The pellets are relatively fragile, and once inside the reformer they may disintegrate to sticky sawdust as they are exposed to moisture, bed agitation, and high gas blast velocity. All of these factors contribute to the flow bridging and plugging. The selection of a more robust, harder fuel may eliminate many of the fuel plugging issues encountered in the study.

Apparently, the oxygen blast of pine wood pellets under the conditions described here causes a very fine char and particle product which can cause downstream flow blockage. This effect was also observed by Reed and co-workers in high pressure oxygen gasification (Reed, T., et al., 1994). The rotating grate was operated at about 0.5 to 1 rpm rotation speed in these studies. Slower speeds would be preferable so as not to agitate or dislodge the fine char from the grate, and discharge it into downstream components causing blockage and high pressure drop. We were not equipped with the proper power conditioning to go to slower grate speeds as a slower speed caused an increased current draw, which caused the controller to shut down.

Ideally, one would like to operate the grate and bed stirrer with independent rotation speeds. The bed agitator can be run at a higher speed that breaks up bridges, channels and hot spots and maintain uniform bed density or porosity, while the grate can be operated at a minimum speed to prevent pressure buildup in the system.

A general rule of thumb is that the total area of the nozzles should be about 5-7% of the reactor diameter. In this manner, a typical blast velocity is on the order of 25-30 m/s. In

these studies, the total nozzle area is about 1.8% of the reactor area, which gives rise to blast velocity of over 50 m/s. These relatively high velocities can potentially cause local hot spots, disruption of the char and fuel bed, and induce channeling. This can be overcome by simply using a larger diameter nozzle in higher flow rate testing.

3.2.3.4. Phase IIIB Summary

A continuous feed system for operating a full scale CO_2-EOR field unit demonstrator was successfully designed and tested. Feed rates up to 9.5 kg/min of wood pellets were demonstrated, which is sufficient for feeding a full scale field unit. Several key GO^{TM} reformer system elements including continuous product gas cleanup, tar destruction, heat integration, were also demonstrated. The Phase IIIB GO system was scaled-up to 6000 SLPM (305,000 SCFD) at 10 bar pressure. This flow rate does not represent the upper limit of reformer flow performance as its ability was limited by thermal and pressure drop excursions. This underperformance is attributed primarily to reformer fuel bridging and/or channeling, and high pressure drop in the reformer and downstream units, but not in the continuous feed system.

These test results are encouraging and demonstrate the viability of the GO^{TM} system for a portable CO_2-EOR system. We note that the Phase IIIA operating conditions were successfully transferred to and executed in Phase IIIB operation, which suggests that the steam-oxygen fired biomass reformer operating conditions developed here can be scaled to generate useful quantities of CO_2 for Enhanced Oil recovery. A simple change out in fuel type, i.e., from soft wood pellets to a harder wood chips, or using independent rotating grate and bed stirrer action may all that need be required to eliminate fuel bridging and channeling.

3.2.4. Field Data Collection and Analysis (NMT)

PRRC researchers completed a comprehensive study including reservoir characterization, geomodel build-up and reservoir simulation for the Grouse Field reservoir, Cheyenne County, Colorado, belonging to a small producer, Pintail Petroleum Ltd. A preliminary reservoir characterization study was also carried out for a reservoir in the Pawnee Pioneer field, Weld County, Colorado belonging to another small producer, Ward Petroleum Ltd. Pintail's Grouse Field Spergen Reservoir was selected for the purpose of CO_2 enhanced oil recovery (CO_2 EOR), because it contains a water injector and interconnected wells, as well as meeting all the necessary criteria for CO_2 EOR.

3.2.4.1. Reservoir Characterization and Modeling

Petroleum Recovery Research Center researchers completed a comprehensive study including reservoir characterization, geomodel build-up and reservoir simulation for the Grouse Field reservoir, Cheyenne County, Colorado, belonging to a small producer, Pintail Petroleum Ltd. Grouse Field Spergen Reservoir was selected for the purpose of CO_2 enhanced oil recovery (CO_2 EOR), because it contains a water injector and interconnected wells, as well as meeting all the necessary criteria for CO_2 EOR. The objective of this study was to evaluate the reservoir for

potential CO_2 EOR operation. Parameters obtained from these studies were applied to generate geomodel for reservoir simulation. The results of this analysis are presented below.

Grouse Field, Cheyenne County, CO

The map of the Grouse Field in Cheyenne County, Colorado, and belonging to Pintail Petroleum Ltd is shown in Figure 60. The stratigraphic column map of the field is described in Technical Report 1. In the Grouse Field, there are only eight producing wells belonging to Pintail Petroleum Ltd: seven wells producing oil from the Mississippian Spergen (Salem) Formation and one well (05-017-06469) producing from the Morrow Formation (MRRW), which will be ignored because it is producing from a different reservoir. All other surrounding wells are drilled and abandoned (DA). Considering the well 05-017-06469 producing from a different reservoir (MRRW), the reservoir area is defined, by nearby DA wells, within the boundaries of the blue rectangle shown in Figure 3.60. Thus the study area of Pintail reservoir is 19,362,600 ft^2 (4164 ft x 4650 ft).

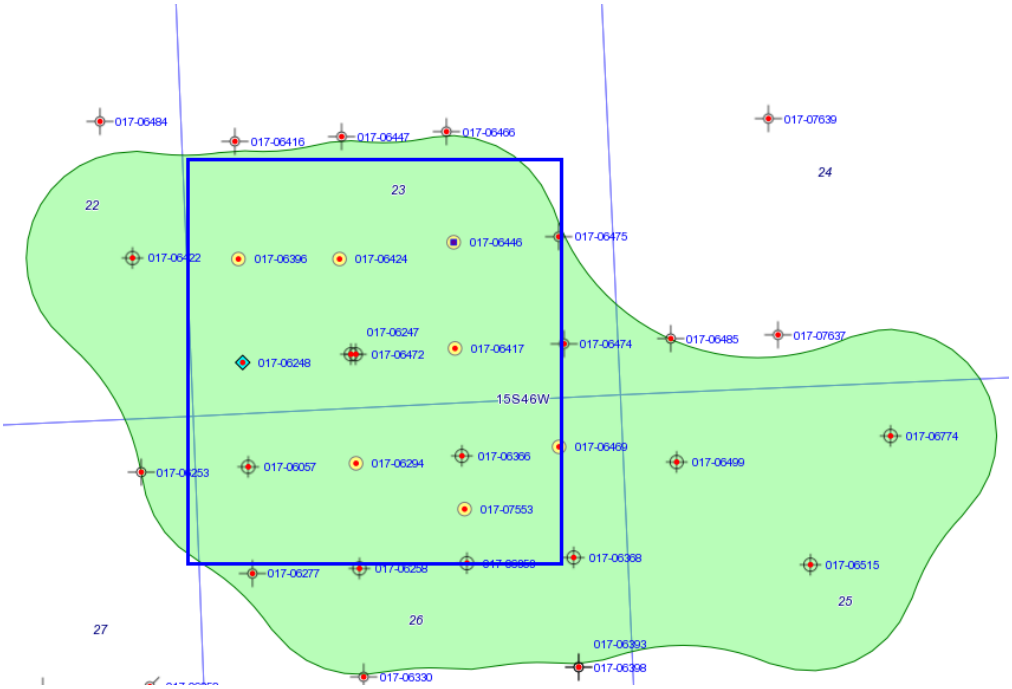

Figure 3.60. *Map of the Grouse Field, Cheyenne County, Colorado (the area in green shadow). Reservoir area is within the blue rectangle. Production wells are marked as a yellow circle with a central red dot.* (http://dnrwebcomapg.state.co.us/mg2010app/?ogw='01706446')

According to the well information from the Colorado Oil and Gas Conservation Commission's (COGCC) website (http://cogcc.state.co.us/), all seven wells belonging to Pintail

PetroleumLtd. were perforated in the Spergen formation. All the wells are producing from the same formation and appear to be connected.

Formation Top Maps

Formation tops for over 20 wells in the Grouse Field around the reservoir study area were acquired from the Colorado Oil and Gas Conservation Commission's (COGCC) website (http://cogcc.state.co.us/). These tops were adjusted according to the elevation depth of well 05-017-06446. Then these top coordinates were used to generate top maps of the Mississippian-St. Louis (seal formation), Spergen (production formation), and Osage formation (Figures 3.61-3.63). The Spergen varies from 79 to 150 feet in thickness in the study area.

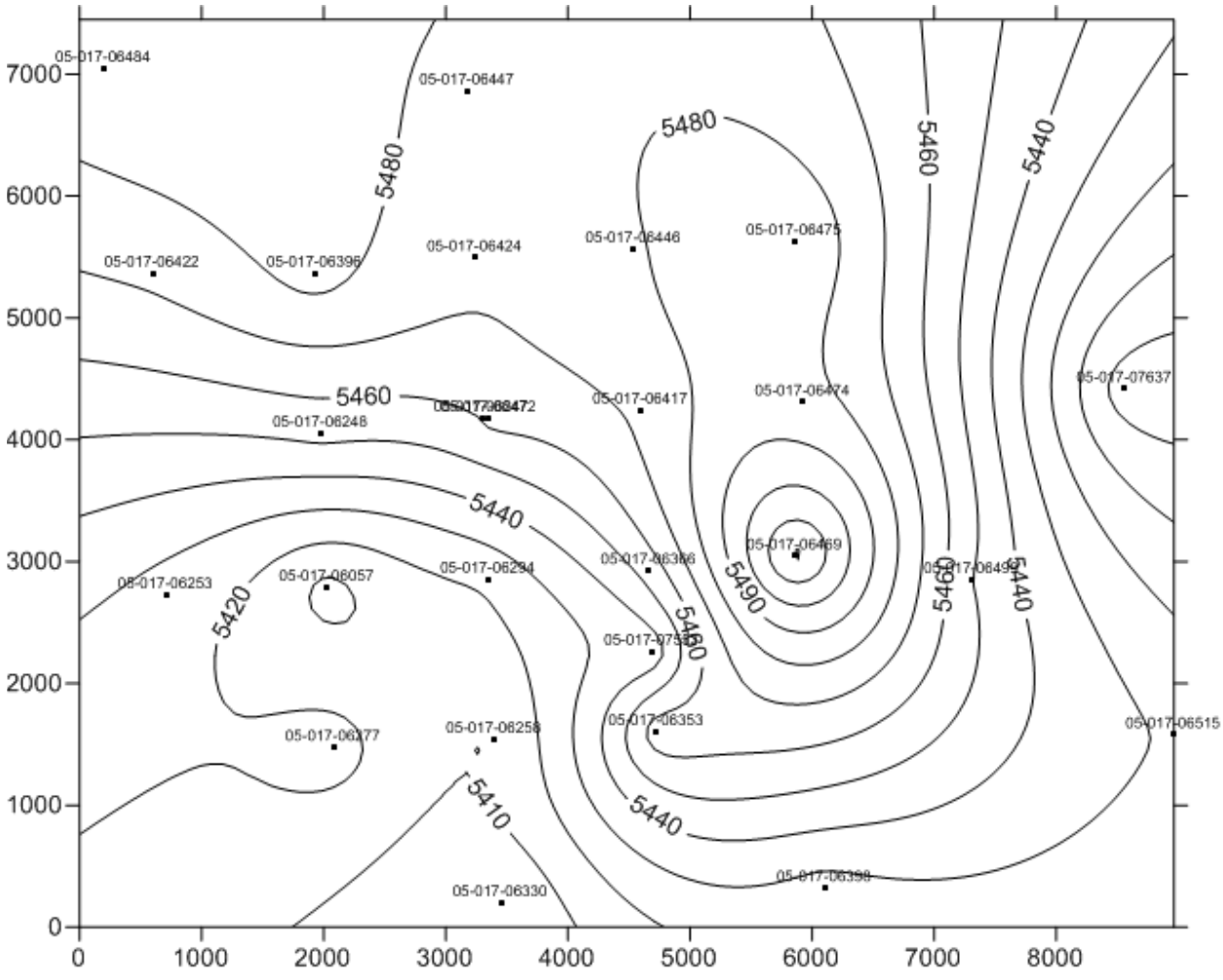

Figure 3.61. *The formation top map of the Mississipian-St. Louis formation.*

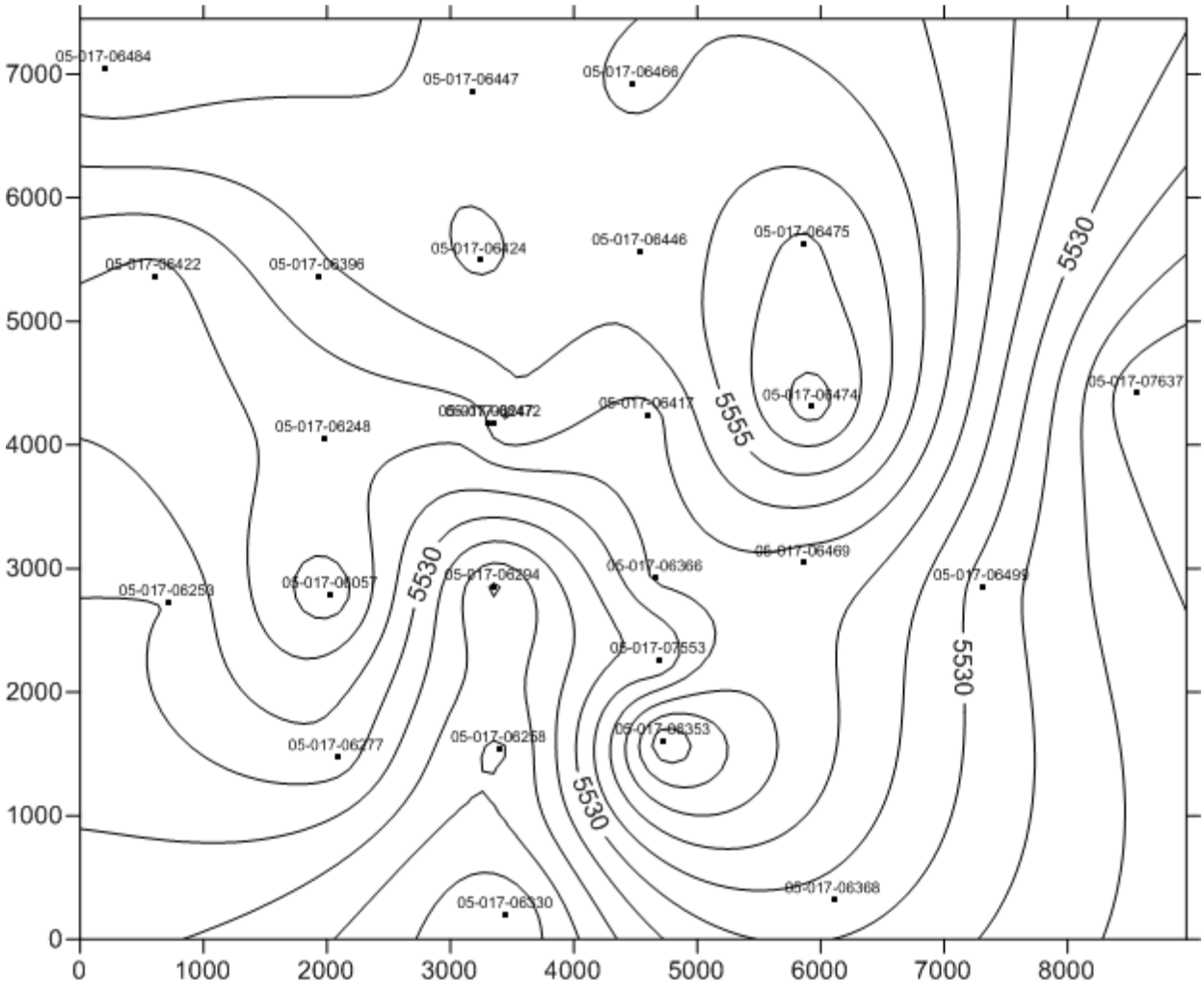

Figure 3.62. *The formation top map of the Spergen formation.*

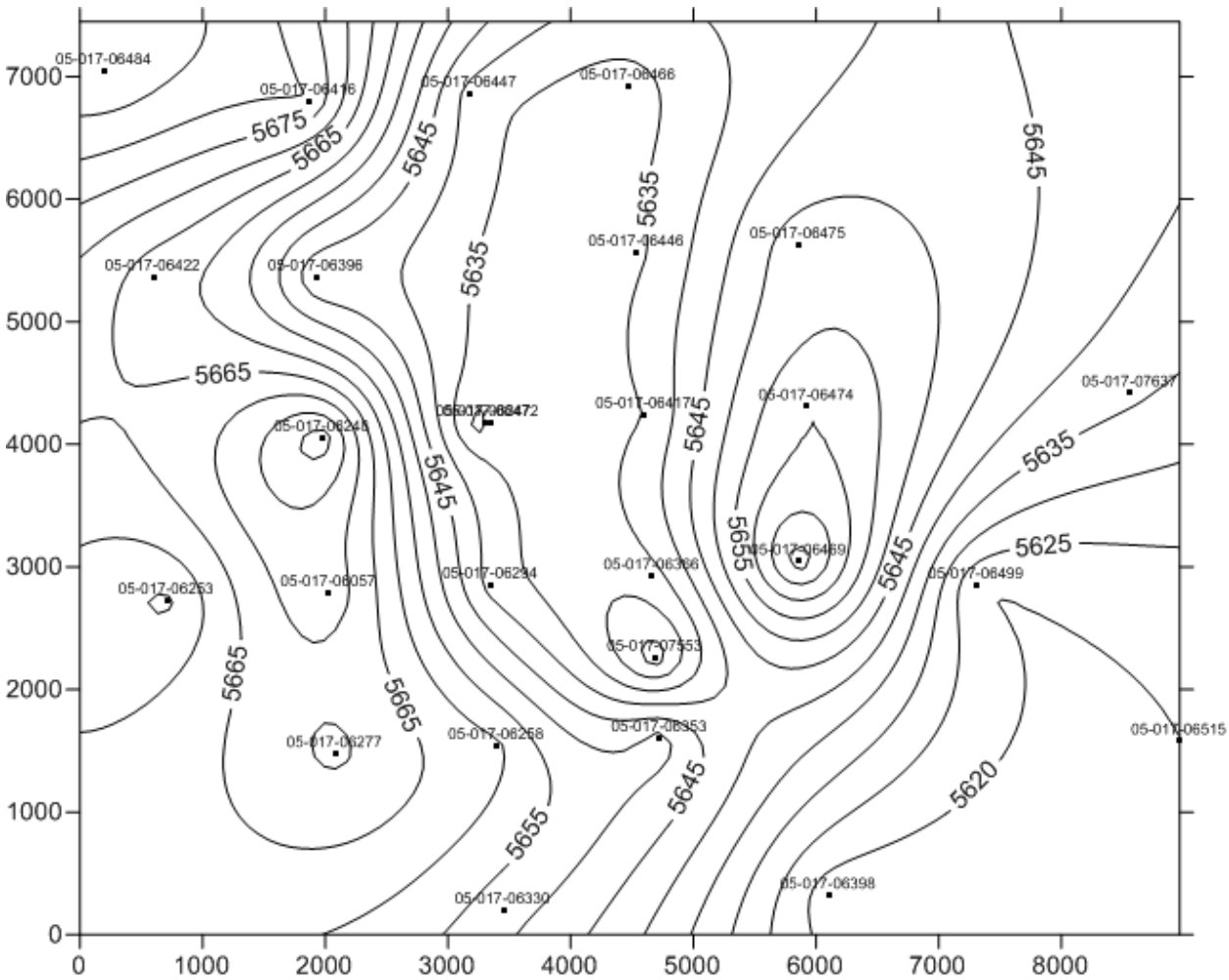

Figure 3.63. *The formation top map of the Osage formation.*

Petrophysical Characterization

Wireline logs are available for these seven wells. Considering this is a small reservoir, well logs for one well were analyzed and normalized for the whole reservoir. Researchers selected the wireline logs for well 05-017-06446, as they are the most comprehensive. Seven well logs (GR, SP, Caliper, Bulk Density, Neutron Porosity, Density Porosity, Resistivity (RILD, RILM, SFLU) were digitized by Neuralog Digitizing software and analyzed by Log Evaluation System Analysis (LESA).The digitized well logs and LESA analysis results are shown in Figures 3.64 and 3.65, respectively. A comprehensive analysis was carried out for the well logs. The analysis shows clearly that there is mudcake in the production formation (~5540-5590 feet), which shows it is a permeable zone. The oil amount and the permeability are both good. The high resistivity in the uninvaded zone (RILD curve), higher than that of the invaded zone (RILM curve), and slightly lower than the resistivity of the flushed zone (SFLU curve) (with freshwater drilling mud) in the dual induction log (track 2) shows the hydrocarbon-bearing zone at the depth of 5540–5590 feet. The porosity is determined through the crossplot of density porosity and

neutron porosity with the range of 0–0.342 within 3000–5700 feet. The permeability calculated by LESA is 0-1094 mD. The combination of PEF, density porosity and neutron porosity shows that the lithology of the hydrocarbon-bearing zone is limestone/dolomite. These important parameters will be input to a geomodel for reservoir simulation. There is a thick shale formation above the production zone, which would be a good seal for CO_2 injection.

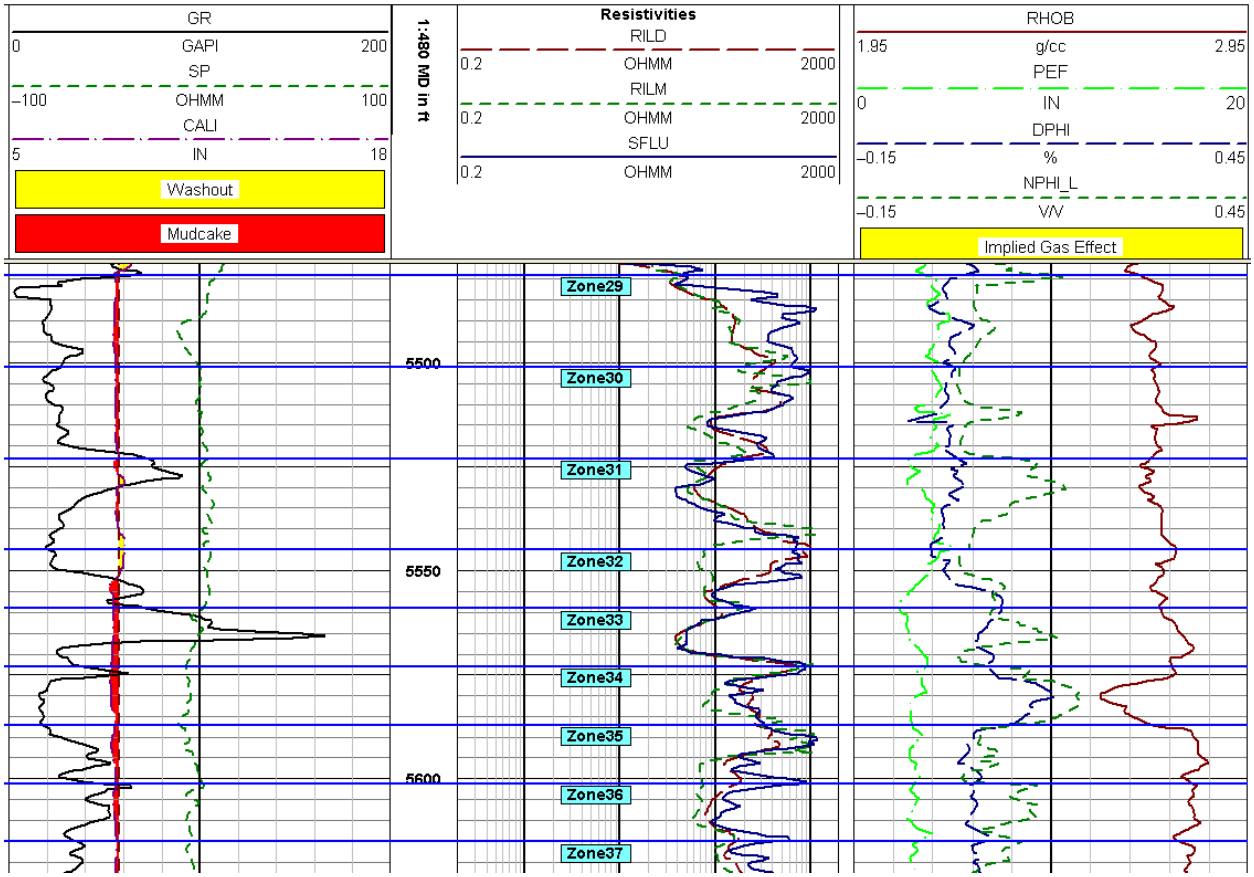

Figure 3.64. *Digitized well logs for well 05-017-06446.*

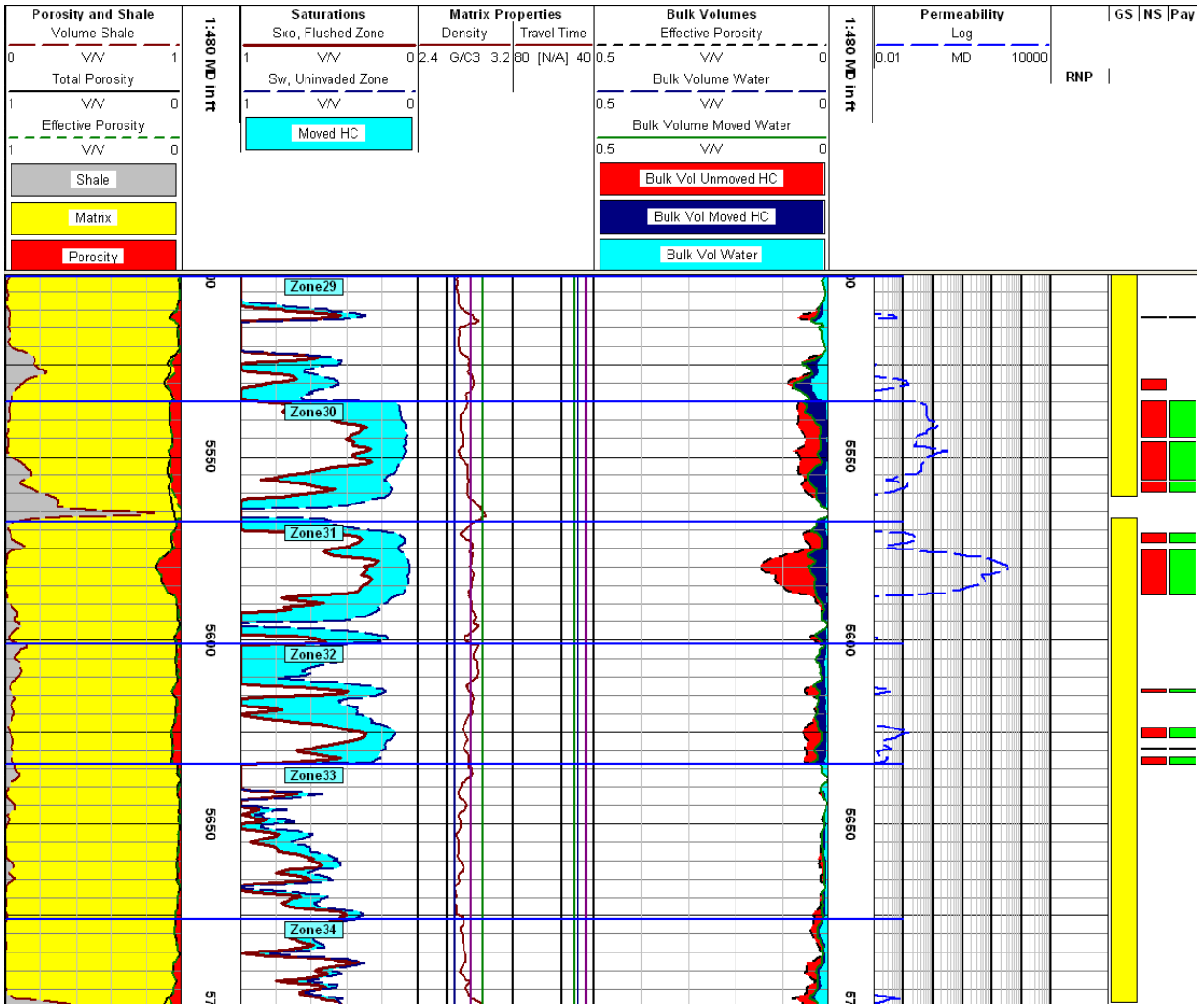

Figure 3.65. *Comprehensive log for well 05-017-06446.*

Reservoir Pressure Change, Temperature, API

The reservoir pressure information was inferred from DSTs, Field Inspection, and Mechanical Integrity tests, and logs for the wells from Colorado online database (http://cogcc.state.co.us/). The final shut-in pressures (FSPs) and initial shut-in pressures (ISPs) recorded shows that there is a remarkable consistency in pressure for all the wells, and that the reservoir has undergone minimal pressure decline between 1973 and 1993, thus indicating the presence of a strong water drive. In addition, the Spergen zone has increasing water cutoff from bottom to top. This corresponds with the hypothesis that the Spergen reservoir is a bottom water drive system. Well records indicate that measured reservoir temperature varied between 130° to 148°F (54.4° to 64.4°C), and that oil API varied between 38 to 42 degrees.

Oil-Water Contact (Free-Water Level, FWL)

This parameter identifies the lowest subsea depth below which DST's always result in water production. The FWL was estimated to be around -1122 feet subsea according the water saturation close to 1 from the wireline logs analyzed by LESA.

Rock Compressibility

The unjacketed pore compressibility in a porous rock is the change in pore volume due to change in pore pressure for constant differential pressure. The rock compressibility of Spergen Limestone is calculated according to the Hart and Wang (1995) measurement of Indiana Limestone with porosity of 0.13 within the pressure range of 2–10MPa.The calculated rock compressibility is 1.49887E-06 1/psi.

Production Data

The monthly production is available by well from January 1, 1999 to present. Prior to 1999, production was reported on a lease basis, which contains multiple wells (1-4 wells). Lease production needs to be assigned to individual wells. Assuming that production from each well keeps the same trend in the available data since 1999, the lease production of pre-1999 production is estimated for each well within the lease according to the production ratio after 1999. According to production data, some wells have performed better than expected while others have underperformed. The fracturing is believed to contribute to the variable productivity. The cumulative oil production of seven wells from Spergen reservoir in the Grouse Field is 1.215 million BBLs.

Bubble Point Pressure

Bubble Point Pressure (Pb) is calculated as 254 psi with the Vasquez and Beggs correlation method, below. The solution gas oil ratio (40–100 scf/bbl) is obtained from online well information.

$$p_b = \left(\frac{R_s}{C_1\, \gamma_g \cdot e\left(C_3 \left(\frac{\gamma_{API}}{(T + 459.67)} \right) \right)} \right)^{\frac{1}{C_2}} \tag{3.34}$$

Coefficient	$\gamma_o \leq 30^o$ API	$\gamma_o > 30^o$ API
C_1	0.0362	0.0178
C_2	1.0937	1.1870
C_3	25.7240	23.9310

Capillary Pressure

The basic relationship between capillary pressure (Pc), interfacial tension (IFT,γ), contact angle (θ) and pore radius (a) is given by

$$P_c = \frac{2\gamma \cos\theta}{a} \bullet A \tag{3.35}$$

where A is $145*10^{-3}$ (constant to convert from KPa to psi)

The rock capillary pressure is measured with Hg capillary pressure. The conversion from Hg-air capillary pressure to other fluid is given by:

$$P_{c(fluid1-fluid2)} = P_c(Hg-air)\frac{(\gamma\cos\theta)_{(fluid1-fluid2)}}{(\gamma\cos\theta)_{(Hg-air)}} \tag{3.36}$$

The capillary pressure of study area is acquired from SPE 21044. The interfacial tension and contact degree are acquired from literature (Churcher, etc (1991), McCaffery (1972), and Rao (1997)). The parameters and calculation results for capillary pressure are shown in Table 3.28. The capillary pressure for oil-water and oil-gas is 1.803 psi and 0.114 psi, respectively.

Table 3.28. Capillary Pressure

	γ, dynes/cm	θ, degree	Pc, KPa
Hg-air	486	140	120[1]
oil-water	47.69[2]	36[2]	
gas-oil	2.6[3]	20[3]	
Pc (oil-water), psi	1.803200335		
Pc (oil-gas), psi	0.114187398		

[1] Churcher, etc (1991), [2] McCaffery (1972), [3] Rao (1997).

Pawnee Pioneer field, Weld County, CO

Ward Petroleum Ltd. owns the reservoir in the Pawnee Pioneer Field that produces from the Upper Cretaceous Richard Member of the Pierre Shale play. A stratigraphic section of rock units is shown in Figure 3.66. Oil and associated gas in the Pierre Shale play are produced from Richard, Terry ("Sussex"), and Hygiene ("Shannon") Sandstone members. Terry and Hygiene reservoir sandstones are mainly offshore marine linear sandbars that are enclosed in shales and fine-grained sandstones of the Pierre Shales from elongate fine-grained sandstones. The thickness of the reservoir sandstones ranges from 4 to 48 ft, with average thickness of 20 ft. The average porosity is 14%; average permeability 0.1–9 mD. Oil gravity ranges from 4–65° API. Seals (Upper Pierre Shale) are overlying and updip marine shales.

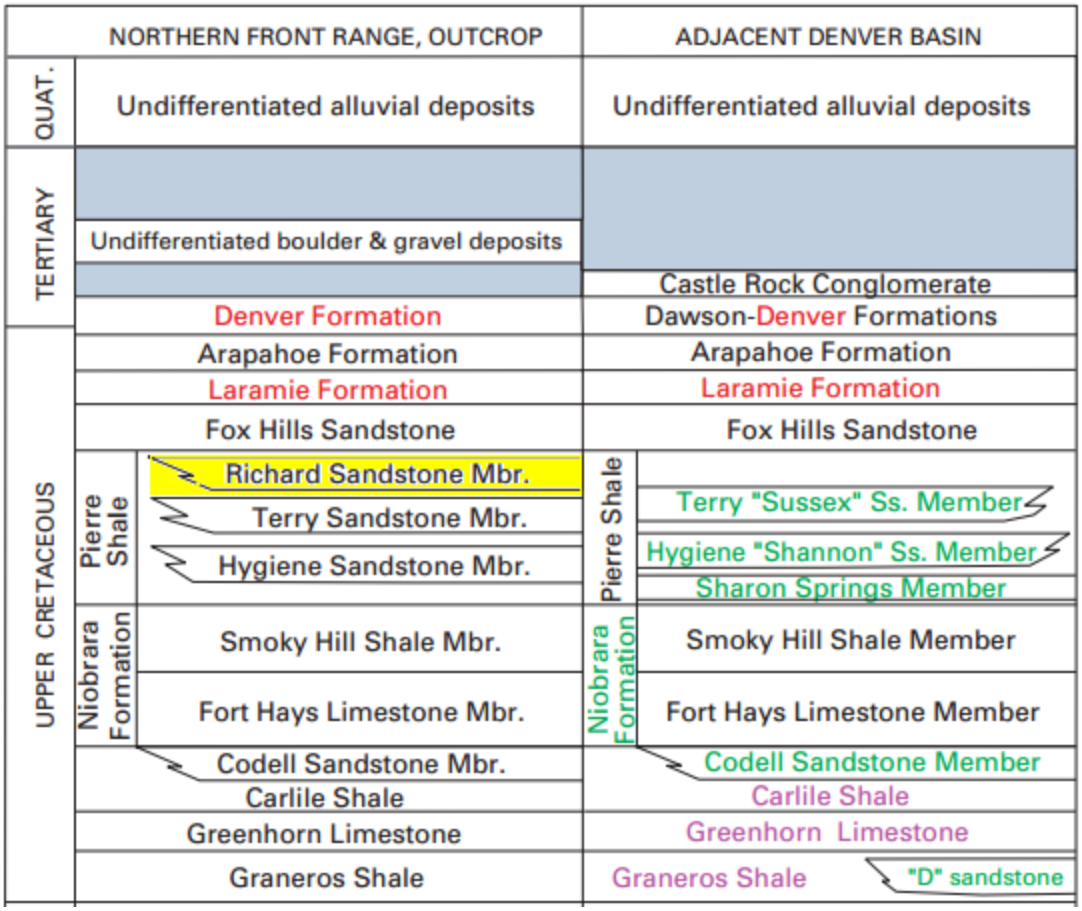

Figure 3.66. *Stratigraphic section of rock units in outcrop and the adjacent Denver Basin. (Higley, D. K., and Cox, D. O., 2007)*

The preliminary model of Ward's reservoir in the Pawnee Pioneer Field has been developed. The surface view of the simulation area is shown in Figure 3.67. The dimensions of the model are 10195 ft (w) x 13605 ft (l) x 170 ft (thickness). The model area consists of three geological formations, seal formation, Richard Sandstone (production formation), and support formation. The formation top is determined from the well logs and online information from 15 wells in the immediate area. The top-depth (z/x=10:1) of the formations are shown in Figure 3.68. A model prepared for initial simulations consists of 16,800 grids (30x40x14).

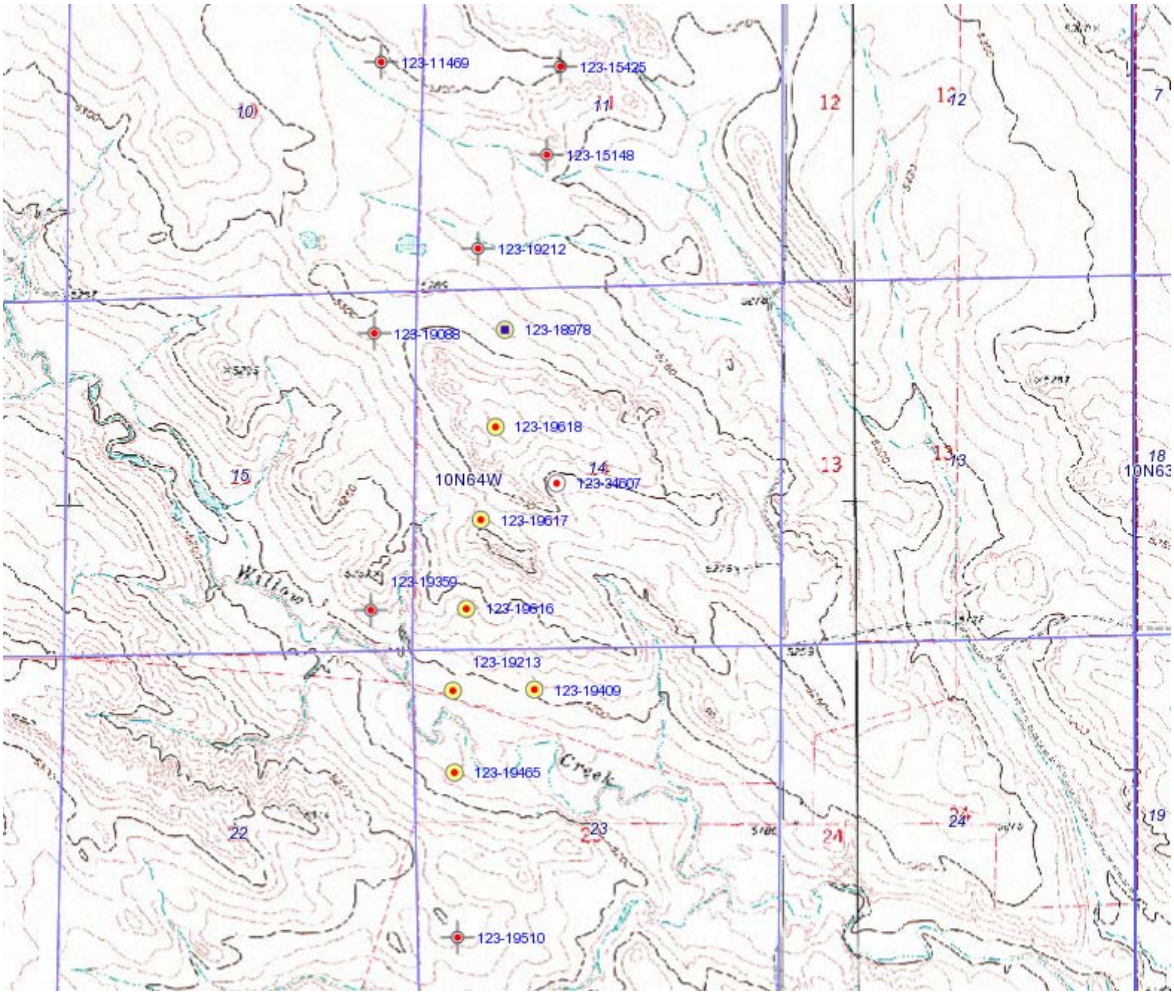

Figure 3.67. *Surface view of the simulation area.*
(http://dnrwebcomapg.state.co.us/mg2010app/?ogw='12318978')

PR: Producing

SI: Shut In

DA: Drilled and Abandoned

IJ: Injecting

Figure 3.68. *Formation top-depth for Ward's Morrow Reservoir in the Pawnee Pioneer Field*

The wireline logs for well 05-123-19213 were analyzed to represent the Pawnee Pioneer reservoir. The digitized well logs are shown in Figure 3.69. For in-depth analysis in LESA, the Rw factor of the formation is required to be calculated. The effort on Ward's Reservoir in the Pawnee Pioneer Field ends here because there is no injector on site, which would require an additional operation cost for CO_2 EOR.

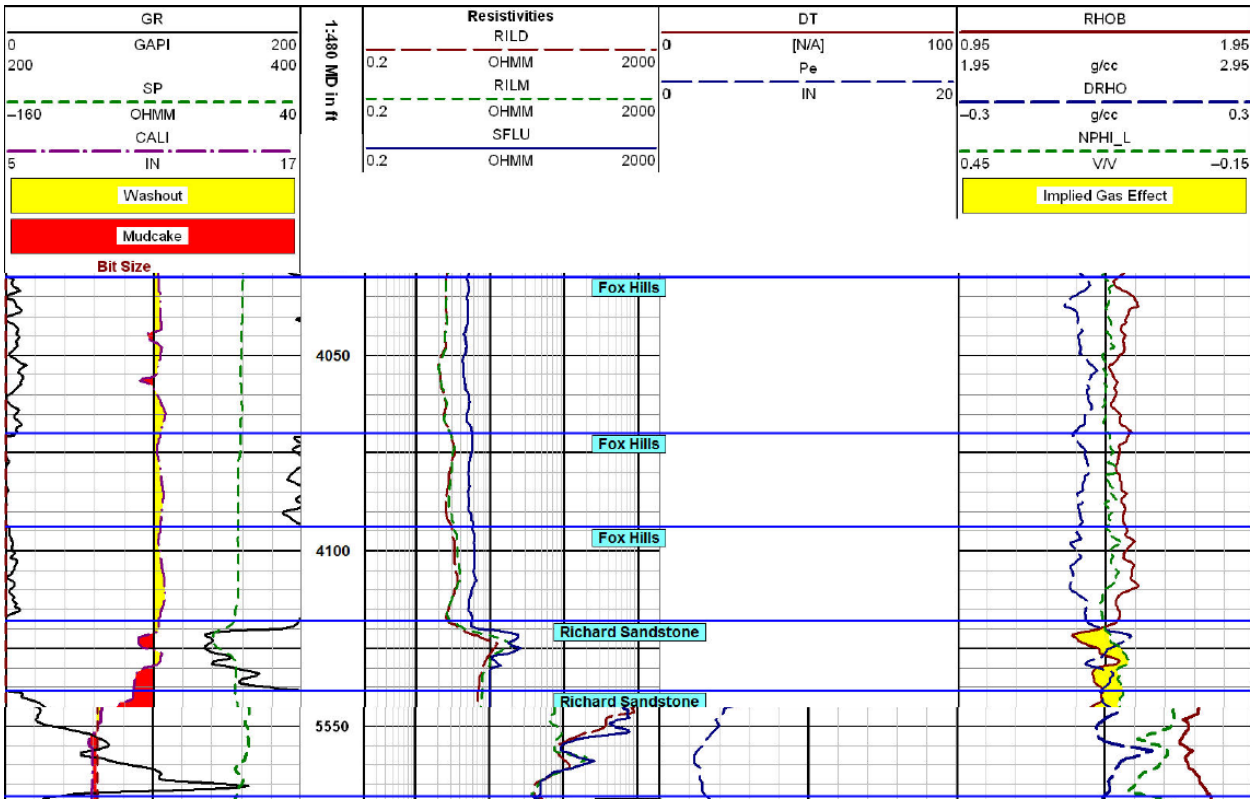

Figure 3.69. *Digitized well logs for well 05-123-19213.*

3.2.4.2. Geomodel Construction and Reservoir Simulations- Grouse Field Spergen Reservoir

Geomodel Build-Up

A geomodel was constructed, including all the wells and geophysical information. Besides seven wells, one well was added as a water injector, which was converted from the original 05-017-06248 well in 1992 and one well was added as a CO_2 injector, which was converted from a water injector in 2012. Accordingly, the simulation model contains nine wells. As described in the previous section, the study area of Pintail reservoir is 19,362,600 ft^2 (4164 ft x 4650 ft). The simulation model grid is 34,200 (40 x 45 x 19) with each grid of 105 ft x 104 ft with varied depth. According to pressure and water cutoff analysis, there is a natural waterflood into the reservoir. An aquifer needs to be added to the bottom of the reservoir. The geomodel of formation top-depth is shown in Figure 3.70. The models containing the porosity and permeability properties are shown in Figure 3.71 and 3.72. The gas-water and water-oil relative permeability is adopted from Schneider's, et al. (1975) research on relative permeability in carbonate rocks, as shown in Figure 3.73 and 3.74.

Figure 3.70. *Formation top-depth for Grouse Field Spergen Reservoir.*

Figure 3.71. *3D view of formation porosity for Grouse Field Spergen Reservoir.*

.

Figure 3.72. *3D view of formation permeability for Grouse Field Spergen Reservoir.*

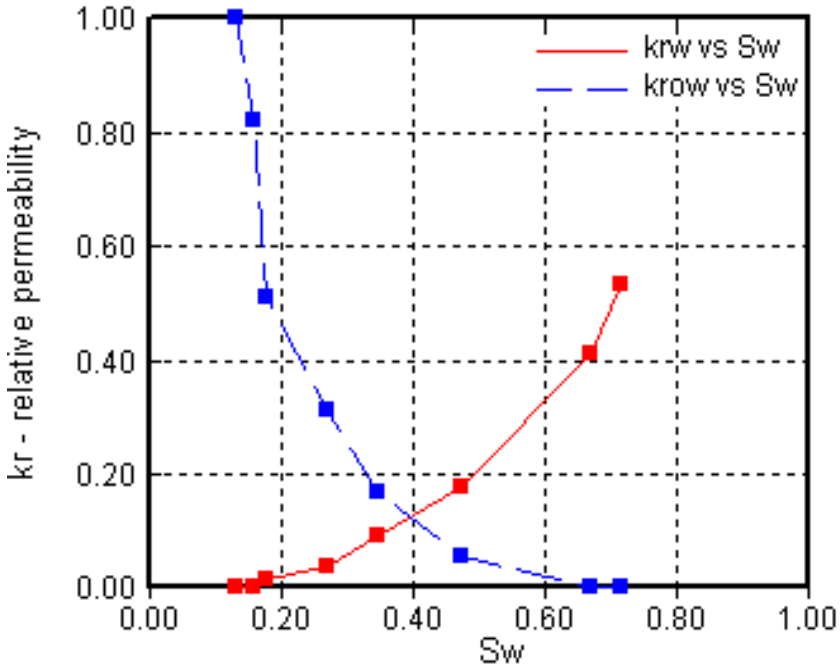

Figure 3.73. *Water-oil relative permeability.*

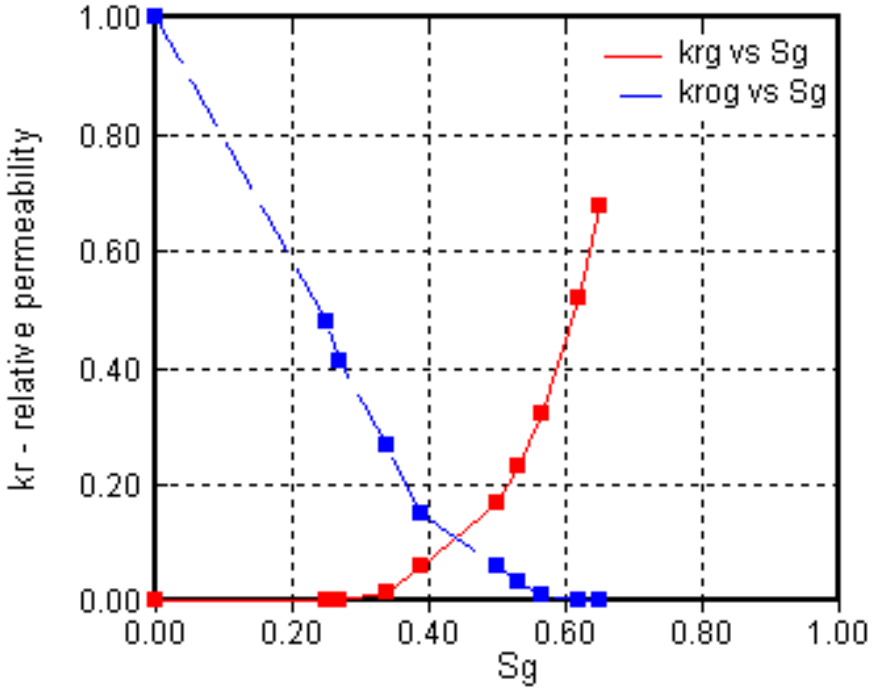

Figure 3.74. *Gas-liquid relative permeability.*

History Match

The history match has been accomplished with two constraints: one fixes the standard surface gas production (STG) and matches the oil production; the other fixes the standard surface oil production (STO) and matches the gas production.

The model was constructed with and without an aquifer at the bottom of the reservoir. The average reservoir pressure with and without aquifer and the aquifer water influx are shown in Figure 3.75. The minimum pressure of the reservoir is 938 psi and 1044 psi at 12/01/1991 (just before the water injection on 01/01/1992) with and without aquifer support, respectively. The aquifer water influx is 101 MSTB over 31 years. The addition of the aquifer does not affect production much because the reservoir pressure keeps well above bubble point pressure.

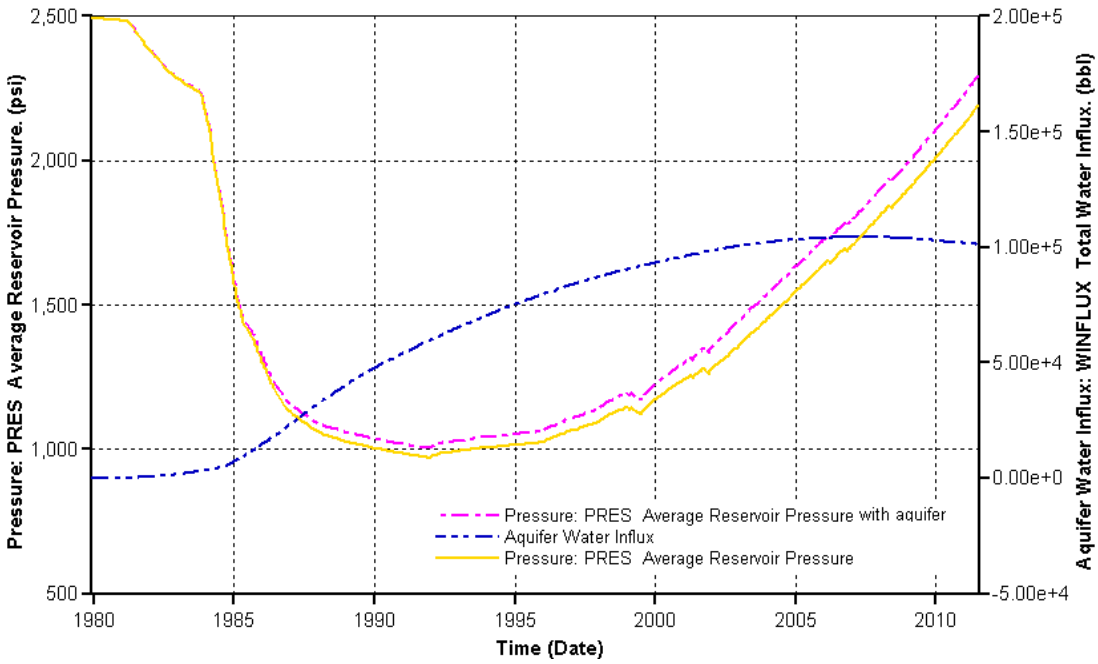

Figure 3.75. *Average reservoir pressure with or without aquifer support.*

The history match results of cumulative gas production and gas production rate of seven wells 05-017-06248, 05-017-06396, 05-017-06294, 05-017-06417, 05-017-06424, 05-017-06446, and 05-017-07553 with STO for updated model are shown in Figure 3.76. The reservoir pressure curve shows that the reservoir pressure remains stable over thirty years. The well maintained pressure is consistent with stable production.

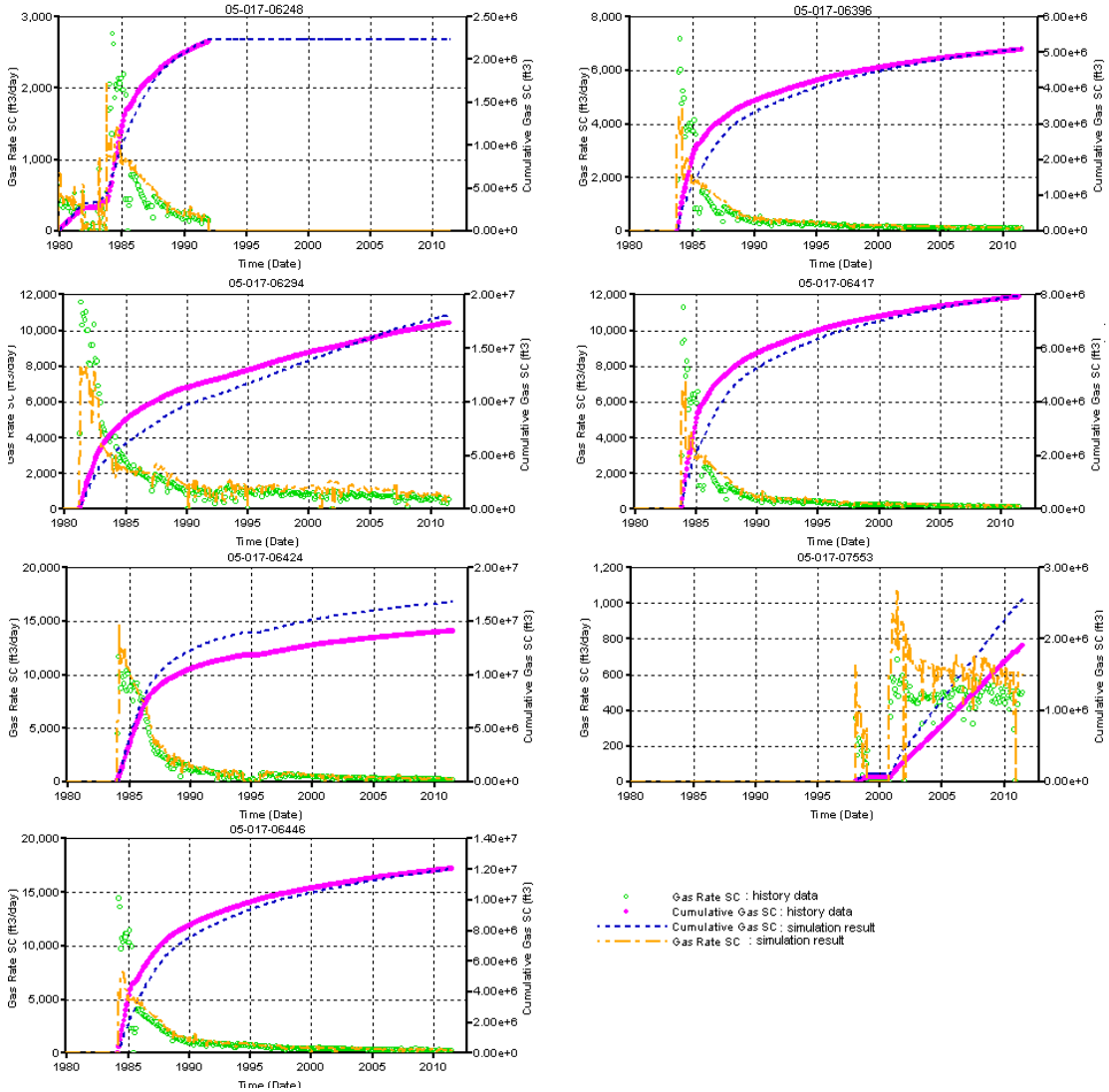

Figure 3.76. *The cumulative gas production and gas production rate of seven wells: 05-017-06248, 05-017-06396, 05-017-06294, 05-017-06417, 05-017-06424, 05-017-06446, and 05-017-07553, with STO compared to history data.*

The cumulative oil production and oil production rate of seven wells with STG are shown in Figure 3.77. Among these seven wells, well 05-017-06248 was shut in on 12/1/1991 and converted to a water injector. The simulation results are listed in Table 3.29. The cumulative oil production of Pintail's Reservoir inthe Grouse Field is 1,215 MSTB. The simulation data is 92% of the production data; thus the simulation results are a good match with history data.

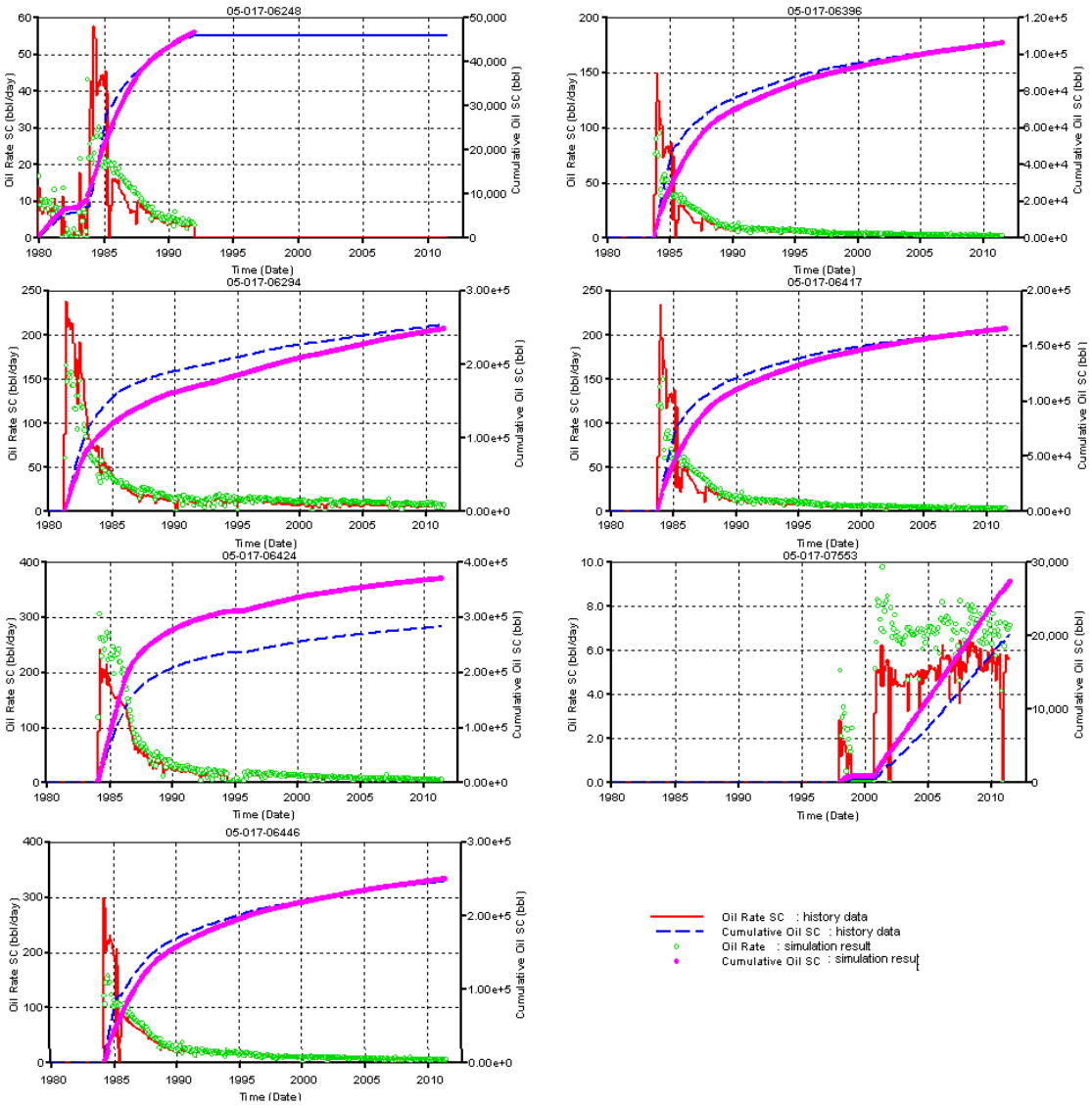

Figure 3.77. *The cumulative oil production and oil production rate of seven wells: 05-017-06248, 05-017-06396, 05-017-06294, 05-017-06417, 05-017-06424, 05-017-06446, and 05-017-07553, with STG compared to history data.*

Table 3.29. Simulation Results for Pintail's Grouse Field Sperger

Parameter	Oil
Original Oil in Place (OOIP)	10,541 MSTB
Mobile Oil in Place (STO)	6,270 MSTB
Average Pressure	2265 psi
Cumulative Production	1,119 MSTB
Recovery Rate (Compared to OOIP)	10.616 %
Recovery Rate (Compared to Mobile STO)	17.85%

Simulation: Grouse Field Spergen Reservoir for Fifty Years with CO_2 Injection

The reservoir performance with CO_2 injection for two years (01/01/2012-12/31/2013) was simulated with a pseudo-miscible model (black oil model) for fifty years of CO_2 injection (through 12/01/2063). The CO_2 injection rates were set as 0.25 MMSCF (5,107 tons/yr) and 1 MMSCF/day (20,427 tons/yr), respectively. The reservoir pressure and aquifer water influx are shown in Figure 3.78.

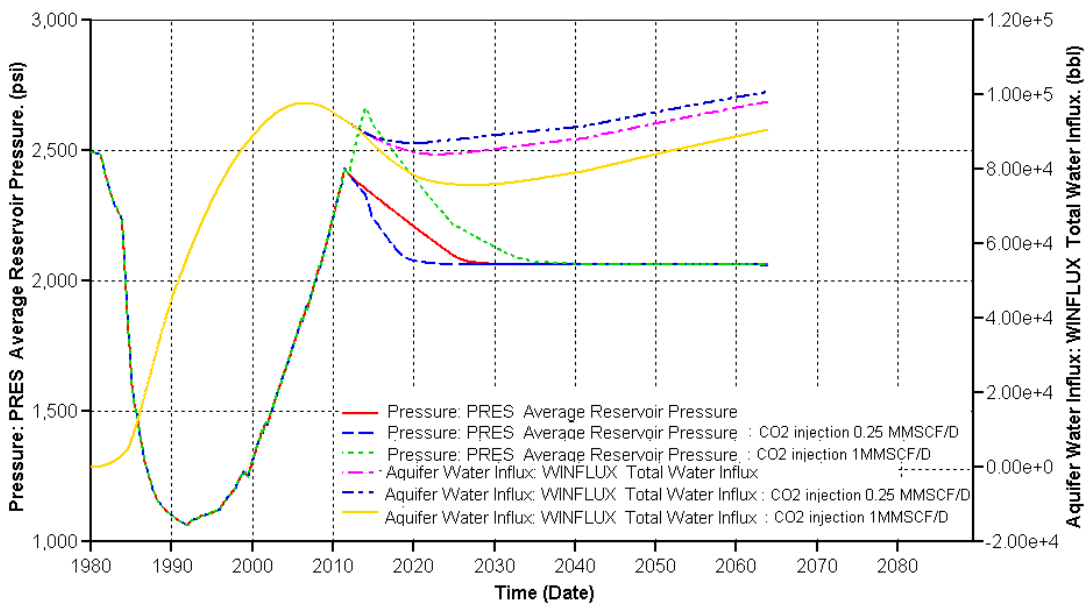

Figure 3.78. *Average reservoir pressure and aquifer water influx.*

The aquifer below the reservoir is set as a "Leakage Aquifer". When the pressure in the reservoir is higher than the aquifer, the mobile fluid in the reservoir will flow into aquifer; when

the pressure in the reservoir is lower than the aquifer, the water in the aquifer will flow into the reservoir. Thus the pressure in the reservoir is buffered by the aquifer.

The simulation results of cumulative oil production of Pintail wells for another fifty years compared to no CO_2 injection are summarized in Table 3.30 and shown in Figure 3.79, which show that CO_2 injection increased oil recovery. CO_2 was injected for only two years. For each incremental barrel of oil produced over the base case 4.20 and 2.97 MCF of CO_2 was required. The higher CO_2 injection rate favors economic recovery.

Table 3.30. Simulation Results Comparison for Pintail's Grouse Field Spergen Reservoir Over Sixty Years (12/01/2063) After Two Years of CO_2 Injection

	No injection	CO_2 injection 0.25 MMSCF/d	CO2 injection 1 MMSCF/d
Original Oil in Place (OOIP)	10,541 MSTB		
Mobile Oil in Place (STO)	6,270 MSTB		
Cumulative Production	1255.5MSTB	1299MSTB	1501.9MSTB
Recovery Rate (Compared to OOIP)	11.626 %	12.323%	14.248%
Recovery Rate (Compared to Mobile STO)	19.546%	20.718%	23.954%
CO_2 injected, tons (MCF)	0	10,227 (182,750)	40,911 (731,000)
MCF CO_2 for incremental barrel of oil produced	0	4.20	2.97

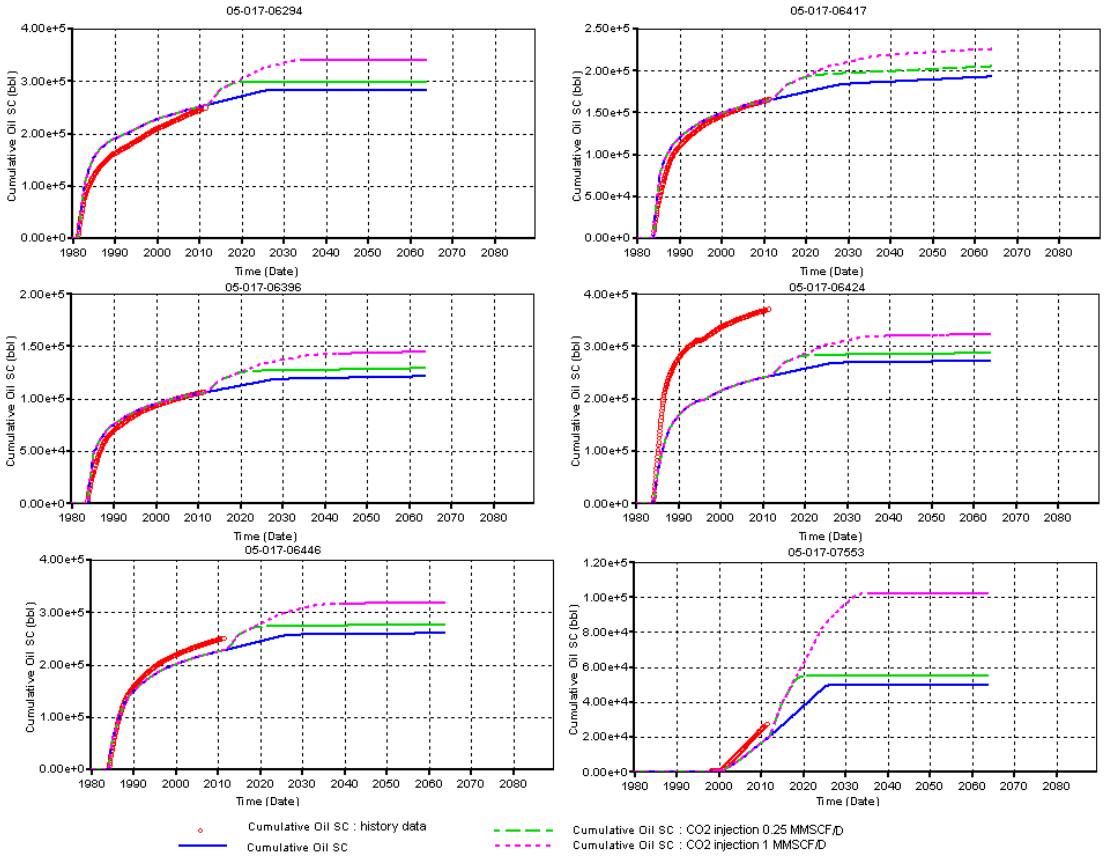

Figure 3.79. *Cumulative oil production of Pintail's wells in the Grouse Field with and without two years of CO_2 injection.*

<u>40 years CO2 Injection with Constant CO_2 Production Rate</u>

A new schedule for 40 years CO_2 injection was accomplished. All produced CO_2 is recycled and new CO_2 is kept at a constant 1MMscf/d. The sum of recycled CO_2 and new CO_2 is then injected, thus the injection rate increases with time. This is in contrast to last month when injected CO_2 was held constant and thus as CO_2 recycle is increased new CO2 was decreased. Figure 3.80 shows the oil production and CO_2 injection rate. CO_2 breaks through after four years (2016 in this case), and at the end of 2052, recycled CO_2 is almost three times of produced CO_2 or a total injection rate of almost 4MMscf/d.

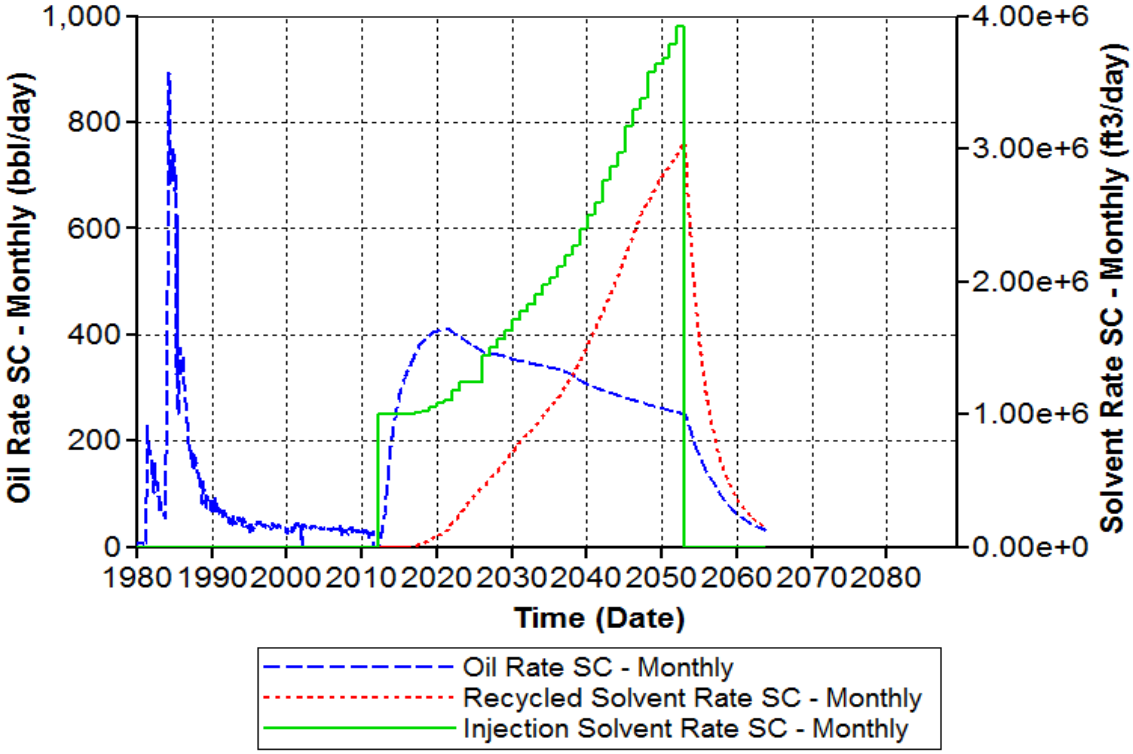

Figure 3.80. *Oil rate, recycled and injection solvent rate plot*

Comparison of Two CO_2 Injection Schedules

Figure 3.81 shows the difference of cumulative oil production between constant CO_2 injection rate 1MMscf/d and constant new CO_2 injection rate 1MMscf/d schedule. Increasing CO_2 injection rate has little influence on well 05-017-07553, but for others wells, it is about a 15% increase in recovery.

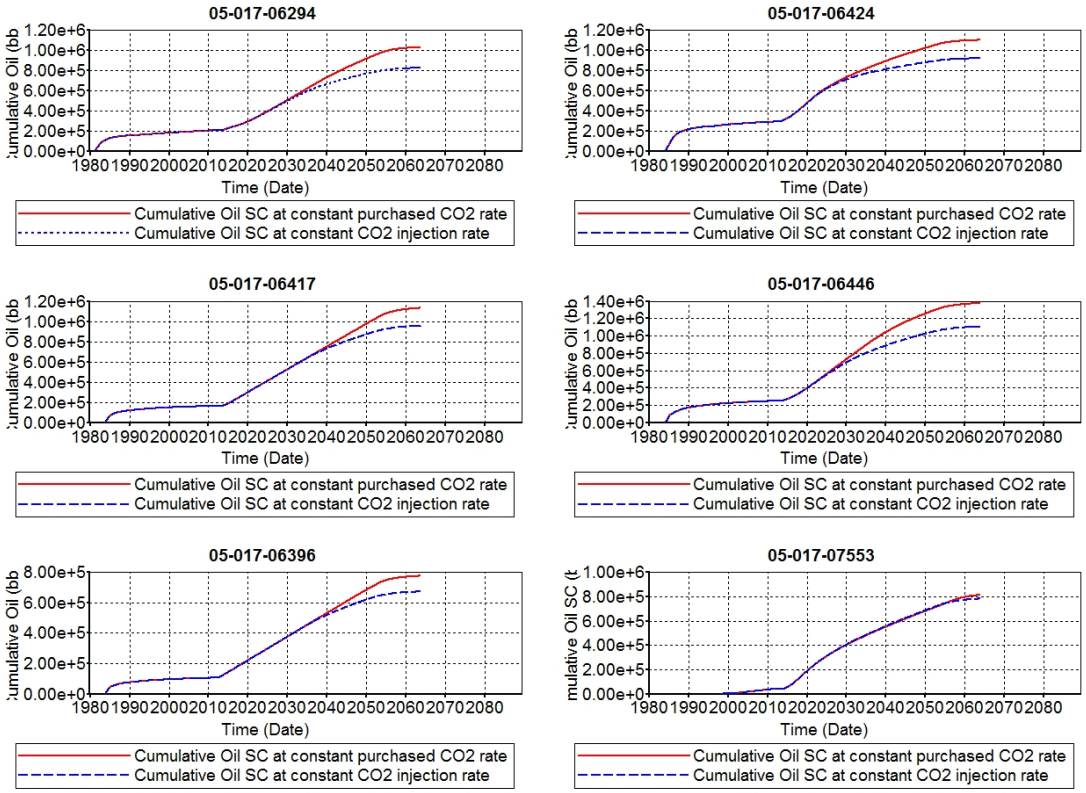

Figure 3.81. *The cumulative oil production of Pintail wells with CO_2 injection in 40 years.*

Figure 3.82 is the comparison of average reservoir pressure and oil rate. Note that surface gas rate is set as the primary constraint for production wells and 1500 psi BHP is set as the second constraint. Simulation runs at primary constraint first until secondary constraint is violated, and then second constraint is automatically set as primary constraint. Average pressure increases first at high surface gas rate constraint because of CO_2 injection. After ten years production at high STG, reservoir pressure begins to decrease. We can see that at the constant purchased CO_2 situation, average pressure and oil rate are both higher than at constant CO_2 injection because more CO_2 were injected into the reservoir. Table 3.31 is the comparison of recovery. More than 9% of OOIP oil is recovered compared with higher injection rate.

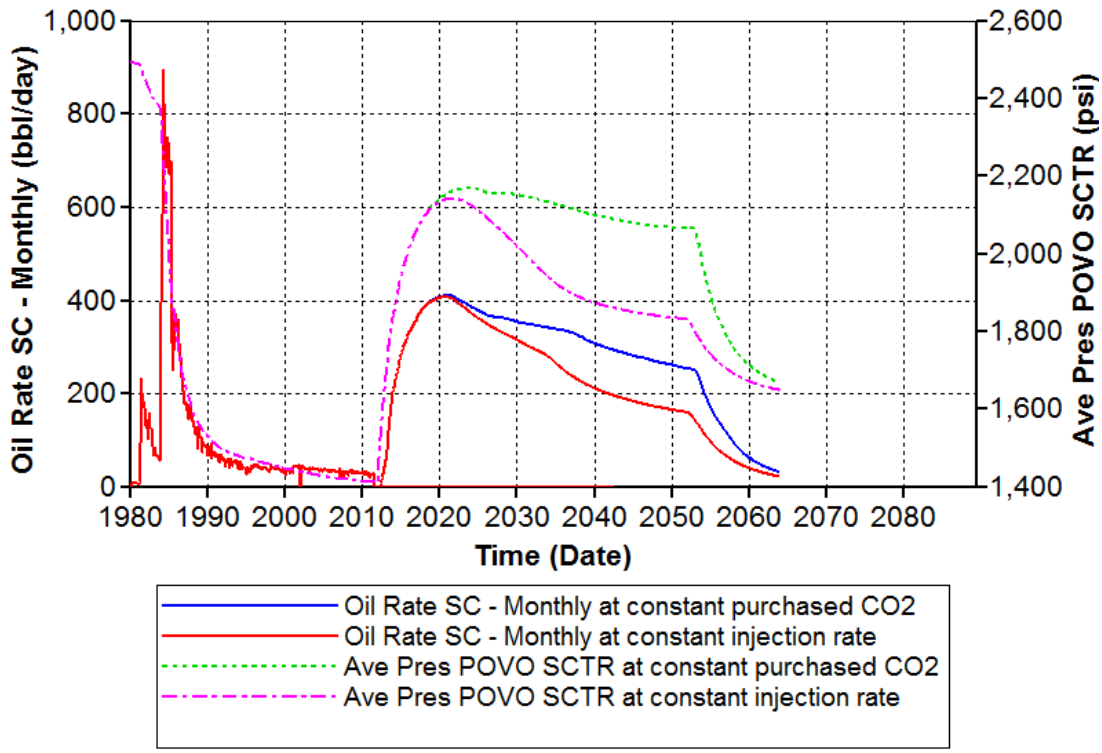

Figure 3.82. *Oil rate and average pressure comparison between constant new CO_2 of 1 MMSCF/day and constant injection rate of 1 MMSCF/day*

Table 3.31. Simulation results comparison for Pintail reservoir in 40 years (12/01/2063)

	CO_2 injection rate constant 1 MMSCF/d	New CO2 rate 1 MMSCF/d plus all recycle
Original Oil in Place (OOIP)	10,541 MSTB	10,541 MSTB
Cumulative Production	5311.0MSTB	6274.4MSTB
Recovery Rate (Compared to OOIP)	50.384%	59.524%
CO_2 injected, (MMSCF)	14,610	30,565

Conclusions

A comprehensive study including reservoir characterization, geomodel construction and reservoir simulation was performed for the Grouse Field Spergen Reservoir, Cheyenne County, Colorado belonging to the small producer Pintail Petroleum Ltd. A preliminary reservoir characterization study was carried out for a reservoir in the Pawnee Pioneer Field, Weld County, Colorado belonging to another small producer, Ward Petroleum Ltd. The Grouse Field reservoir was selected for reservoir simulation considering that it contains a water injector and the wells are interconnected; in addition, it meets with all the necessary criteria for CO_2 EOR.

History matching with STG as the main constraint obtained simulated cumulative oil production as 92% of the history production data, which shows that the simulation results are a good match with history data.

The reservoir performance with CO_2 injection for two years (01/01/2012-12/01/2013) was simulated with a pseudo-miscible model (black oil model) for fifty years. The CO_2 injection rates are set as 0.25 MMSCF (5,107 tons/yr) and 1 MMSCF/day (20,427 tons/yr), respectively. For 0.25 and 1 MMSCF/day CO_2 injection rates, 4.20 and 2.97 MCF of CO_2 was required for each incremental barrel of oil produced over the base case, respectively, which shows higher CO_2 injection rate favoring economic recovery.

3.2.4.3. Economics of CO_2-EOR

An economic calculator has been designed to calculate several important economic values, including initial or capital investment, net present value, and payout. The main inputs for the calculator include an oil price forecast, current production trend, oil production forecast with CO_2 injection, operational expense, horsepower requirements for compression, and pipeline estimates. After the Economic Calculator has performed some initial calculations it can then be sent to small producers, for example, Pintail Petroleum, who can then fine-tune some of the estimates and have an accurate net present value (NPV).

Capital Investment

The capital investment was roughly calculated following steps outlined in previous research. Due to the uncertainty of the capital investment estimation, this tool allows the value to be changed, allowing more accurate calculations when accurate cost estimations are available. Three major facilities were considered in the capital investment. First the compression was calculated using a simple correlation between the flow rate and the cost. Next, a separator cost was estimated by researching prices online. The challenge of estimating the cost of equipment lies in the discounts and reduced prices that many companies receive. Finally the cost of pipeline was estimated using a simple calculation:

$$C_{pipe} = \frac{\$60{,}000}{inch*mile} * Dia_{pipe} * L_{pipe} \tag{3.37}$$

Net Present Value

Net present value is a common method of analyzing the present value of an investment. The formula used to calculate NPV is:

$$NPV = \sum_{t=1}^{n} \frac{R_t}{(1+i)^t} \tag{3.38}$$

where R_t is the cash flow for period of length t, t is the time period, i is the discount rate, and n is the number of time periods for which the NPV is calculated. The calculator estimates a net

present value over the next 20 years (n=20) and the time period t= 1 year. For this project i has been set at a modest value of 10%.

Payout

Finally, the payout is calculated to show the time required for the project to pay for itself. The payout is calculated by subtracting the cash flow from the capital cost each month until the investment is paid. The payout in this project is long; the cash flow of the project is negative for two years.

Economic Calculator for CO2 Flooding Project	
Investment	$1,105,089.88
Monthly OPEX	2950
Discount rate	0.1
NPV	$1,470,146.74
Payout (Months)	92

OPEX Itemized list				Initial Investment	
Item	Current cost	Expected Cost	Difference	Item	Cost
Overhead	200	500	300	Pipeline	720,000.00
Water Disposal	500	550	50	CO2 Seperator	25,000.00
Lifting costs	700	900	200	Compression	360,089.88
Maintenance	150	350	200		
CO2	0	2000	2000		
Compression(DPC2202LE)	0	200	200		
			0		
			0		
			0		
			0		
			0		
			0		
			0		
		Total	2950	Total	1,105,089.88

Figure 3.83. *Economic calculator sheet for CO_2 flooding*

Calculator Inputs

The calculator uses several inputs. First is the production trend (production forecast without CO_2 injection). This was achieved by running the CMG model with water injection only until 2052. This trend provides a baseline to calculate oil rate uplift. Next the production forecast (forecast with CO_2 injection) is used to estimate the production of the field when CO_2 is injected until 2032. Several different forecasts were run to describe different scenarios. Ultimately an injection rate of 1MMscf at 2000 Psi was used. The revenue for this project is based on the oil rate uplift:

$$Uplift = Production_{CO2} - Production_{trend} \tag{3.39}$$

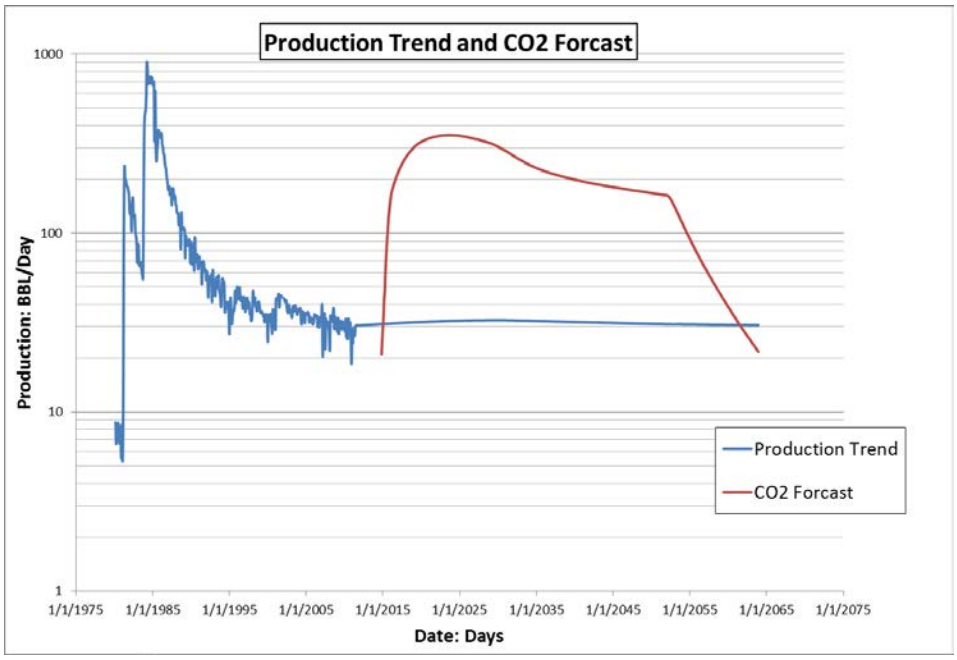

Figure 3.84. *Production Trend and CO_2 Forecast*

Next an oil price forecast was obtained from the Energy Information Administration website (https://www.eia.gov). The price deck was then used with the oil rate uplift to calculate the revenue generated. The gas rate is not used for two reasons. First, the field has a very low gas:oil ratio. Low gas production combined with low gas prices will not substantially affect the economics. Second, Pintail Petroleum does not report any gas production.

Operational expense was also roughly estimated. The OPEX was subtracted from the revenue to find the monthly cash flow. One of the additions to the capital investment was payment of the increased OPEX until uplift started two years after CO_2 injection began.

Sensitivities

Finally, sensitivities were performed to determine which cost/price estimates should be the most accurate. In the graphs below, two parameters were varied at 75%, 100%, and 125%. The price deck and the oil rate forecast had the greatest impact on the NPV. This confirms our plan to focus our efforts on the CMG model and accept the rough estimates on the capital cost and OPEX.

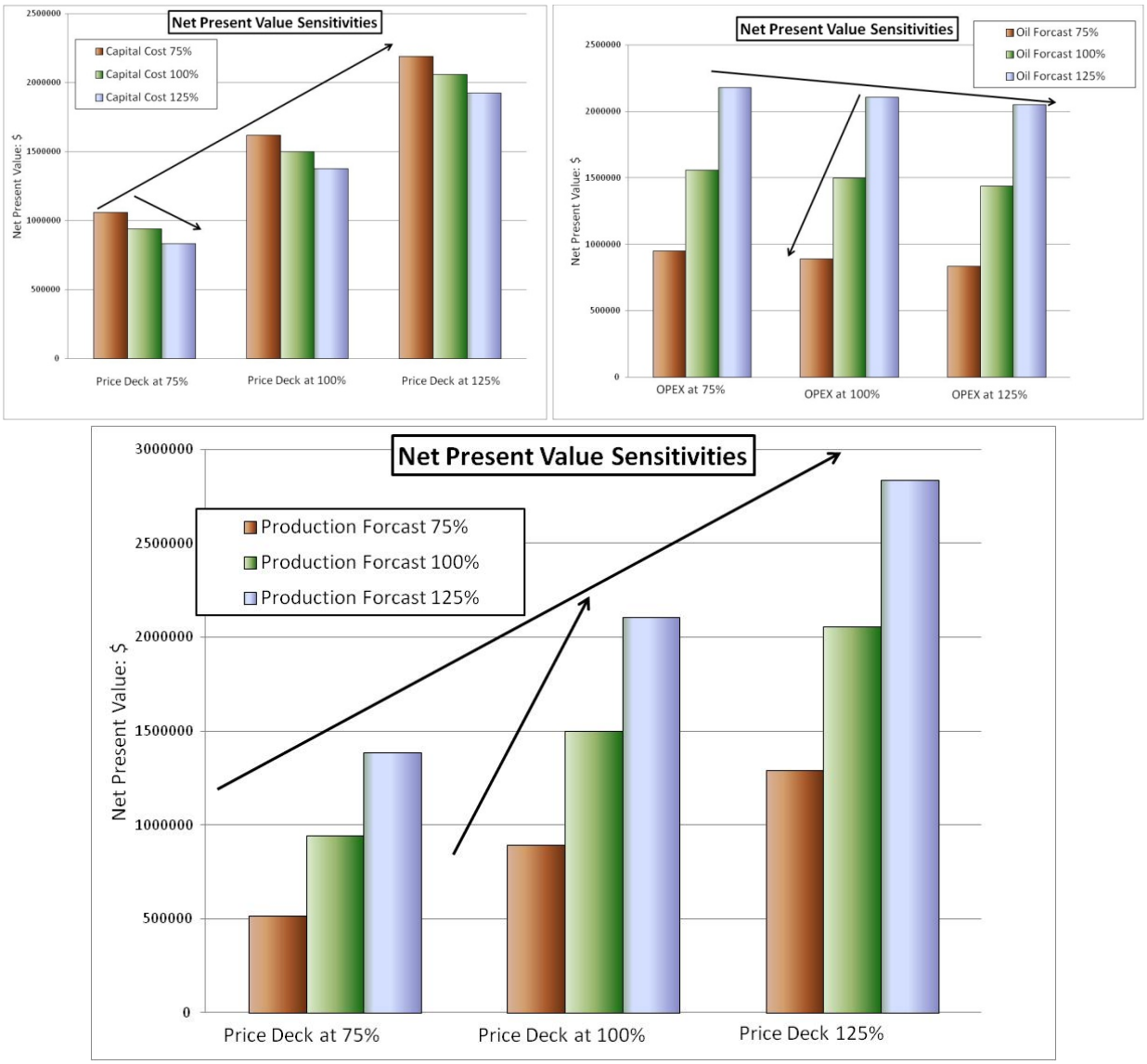

Figure 3.85. *Net Present Value Sensitivities*

<u>Summary</u>

Presently the price deck and the oil forecast are the most accurate inputs. It is recommended to refine the capital costs: there is an option that can reduce the capital cost, thus reducing the risk of the project. Renting compression from a company would eliminate a majority of the initial compression costs. By renting a compressor, the project can more easily be abandoned if minimum oil uplift is not met. Many rental companies also perform routine maintenance, which lowers the maintenance OPEX. Several compression companies in the Denver area have been asked to provide an estimate.

The forecast of enhanced oil production from CO_2 used in this analysis is considered optimistic, while the first increased production due to CO_2 injection is considered very conservative. This field has not been water-flooded except for injection of the small amount of

water that has been produced; thus, all the production to date has been primary production, though it is believed to have a natural water drive. Thus this high production due to CO_2 injection may not be too optimistic. Also from field experience, first oil breakthrough is usually six to twelve months after the start of CO_2 injection. It is believed that the reservoir model is too homogeneous and thus breakthrough is slower than normal. For economics the earlier breakthrough provides earlier cash flow and thus an earlier payout. The later breakthrough indicates a better sweep and thus a higher ultimate recovery, but poorer economics, due to a later date of return. It is recommended to run future sensitivities to the recovery timing and rate.

3.3. Impact to Producers

Enhanced Oil Recovery using CO_2 injection into the ground is a well-known technique that allows a typical well to increase its overall yield by as much as 40%. However, as currently practiced, EOR requires pipelines to deliver CO_2 from natural reservoirs to oilfields. This technique is only practical for oilfields within limited distance from such reservoirs, as the capital cost of building pipelines over long distances is prohibitive. In general, such pipelines only serve major oilfield customers as the return from EOR from isolated small fields is insufficient to justify the capital cost of pipeline construction, and small producers typically do not have the cash to pay for such construction. In addition, pipeline CO_2 is only available in a few very limited regions of the country which possess natural CO_2 reservoirs.

What is needed is a system that can deliver CO_2 directly to small producers, wherever they may be, without major capital expenditures, in a timely fashion after a decision has been made to undertake EOR, on a scale relevant for small-field operations.

To meet this unmet need, Pioneer Astronautics in this program developed a modular, truck-portable renewable energy system for CO_2-EOR called Green Oil^{TM} . The Green Oil^{TM} technology, operates through the steam-oxygen reforming of biomass into CO_2 and hydrogen. This is followed by product gas cleanup, conditioning, CO_2-H_2 enrichment and gas separation. The system simultaneously generates CO_2 for on-site well flooding and H_2 for carbon-free electrical power for local or grid use. It is designed to generate 1million cubic feet of CO_2 per day for the recovery of about 100 barrels of oil per day. The hydrogen produced is capable of generating about one to two megawatts of carbon-free electricity. This power can be used locally or sold to the local grid to reduce capital and operating expenses. In contrast to approaches involving the construction of pipeline, large power plants, or other mega projects which typically take many years, the transportable Pioneer Astronautic system can go directly to the small producer fields where it is needed, and do so in a timely manner. As an additional advantage, the system sequesters more biomass-derived carbon than is released by the burning of the oil it yields, and thus can be said to not only produce carbon-free electricity, but carbon-free oil.

3.4. Technology Transfer Efforts

This project has demonstrated the unique characteristics of the Green Oil™ project of co-generating CO_2 for Enhanced Oil Recovery and H_2 for electrical generation at scale suitable for small oil producers through the steam-oxygen reforming of biomass fuel. To gain technology visibility for potential end users, several technology transfer efforts were conducted in this effort. These included participation in technical conferences/workshops, the construction of a website, and article publication in a trade magazine. These are summarized below:

3.4.1. Conference Presentations

Robert Zubrin, "Green Oil: CO_2 – Enhanced Oil Recovery for America's Small Oil Producers," RPSEA Onshore Production Conference, November 29, 2012, Houston, TX.

Mark Berggren, "Green Oil: CO_2 – Enhanced Oil Recovery for America's Small Oil Producers," RPSEA Onshore Production Conference, April 10, 2012, Midland, TX.

3.4.2. Website Construction

A website has been constructed that explains our modular and truck-portable biomass-based steam reforming technology to create CO_2 for EOR, H_2 for electricity generation, and how it meets the needs of the small producer. The URL is given below:
http://www.pioneerastro.com/RPSEA.html

3.4.3. Article Publication

An article summarizing our technology development was accepted to World Oil, April 2013, Vol. 234 No. 4. The URL is given below.
http://www.worldoil.com/CurrentIssue.aspx

4. Summary and Recommendations for Future Work

Pioneer Astronautics has demonstrated a unique truck-portable, high pressure, steam-oxygen biomass reforming technology that can supply high concentrations, pressures and flow rates of CO_2 suitable for Enhanced Oil Recovery, and H_2 for power generation for the small oil producers. The Green Oil™ portable technology demonstrated 6000 SLPM product gas, 35 -40% CO_2, and 45 - 50% H_2 at 10 bar. Fuel bridging and high pressure drop in the reformer limited the scale-up to higher flow rates Techno-economic reservoir modeling analysis indicates that at full scale the device has the potential to generate a favorable economic recovery of oil. Further development is required to demonstrate long duration, full scale operation. The two main areas for additional development are establishing stable, bridge-free reformer operation and heat integration of the Water Gas Shift reactor/ Steam Generator. The following

recommendations are made for further development of this process and achieve full scale operation:

- Operate the grate and bed stirrer with independently for more effective disruption of bridging and char/ash removal in the reformer
- Integrate the WGS reactor with heat recovery for simultaneous thermal control of catalyst exotherms and steam generation for the reformer
- Re-size the catalytic Tar Destruction reactor for sufficient residence time

Together with Pioneer Energy, Pioneer Astronautics is continuing to develop the Green Oil system. Pioneer Energy is developing an oxygenated steam reformer that generates carbon dioxide and hydrogen from natural gas, while Pioneer Astronautics has begun to develop an oxygenated steam reformer that can utilize coal feedstock. Coal fuel has numerous advantages, and Table 4.1 summarizes our motivation for pursuing coal reforming for CO_2-EOR for the small oil producer.

Table 4.1. Advantages of Coal Reforming CO_2-EOR for the Small Producer

Benefit	Payoff/Utility
High C content	High energy density
Widely available feedstock	Service small oil producers throughout Rocky Mountains, Southwest and Appalachia
Inexpensive feedstock	PRB coal is estimated to be ~27$/ton delivered, w/in 50 miles
Green technology	Sequesters more coal-derived carbon than is released by the burning of the oil Generation of carbon-free electricity Established emissions control technology in place
Value-added products	Ash is a valuable additive in concrete, reduces the cost/energy demand in manufacturing and greenhouse emissions Sulfur is a salable chemical precursor for fertilizer

These two approaches are complimentary, as natural gas offers the advantage of ease of use, while coal provides the cheapest potential feedstock. The latter is especially true in the Rockies, where very low cost coal is readily available. All three reformer systems – biomass, coal, or natural gas – can be readily mated to the same portable gas separation system, allowing EOR to go forward at both large and small producer oil wells anywhere in the country using the most locally-advantageous feedstock.

5. References

Aznar, M. P., Caballero, M. A., Gil, J., Martin, J. A., and Corella, J., 1998. "Commercial steam Reforming catalysts To Improve Biomass Gasification with Steam-Oxygen Mixtures. 2. Catalytic tar Removal," Ind. Eng. Chem. Res. 36, 2668.

Aznar, M. P., Caballero, M. A., Corella, J., Molina, G., and Toledo, J. M., 2006. "Hydrogen Production by Biomass Gasification with Steam-O2 Mixtures Followed by a Catalytic Steam Reformer and a CO-Shift System," *Energy & Fuels* 20, 1305.

Baker E. G., et al., 1984. "Oxygen/Steam Gasification of Wood in a Fixed-Bed Gasifier," *Ind. Eng. Chem. Process Des. Dev.* 23, 725-728

Casal, J. and Martinez-Benet, 1983. "A better way to calculate cyclone pressure drop," *Chem. Eng*., Jan. 24, 1983, 99.

Churcher, P.L., French, P.R., Shaw, J.C., Schramm, L.L., Rock Properties of Berea Sandstone, Baker Dolomite, and Indiana Limestone, SPE 21044-MS, presented at SPE International Symposium on Oilfield Chemistry, 20-22 February 1991, Anaheim, California.

COGCC, 2011. Colorado Oil and Gas Conservation Commission. http://dnrwebcomapg.state.co.us/mg2010app/. Accessed November 2011.

COGIS, 2011. Colorado Oil and Gas Information System, 2011. www.cogcc.state.co.us. Accessed November 2011.

Crane Company. 1988. "Flow of fluids through valves, fittings, and pipe." Technical Paper No. 410 (TP 410).

Devi, L., Ptasinski, K. and Janssen, F. J. J. G., 2005., "Pretreated olivine as tar removal catalyst for biomass gasifiers: investigation using naphthalene as model biomass tar", Fuel Processing Technology 86, 707.

DOE/NETL, 2008. "Storing CO2 with Enhanced Oil Recovery," DOE/NETL-402/1312/02-07-08 ISO, 2003. "Measurement of fluid flow by means of pressure differential devices, Part 1: Orifice plates, nozzles, and Venturi tubes inserted in circular cross-section conduits running full." International Standards Organization, Reference number: ISO 5167-1:2003.

Esco Engineering, 1998. "Cyclone Size and Efficiency Calculations", Neil Stone, Esco Engineering. http://www.esco-engineering.ca/. Accessed November 2011

Gil, J., Aznar, M. P., Caballero, M. A., Frances, E., and Corella, J., 1997. "Biomass Gasification in Fluidized Bed at Pilot Scale with Steam-Oxygen Mixtures. Product Distribution for Very Different Operating Conditions," *Energy & Fuels* 11(6), 1109.

Gil, J., Corella, J., Aznar, M. P., and Caballero, M. A., 1999. "Biomass gasification in atmospheric and bubbling bed: Effect of the type of gasifying agent on the product distribution," *Biomass and Bioenergy* 17, 389.

GO-TECH, 2011. http://octane.nmt.edu/gotech/Main.aspx. Accessed November 2011.

Harris, M. Lee. "Validation and Comparison of Carbon Sequestration Project Cost Estimation Models with Project Cost Data Obtained from the Southwest Carbon Sequestration Partnership." Petroleum Recovery Research Center, 2010.

Hart, D. J. and Wang, H. F. Laboratory Measurements of a Complete Set of Poroelastic Moduli for Berea Sandstone and Indiana Limestone. *J. Geophysical Research*, 100 (B9), pp. 17741-17751, 1995.

Higley, D. K., and Cox, D. O.,2007. "Oil and Gas Exploration and Development along the Front Range in the Denver Basin of Colorado, Nebraska, and Wyoming," U.S. Geological Survey Digital Data Series DDS-69-P, http://pubs.usgs.gov/dds/dds-069/dds-069-p/REPORTS/69_P_CH_2.pdf)

Kansas Geological Survey, Energy Research, 2011. http://www.kgs.ku.edu/Publications/Bulletins/Sub9/index.html). Accessed November 2011.

Kitzler, H., Pfeifer, C., and Hofbauer, H., 2011. "Pressurized gasification of woody biomass- Variation of parameter," *Fuel Processing Technology* 92, 908.

Koch, W.H., and Licht, W., 1977. "New design approach boosts cyclone efficiency", *Chem. Eng*. Nov 7 1977, 80

Lv, P., et al., 2007. "Hydrogen rich gas production from biomass air and oxygen/steam gasification in a downdraft gasifier," Renewable Energy 32, 2173-21-85

McCaffery, Frank G., Measurement of Interfacial Tensions and Contact Angles at High Temperature and Pressure. JCPT 72-03-03, Journal of Canadian Petroleum Technology, 11 (3), Jul-Sept 1972. (Presented at the 23rd Annual Technical Meeting of The Petroleum Society of CIM, Calgary, Alberta, May, 1972.)

Meng, X., et al., 2011. "Biomass gasification in a 100 kW steam-oxygen blown circulating fluidized bed gasifier: Effects of operational conditions on product gas distribution and tar formation," *Biomass and Bioenergy* 35, 2910.

Moe, J.M., 1962. "Design of Water-Gas Shift reactors," *Chem. Eng. Progress*, **58** (3), 33

New Mexico Bureau of Geology & Mineral Resources, 2011. http://geoinfo.nmt.edu/faq/energy/petroleum/home.html. Accessed November 2011,

NIST-JANAF Thermochemical Tables, Fourth Edition, 1998. *J. Phys. Chem. Ref. Data*, Monograph 9, 1-1951

Ohio Division of Geological Survey, 2004. Oil and gas fields map of Ohio: Ohio Department of Natural Resources, Division of Geological survey Map PG-1. http://www.ohiodnr.com/Portals/10/pdf/pg01.pdf. Accessed November 2011.

Rao, D.N., A New Vanishing Interfacial Technique for Miscibility Determination, Elsevier, *Fluid Phase Equilibria*, volume 127-139, 1997.

Ran, J. and Li, C., 2012. "High temperature gasification of woody biomass using regenerative gasifier," Fuel Processing Technology 99, 90.

Reed T.B., and Gaur S., 2001. "A Survey of Biomass Gasification 2001," 2nd Edition, National Renewable Energy Laboratory and the Biomass Energy Foundation.

Reed, T. B., Graboski, M. S., And Levie, B., 1994, "Fundamentals, Development and Scaleup of the Air-Oxygen Stratified Downdraft Gasifier," SERI/PR-234-2571, Biomass Energy Foundation Series.

Schneider, F. N., Owens, W.W. Relative Permeability Studies of Gas-Water Flow

Following Solvent Injection in Carbonate Rocks. SPE 5554, wt. s presented at the SPE-AIME 50th Annual Fall Meeting, held in Dallas, TX, Sept. 28- Oct. 1, 1975.

Siedlecki, M. and de Jong, W., 2011. Biomass gasification as the fist hot step in clean syngas production process – gas quality optimization and primary tar reduction measures in a 100 kW thermal input steam-oxygen blown CFB gasifier," Biomass and Bioenergy 35, S40-S62.

Tillman, D. A., "Wood as an Energy Resource." (1978) Academic Press.

"U.S. Energy Information Administration - EIA - Independent Statistics and Analysis." *Analysis & Projections*. N.p., 25 June 2012. Web. 17 Sept. 2012. http://www.eia.gov/analysis/projection-data.cfm

Waldheim, L., Nilsson, T., 2001. "Heating value of gases from biomass gasification," TPS-01/16, Report prepared for: IEA Bioenergy Agreement, Task 20 - Thermal Gasification of Biomass

Wang, Y. and Kinoshita, C. M., 1992. "EXPERIMENTAL ANALYSIS OF BIOMASS GASIFICATION WITH STEAM AND OXYGEN," Solar Energy 49(3), 153.

Wickstrom, L., et al., 2008. "Enhanced Oil Recovery Potential and CO2. Sequestration in the Michigan and Northern Appalachian Basins Region," Eastern Section AAPG Pittsburgh October, 2008.

6. List of Acronyms and Abbreviations

Acronym/Abbreviation	Full Name
Act	Actual conditions
Atm	atmosphere
bio	biomass
C	Concentration
C_0	Initial concnetration
^oC	Degrees centigrade
CE	Carbon Conversion Efficiency
CGE	Cold Gas Efficiency
cm	centimeter
DAC	Data Acquisition and Control
EOR	Enhanced Oil Recovery
ER	Equivalence Ratio
FPS	Feet Per Second
FW	Feed Water flow rate to Boiler -1
GO	Green Oil
GPH	Gallons per Hour
GR	Gasification Ratio
GY	Gas Yield
hr	hour
in	inches
J	Joule
K	Degrees Kelvin
k	Rate coefficient

k	kilo
kg	kilogram
kPa	Kilopascals, 10^3 Pascals
lb	pound
$\dot{m}$	Mass flow rate
m	meter
m_C	Mass fraction carbon
m_H	Mass fraction hydrogen
m_O	Mass fraction oxygen
m_S	Mass fraction sulfur
min	minute
MJ	MegaJoule, 10^6J
mol	mole
MW_{avg}	Average Molecular Weight Product Gas
$\dot{n}$	Molar flow rate
Nm^3	Normal cubic meter
OOIP	Original Oil In Place
P	Pressure
P & ID	Process and Instrumentation Diagram
Pa	Pascal
PFD	Process Flow Diagram
PG	Process Gas
PSI	Pounds Per Square Inch
PT	Pressure Transducer
Q	Volume flow rate
QP	Flow Rate of Propane
R	Gas Constant
s	second
SCFD	Standard Cubic Feet per Day
SCFM	Standard Cubic Feet Per Minute
SLPM	Standard Liters Per Minute
SOBV	Solenoid Operated Ball Valve
S/B	Steam to Biomass Ratio
S/O	Steam to Oxygen Ratio
SP	Stream Point
SV	Superficial gas velocity
Stoich	Stoichiometric
TC	Thermocouple
TCD	Thermal Conductivity Detector
vol. %	Volume percent
WGS	Water Gas Shift reactor
η	Efficiency
η_{CE}	Carbon conversion efficiency
η_{CGE}	Cold gas efficiency

τ_R	Residence time

Appendix

A.1. Process Model Stream Table Summary

A system process model was developed with the goal to predict process behavior, mass and enthalpy balances, and hardware design. The calculation assumptions include:

- Pine wood feedstock with a base formula of $CH_{1.5}O_{0.67}$, formula weight 24.0715 g/mole
- Moisture and ash content of 10% and 7.0%, respectively
- Biomass heat of formation of -1.175 x 10^8J/kmol per $CH_{1.5}O_{0.67}$
- 70% boiler efficiency
- The steam and oxygen reactant temperature and pressure to the reformer is 453K and 1000 kPa, respectively.
- A water gas shift reaction temperature of 523K is assumed

The model flow sheet is presented in Figure A.1.1, and contains the core unit operations of the 4000 SLPM (200,000 SCFD) reformer system including boilers, super heater, reformer, cyclone, water gas shift reactor and condensers described in the process flow diagram in Figure 3.1. The model calculates the material and enthalpy flows for the reformer system. Enthalpy flow for the gas streams are shown as the sum of the heat of formation plus the enthalpy of gas components at a reference temperature of 298 K. Tar formation is not presently accounted for in the calculation.

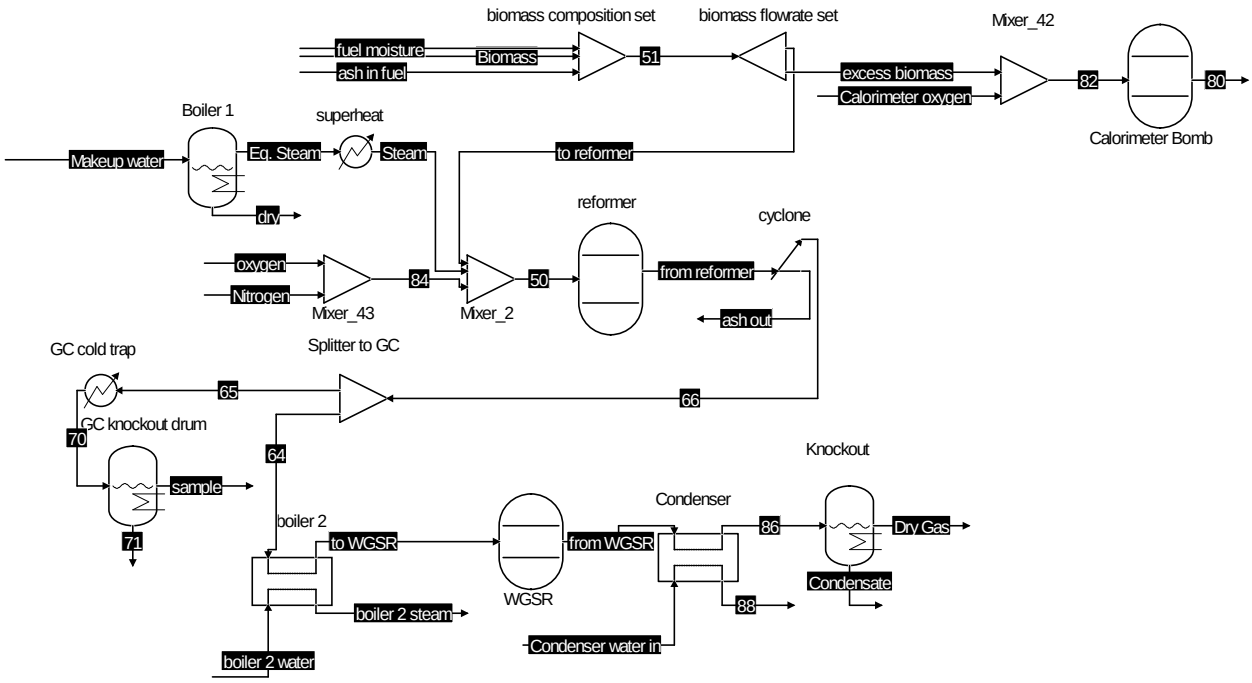

Figure A.1.1. *Process Model Flow Sheet*

A stream table comparison between experimental and calculated data is provided in Table A.1.1. These data summarize the gas vapor compositions, molar flow rates, pressure, temperature for the flow entering and exiting the biomass reformer. Good agreement exists between the observed experimental gas product composition given and that calculated by the model.

Table A.1.1. Comparison of Experimental and Process Model Results for the Reformer

System Parameter	Experimental Value	Model Calculation
Reformer Pressure	1103 kPa	1000 kPa
Steam Feed Rate	1464 SLPM	1613 SLPM
Oxygen Feed Rate	343 SLPM	403 SLPM
Biomass Feed Rate	1.95 kg/min	1.81 kg/min
Steam/Oxygen Mole Ratio	4.3	4.0
Reformer Exit Temperature	1014 K	1028 K
Reformer Product Gas Composition (mole fraction)		
H_2	0.25	0.33
CO_2	0.18	0.17
CH_4	0.03	-
CO	0.18	0.17
H_2O	.36	0.33

A.2. GO™ Piping and Instrumentation Diagram (P & ID)

A piping and instrumentation diagram was constructed for the GO™ system. These drawings identify all of the instrumentation and control functions for the system. The P&ID was also used to generate a bill of materials for valve, piping, and other instrumentation lists in advance of fabrication. Valves are shown in their normal operating states. For example, the steam vent valve, solenoid operating valve SOBV-01 in Figure A.2.1, is in the normally open position. Similarly the steam feed valve, solenoid operated ball valve SOBV-02, is normally closed. The feed gases (N_2, O_2, H_2 and propane) pass sequentially through regulator pressure indicators, control valves, orifice flow meter, mass flow controller valves, and a check valve. Bottled nitrogen was fed from a trailers consisting of individual 12 cylinders manifolded together. Similarly, oxygen was fed from two trailers containing 6 manifolded cylinders. Oxygen, hydrogen, and propane flow rates are measured with calibrated mass flow controllers. H_2 and propane are fed from individual gas bottles. The nitrogen supply purge is primarily to prevent temperature and pressure excursions and is used for purging out air (O_2) through the system before and during startup, for purging the biomass magazine during operation, and to purge the system during and after shutdown.

Steam for the initial start-up is generated using propane heating of water. Bottled propane gas is injected into the Boiler-1 assembly through a burner nozzle. Ambient air is entrained into the propane flow. The burner is equipped with a glow plug and is ignited remotely using the automated control system. Water is converted to steam in a pressurized steam vessel (Steam Vessel-1). The steam feeds into an orifice flow meter and super heater before it enters the-inlet gas injector of the reformer. The steam flow orifice uses a differential pressure transmitter for measuring the pressure drop across the orifice. Oxygen feed gas mixes with steam downstream of the steam flow orifice and before the super heater. Superheated steam is created by flowing H_2 into the steam/oxygen mixture and igniting the mixture using an automatic and remotely controlled glow plug. The super-heated steam is injected into the gasifier in a downdraft configuration. Temperature readings at various points along the bed are measured using Type-K thermocouples. Pressure measurements at several points along the gasifier reactor are made with pressure transmitters and are continuously read by the automatic control system. The pressure port lines are purged with argon to keep them particle free. Two sampling ports are used to extract gas samples in the biomass reactor and downstream of the reactor exit for measuring oxygen content. The product gas from the gasifier passes through a cyclone for particle removal, through a water gas shift (WGS) reactor, through a heat exchanger (for a second steam generator), a series of water condensers, and out through a tail gas flare unit. A back pressure control valve (BPCV 01) in the tail gas exit line serves to set the upstream system pressure. The product gas flow rate is measured after the BPCV with an orifice flow meter. There are two slipstream ports which divert the reactor effluent to a gas chromatograph (GC) for determining the gas composition. These occur before and after the WGS reactor. Downstream of the ports and before injection into the GC, a series of in line water condensers and desiccant traps are placed to remove water from the sample.

There are several levels of protection against over-pressurization. These include the pressure relief valves on the inlet gas supplies, the steam generators, the super heater, the gasifier, and the water gas shift reactor. Additional flow control valves and check valves are also inserted in steam and feed gas lines to properly direct the gas flow and to keep oxygen out of the water gas shift reactor which would oxidize its catalyst. To prevent a process excursion during startup and shut down, the product gas is vented through a pneumatically operated valve (BV 06) downstream of the gasifier until the designed system state is reached. There are also protections against system overheating. Temperature in the reactor vessel is monitored, and if it raises above a specified point, a series of solenoid control valves shuts off the oxygen (SOBV16), propane gas (SOBV17) feed gas valves, and steam (SOBV02) supply valve, and opens the emergency argon supply. Similarly, if the temperature/pressure of the Boiler-1 becomes too high, the control system opens SOBV01 opens and closes SOBV02 to vent steam, closes the feed gas valves, shuts off the air, natural gas, and steam, and opens the emergency N_2 purge.

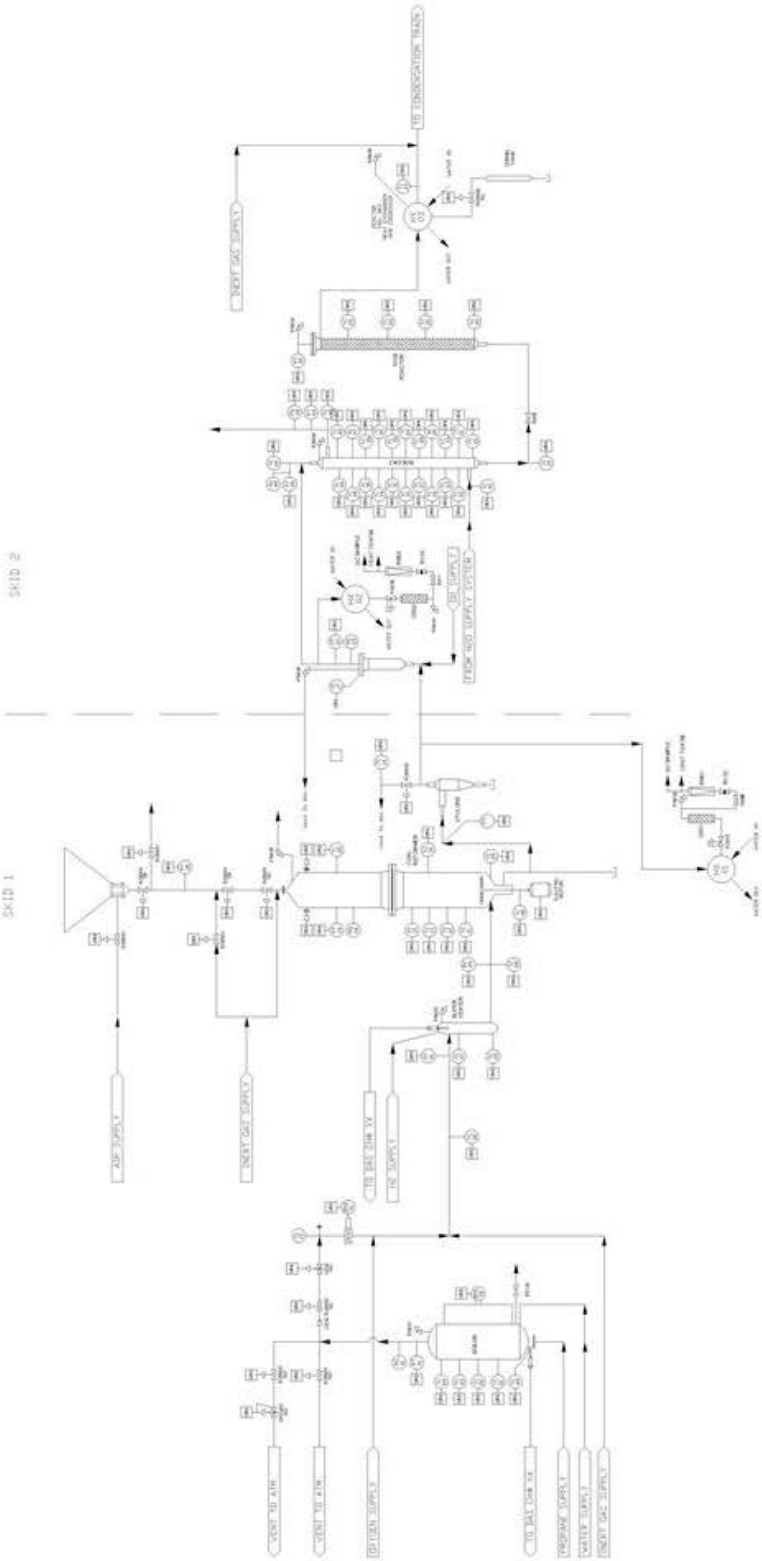

Figure A.2.1 *Piping and Instrumentation Diagram*

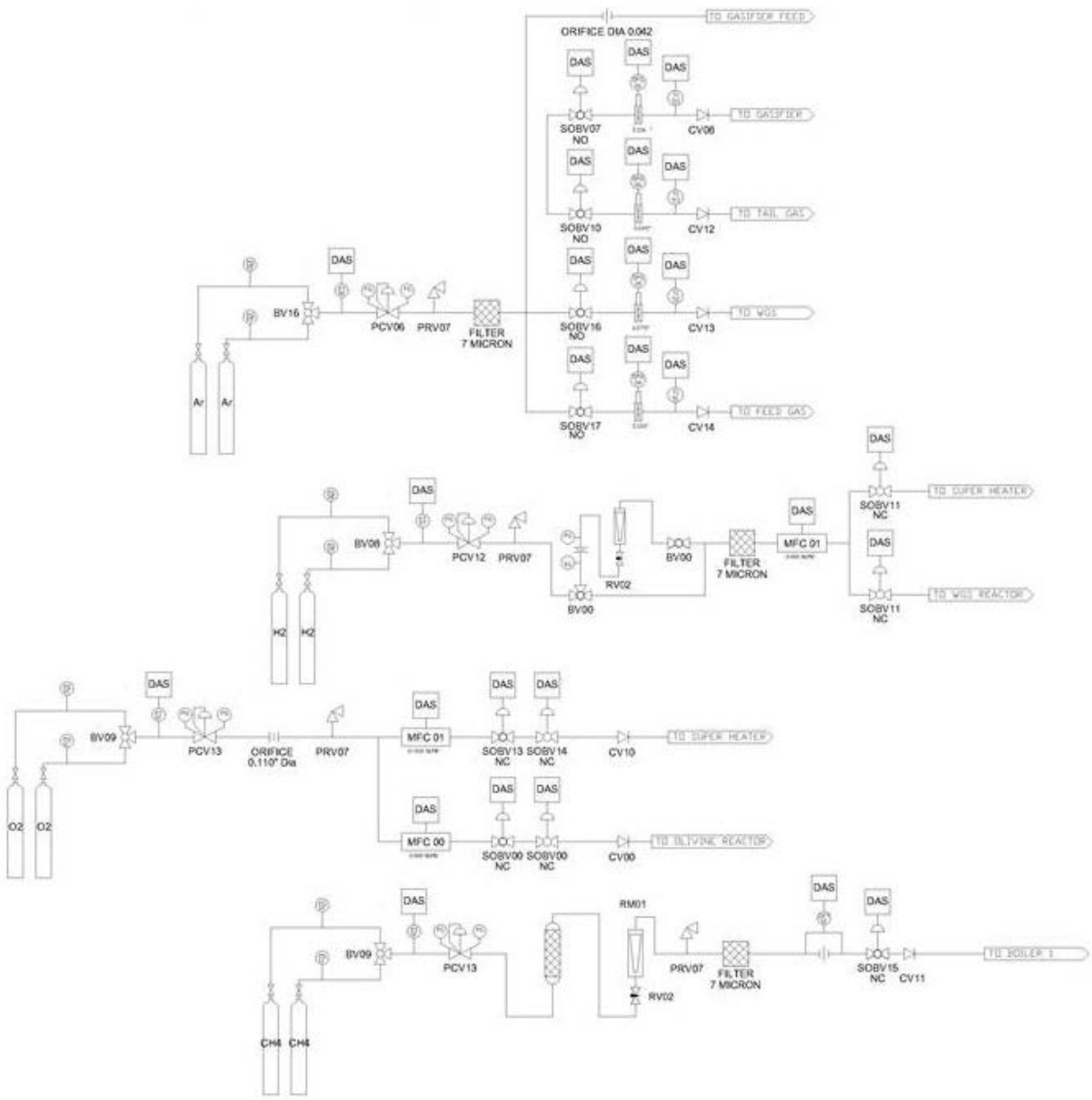

Figure A.2.2. *Piping and Instrumentation Diagram (Continued)*

A.3. Proximate and Ultimate Analysis of the Wood Pellets Fuel

Table A.3.1. Pine Wood Pellet Report of Analysis

REPORT OF ANALYSIS

Proximate Analysis Method: ASTM D-5142	As Received	Moisture Free	Moisture & Ash Free
Moisture, wt%	6.20	******	******
Ash, wt%	0.58	0.61	******
Volatile Matter, wt%	76.94	82.04	82.54
Fixed Carbon, wt%	16.28	17.35	17.46
Total	100.00	100.00	100.00

Ultimate Analysis Method: ASTM D5142/5373			
Moisture, wt%	6.20	******	******
Hydrogen, wt%	5.39	5.74	5.78
Carbon, wt%	50.50	53.84	54.17
Nitrogen, wt%	0.25	0.26	0.27
Sulfur, wt%	0.07	0.07	0.07
Oxygen, wt%	37.01	39.48	39.71
Ash, wt%	0.58	0.61	******
Total	100.00	100.00	100.00

Heating Value, Btu/lb Method: ASTM D-5865	7,953	8,478	8,531

Hydrogen and Oxygen values reported do not include hydrogen and oxygen in the free moisture associated with the sample.

Monte L. Ellis
Laboratory Manager

WYOMING ANALYTICAL LABORATORIES, INC.
1660 Harrison St.
Laramie, WY 82070
Wallaramie@wal-lab.com
(307) 742-7995
Fax: (307) 721-8956

A.4 Test Case Summary

Table A.4.1. Test Case Log

Test Number	Date	Objectives, Remarks and Observations
005-1	1-5-12	Phase IIIA first fire, batch operated checkout of instrumentation
010-2	1-10-12	System checkout with charcoal, uneven thermal profile burn
013-3	1-13-12	System checkout with reduced reformer nozzle area, more uniform burn profile observed
018-4	1-18-12	Checkout of O2 feedback loop and PID tuning
020-5	1-20-12	Checkout of new system and DAC updates
025-6	1-25-12	Checkout of auto fill of Boiler-1, generation of higher product gas flow rates
032-7	2-1-12	Added upper fuel magazine, increase run time, generated higher product gas flow rate
037-8	2-6-12	Batch flow rate scale-up with charcoal, Aborted run due to glow plug failure in super heater
044-9	2-13-12	Batch flow rate scale-up, activate auxiliary boiler
047-10	2-16-12	Test WGS reactor with Fe-Cr catalyst
053-11	2-22-12	Flow rate scale up of product gas flow rate
055-12	2-24-12	Batch flow rate scale-up, Achieved Phase IIIA goal of 4000 SLPM with charcoal fuel
069-13	3-9-12	Checkout of new WGS reactor and CuO-ZnO catalyst, develop reduction procedure
076-14	3-16-12	Reduction of Cu-Zn oxide catalyst in WGS reactor
079-15	3-19-12	Performance optimization of WGS
081-16	3-21-12	Performance optimization of WGS
088-17	3-28-12	Batch flow test with wood pellets, performance optimization
095-18	4-4-12	Batch flow test with wood pellets, performance optimization
102-19	4-11-12	Batch flow test with wood pellets, 4000 SLPM achieved, achieved Phase IIIA goal with representative biomass fuel
124-20	5-3-12	Continuous biomass feed system integrated into system, system checkout test performed, The influence of operational conditions on product gas evaluated
138-21	5-17-12	Checkout test with continuous biomass feed assembly Influence of the operational condition on product gas evaluated
143-22	5-22-12	Checkout test with continuous biomass feed assembly Influence of the operational condition on product gas evaluated
146-23	5-25-12	Checkout with continuous biomass feed assembly Influence of the operational condition on product gas evaluated
152-24	5-31-12	Aborted run due to DAC malfunction
153-25	6-1-12	Demonstrate extended run with biomass feed assembly, 2.5 hr run
163-26	6-11-12	Extended run with biomass feed assembly, 2 hr run
167-27	6-15-12	Checkout of modifications to biomass feed assembly
171-28	6-19-12	Extended run with biomass feed assembly, 4000 SLPM achieved

200-29	7-18-12	Installation and checkout of modified rotating grate for higher ash removal rate
205-30	7-23-12	Test with biomass feed assembly, rotating grate Influence of the operational condition on product gas evaluated
209-31	7-27-12	Test with biomass feed assembly, rotating grate Influence of the operational condition on product gas evaluated
215-32	8-2-12	Test with biomass feed assembly, rotating grate Influence of the operational condition on product gas evaluated
275-33	10-1-12	Checkout test tar destruction reactor
278-34	10-3-12	Checkout test with tar destruction reactor
278-35	10-9-12	Phase IIIB first fire and baseline test with full scale feed assembly, rotating grate, tar destruction units
278-36	10-16-12	Scale-up and performance test as a function of feed rate Test terminated due to fuel bridging
292-37	10-18-37	Scale-up and performance test as a function of feed rate, Grate repaired, new operating procedures for steam addition, nitrogen blast added Temperature excursion observed, high reformer exit gas temperature terminated test
300-38	10-26-12	Product gas flow rate scale-up and performance test, New back pressure control valve and steam orifice Temperature excursion in reformer exit gas
305-39	10-31-12	Product gas flow rate scale-up and performance test New grate fabricated Bridging encountered/temperature excursion
310-40	11-5-12	Product gas flow rate scale-up and performance test Upper nozzle bank used to create longer residence time and reduce temperature Sudden drop in PG flow rate, increased pressure drop in reformer, and temperature increase
319-41	11-14-12	Product gas flow rate scale-up and performance test Tapered transition duct installed in magazine to reduce fuel bridge Upper nozzle bank tested Fuel channel formed as evident from unusual product gas distribution- < 10% of H2 and CO, and > 45% CO2 > 30% O2
325-42	11-20-12	Test with full scale feed assembly, 6000 SLPM peak flow rate achieved Bridging encountered with rat hole formed around stirrer shaft
331-43	11-26-12	Test with full scale feed assembly, 5 inch bed stirrer installed, High pressure drop
334-44	11-29-12	Test with full scale feed assembly, 10 inch bed stirrer, High pressure drop in system

A.5. Linear Slider Feed Cup Drawing

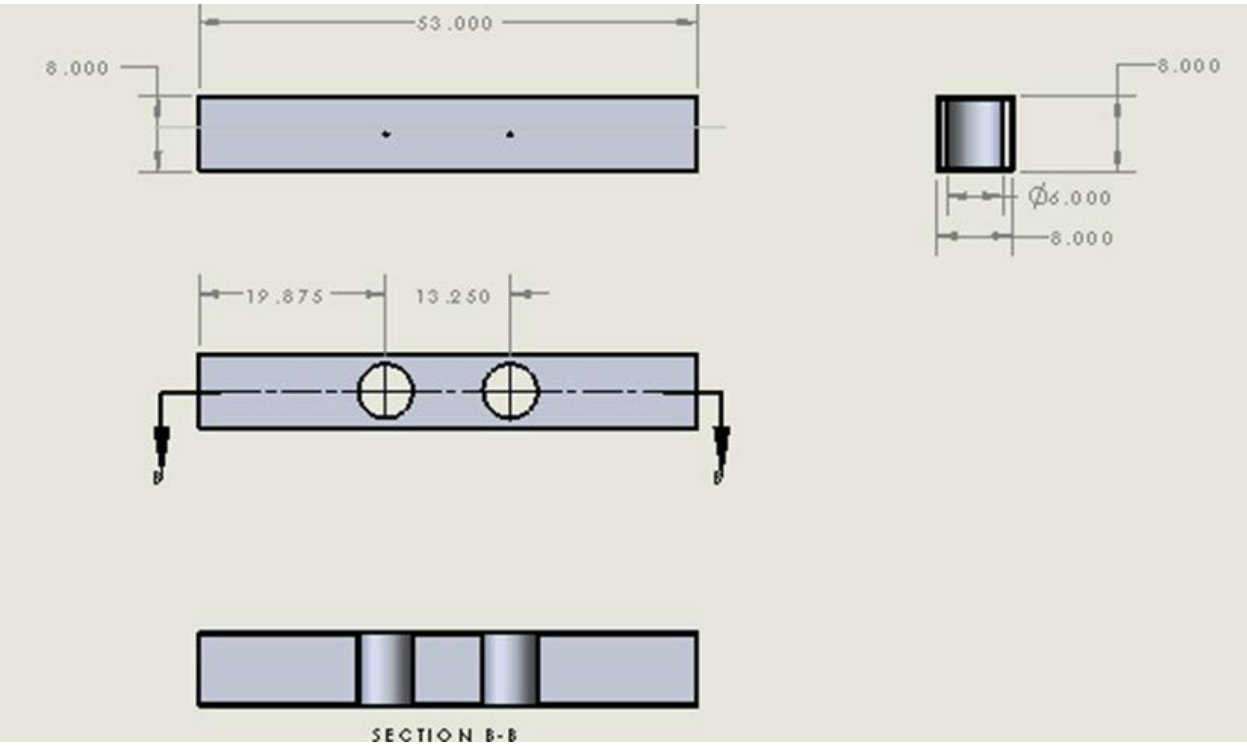

Figure A.5.1. Slider Cup

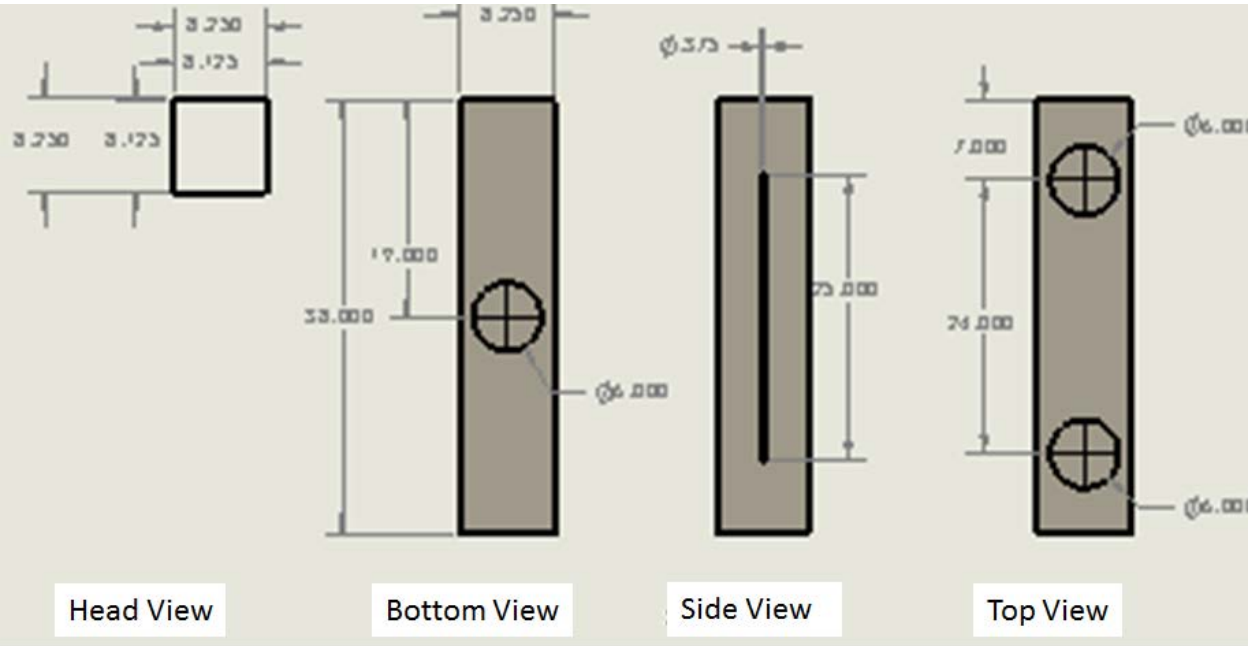

Figure A.5.2. Slider Cup Housing